Role of defects comprise of antidot, Boron/Nitride doping, and uniaxial strain on the electronic/transport properties of GNR, and CNT based RTD devices

Milad Zoghi

A Thesis

in

The Department

of

Electrical and Computer Engineering

Presented in Partial Fulfillment of the Requirements

For the Degree of Master of Applied Science at

Concordia University

Montreal, Quebec, Canada

July 2019

CONCORDIA UNIVERSITY
SCHOOL OF GRADUATE STUDIES

This is to certify that the thesis prepared

By: Milad Zoghi

Entitled: Role of defects comprise of antidot, Boron/Nitride doping, and uniaxial strain on the electronic/transport properties of GNR, and CNT based RTD devices

and submitted in partial fulfillment of the requirements for the degree of

Master of Applied Science

Complies with the regulations of this University and meets the accepted standards with respect to originality and quality.

Signed by the final examining committee:

_____ Chair
Dr. Steve Shih

_____ Examiner, External
Dr. Saifur Rahaman (BCEE) To the Program

_____ Examiner
Dr. Steve Shih

_____ Supervisor
Dr. M. Zahangir Kabir

_____ Co-Supervisor
Dr.

Approved by: _____
Dr. Yousef R. Shayan, Chair
Department of Electrical and Computer Engineering

_____20_____ _____
Dr. Amir Asif, Dean
Gina Cody School of Engineering and
Computer Science

ABSTRACT

Defects, Graphene nanoribbons, and Carbon nanotubes

Milad Zoghi

Silicon technology has been the main driving force for miniaturizing electronic device dimensions to reduce cost and improve performance. However, Silicon industry is reaching to fundamental limits that size shrinking trend cannot be continued. Hence, alternative low dimensional materials such as Graphene nanoribbons (GNRs) and Carbon nanotubes (CNTs) have attracted great amount of attention to be used in the future electronic devices. Although, GNRs and CNTs carry promising electronic and transport characteristics, additional flexibility and control over fundamental properties like band gap level is highly desirable. In this thesis, three kinds of defects comprise of antidots, Boron Nitride (BN) doping, and uniaxial strain are used to modify intrinsic properties of GNRs and CNTs. Using Tight Binding (TB) with accompany of Non-equilibrium Green Function (NEGF), it is found that pristine properties of AGNR and ZCNT such as band gap can be modulated upon introduction of periodic antidot, BN defect topologies. Next, novel ZCNT RTD platform is designed by mean of defects, showing potential applications of defected ZCNT in fundamental electronic components such as RTDs. In addition, role of uniaxial strain on the performance of two AGNR RTD platforms is examined. Width-modified and field-modified AGNR RTD platforms go under both local and whole-body uniaxial strain. The analysis manifests that Peak to Valley Ratio (PVR) might be totally lost if imposed whole-body strain is strong enough. However, local strain can either totally damage the PVR or improve it up to 7 times, depending on the type of strain and utilized platform. As a result, AGNR RTDs may not be considered as the ideal candidates for the flexible electronics since their properties are subject to intense variation upon mechanical deformation. This mechanically dependent performance of AGNR RTDs would be promising in design of motion-based sensors.

ACKNOWLEDGMENTS

Foremost, I would like to express my sincere gratitude to my advisor Prof. M. Zahangir Kabir for the continuous support of my Master study and research, for his patience, understanding, great attitude, and immense knowledge. His guidance helped me in all the time of research and writing of this thesis. I could not have imagined having a better advisor and mentor for my Master study.

Besides my advisor, I would like to thank my friend S. Mohammad Mirjalili and Dr. Arash Yazdanpanah for their sincere help, comments, and encouragement.

I think I can never truly appreciate my mother's dedication whose kindness and full support allowed me to focus on my education at all stages and achieve my goals. I would like to thank deeply my mother and brothers, Mohammad and Mehdi, for supporting me throughout my life.

Last but not least, I want to appreciate my best friend Mozhdeh Yamani whose encouragement and sincere support accompanied me throughout my Master to overcome problems and hard times.

Table of Contents

List of figures

List of tables

List of Acronyms

ACNT: ..…….. Armchair Carbon Nanotube

AGNR: ……. Armchair Graphene Nanoribbon

ASL: …….. Antidot Super Lattice

BN: ……. Boron Nitride

CNT: …… Carbon Nanotube

DBQW: ……... Double Barrier Quantum Well

DFT: …….. Density Functional Theory

DSL: …….. Doping Super Lattice

GNR: …… Graphene Nanoribbon

LDOS: …… Local Density Of States

NDR: …… Negative Differential Resistance

NEGF: …… Non-Equilibrium Green Function

PVR: ……... Peak to Valley Ratio

RTD: ……. Resonant Tunneling Diode

SWCNT: …….. Single Wall Carbon Nanotube

ZCNT: ……. Zigzag Carbon Nanotube

ZGNR: …….. Zigzag Graphene Nanoribbon

Chapter 1 Introduction

1-1 From Bulk Silicon to Defected Carbon Derivatives

Silicon-based microelectronic devices have revolutionized our world in the past four decades. Every electronic of our modern world is being controlled by integrated circuits, made of many Silicon transistors and diodes on a single chip. Each year, consumers expect their electronic devices to become smaller and more powerful while also featuring exciting new capabilities. While advances in Silicon have made this trend possible, it is now clear that Silicon can't keep up with this rate of innovation [1-6]. One main stream technological trend of the Silicon industry is scaling down the device sizes. For instance, the gate length has been reduced down to ~20 nm under current optical lithography technique, and the count of transistors in a commercially available CPU numbers more than 5 billion [1]. In a transistor, the gate oxide insulates the voltage electrode from the current-carrying electrodes. At a thickness of less than four layers of Silicon atoms, current will penetrate through the gate oxide causing the chip to fail [3]. Moreover, because single-crystal Silicon based electronic devices are fabricated onto Si wafer, which cannot be flexible, these devices are restricted to small areas. Flexibility that Si devices lack is crucial quality for large-area electronic applications such as flat panel displays, large-area sensor arrays, smart card, inventory tags, and wearable electronics [1, 3, 7, 8].

As a result, various prospective low-dimensional materials have been proposed to overcome the problems of conventional Si technology [6, 8-18]. The term "low-dimensional materials" combines a wide range of two dimensional (2D), one dimensional (1D) crystalline materials with exciting electro-physical, magnetic and optical properties. Although the first studies of 2D

materials are known since the late sixties [19, 20], an intensive research in this direction has started only in the last 15 years [5, 7, 8, 18, 21-23]. In particular, nano-scale carbon derivatives such as graphene (nanoribbons) (GNRs) and carbon nanotubes (CNTs) are promising due to outstanding electronic properties as well as an excellent combination of elastic, optoelectronic, and thermal properties compared to conventional bulk Silicon [24-28]. The uniqueness of these nano-carbon materials has opened new possibilities for the next generation electronics.

Since discovery of GNRs and CNTs, diverse work has been done to improve the quality of the materials (crystallinity and uniformity) and to control other parameters (chirality, density, and doping levels) and morphology (length, area, dimension, and thickness) [21, 24, 25, 27-33]. However, it is probable that original lattice and properties of the nano-scale materials deviate from expected ones due to the existence of defects [26, 34-37]. The expression "defects" involves a broad case of imperfectness with respect to ideal nanostructure. In this thesis, three most common and interesting types of defects on the carbon derivatives are studied, namely: antidots, Boron/Nitride (BN) doping, and uniaxial strain. Although defects might exploit anticipated properties of a material/device, however, defects could be implemented to tune pristine behavior of the material/device as well [26, 35-39]. This is the case if defects are created intentionally in specific order. Indeed, it is insightful to understand, in which mechanism electronic and transport properties of GNRs and CNTs are modulated upon imposing aforementioned types of defects. Furthermore, it'd be valuable to know whether one can implement modulated properties to design nano-electronic devices such as resonant tunneling diode (RTD) or how performance of well-know RTD platforms could be influenced via mechanical deformation defect.

1-2 Graphene Nanoribbons

Graphene is one atom thick sheet of carbon atoms in honeycomb lattice which is 2D material. GNRs are considered 1D strips of graphene sheet meaning they contain finite width. Depending on the edge shape, GNRs are divided into zigzag GNR (ZGNR) and armchair GNR (AGNR), See Figure 1-1 [40, 41]. It is assumed that Carbon atoms at the edges are passivated by Hydrogen, implying there is no dangling bonds at the edges and hexagonal structure is perfect all over lattice. GNRs are named by the number of atoms across the ribbons as illustrated Figure 1-1.

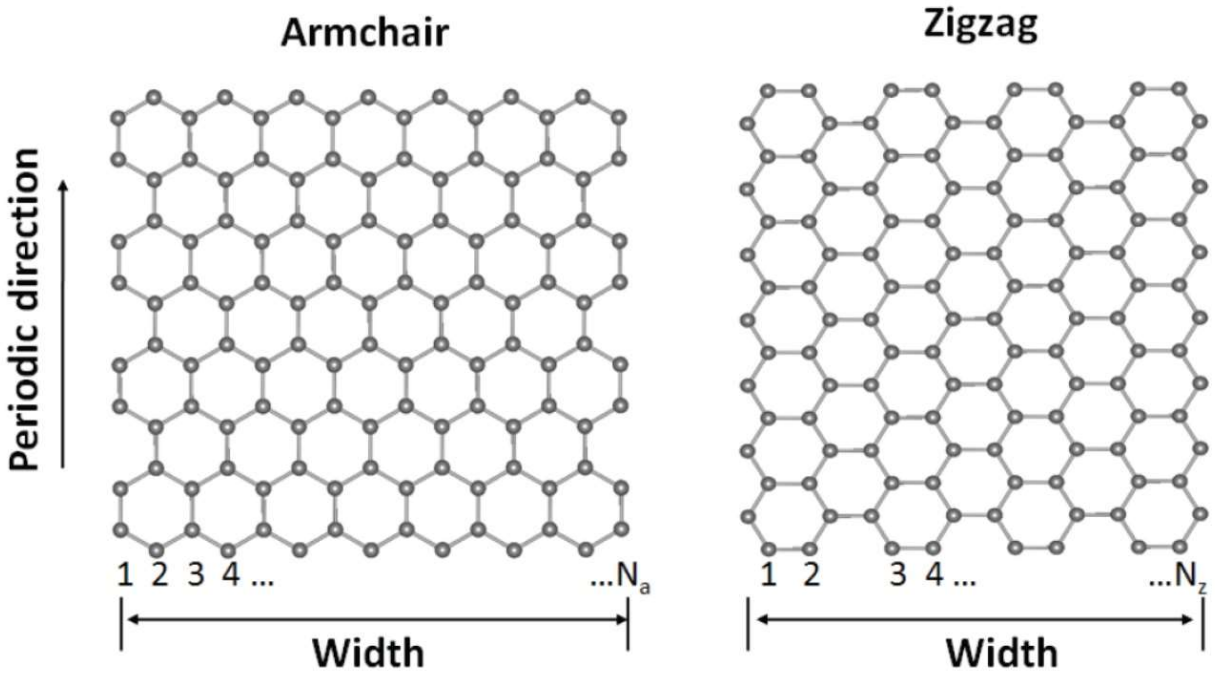

Figure 1-1: Lattice view of AGNR and ZGNR [40].

Under non-spin state consideration, ZGNRs are metallic with no band gap, whereas AGNRs own interesting band gap range, depending on the number of dimer lines (N_a) across on their widths [40, 41]. In fact, AGNRs are categorized in three families N_a= 3P, 3P+1, and 3P+2, where P is an integer. As shown in Figure 1-2, family 3P+2 is semi-metallic while two others are semiconducting. Indeed, band gap size of AGNR can be justified by opting proper width, which makes AGNRs ideal for many electronic and optoelectronic applications.

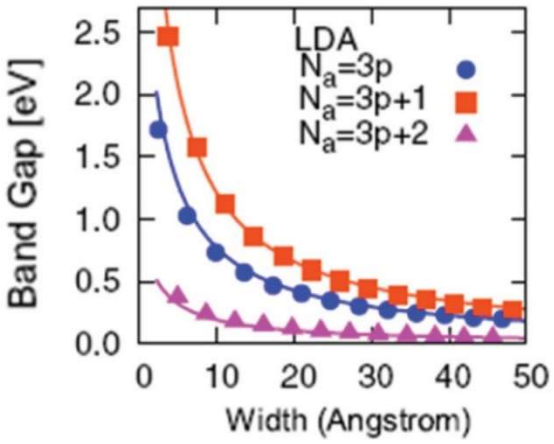

Figure 1-2: Band gap versus width size for three families of AGNRs [40].

1-3 Carbon Nanotubes

CNTs can be viewed as strip cut of graphene sheet and rolled up to shape a cylinder, Figure 1-3-a. Notably, CNTs could made of single or multiple walls [2, 30, 42]. In this work, "CNTs" refers to mono layer CNTs. Diameter and helicity of CNTs is defined by the roll-up vector $C_k=n_{a1}+m_{a2}$ ~ *(n,m)*, refer to Figure 1-3-a . *a1* and *a2* are the graphene lattice vectors and *n, m* are integers.

Zigzag *(n,0)* and armchair *(n,n)*, and chiral *(n≠m)* CNTs have been depicted by back solid lines. Relative values of *n* and *m* determines whether a CNT is metal or semiconductor. CNTs are either metallic or semiconducting depending on the tubular axis. For a given *(n,m)* nanotube, if *n=m*, the nanotube is metallic; if *n−m* is a multiple of 3 and *n≠m* and *nm≠*0, then the nanotube is quasi-metallic with a very small band gap, otherwise the nanotube is a moderate semiconductor [43].

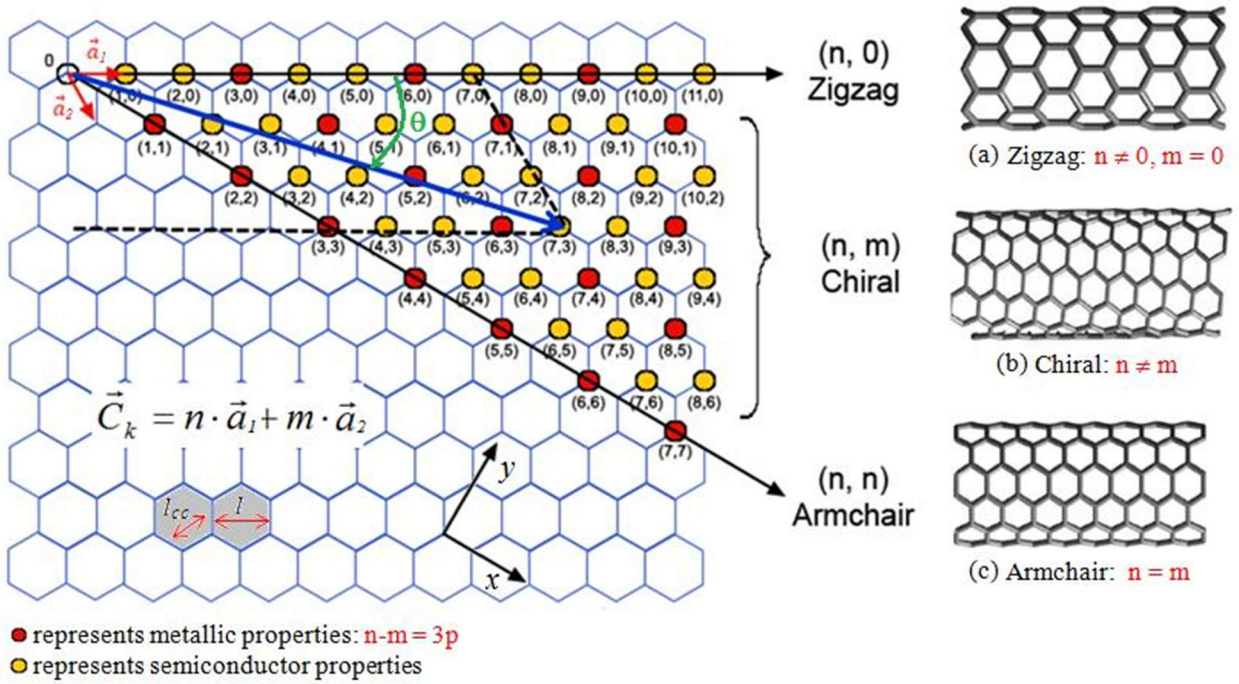

Figure 1-3: Schematic of a 2D graphene sheet illustrating roll-up vector for CNTs and a) ZCNT, b) Chiral CNT, c) ACNT [44].

1-4 Resonant Tunneling Diodes

Resonant Tunneling Diode (RTD) is kind of diode that electron transmission occurs by tunneling through quantum barriers using quasi energy states [45-48]. As shown in Figure 1-4, RTD is built of double barrier quantum well (DBQW) structure. Such DBQW leads to formation of quasi energy states within quantum well. Electrons can use these energy states to tunnel through barriers and contribute to conductance. As a result, upon increasing bias voltage, first, the number of electrons that using tunneling rises gradually, reaching a peak point, where Fermi level of emitter matches the first energy state, Figure 1-4-b. Next, due to mismatch between Fermi level at emitter side and first energy state, electrons are less likely to tunnel and therefore current amount decreases. This trend continues till second energy state or when emitter Fermi level go over barrier height. Thereby, RTD proposes negative differential resistance (NDR) characteristic between peak and valley points. The peak to valley ratio (PVR) of current amount is the most important factor of RTD device and higher value of PVR is very desirable. Tunneling diodes can be very compact and are also capable of ultra-high-speed operation because the quantum tunneling effect through the very thin layers is a very fast process. Also, NDR property of RTDs could be implement on a variety of applications such as oscillators, switches, and amplifiers [45-48].

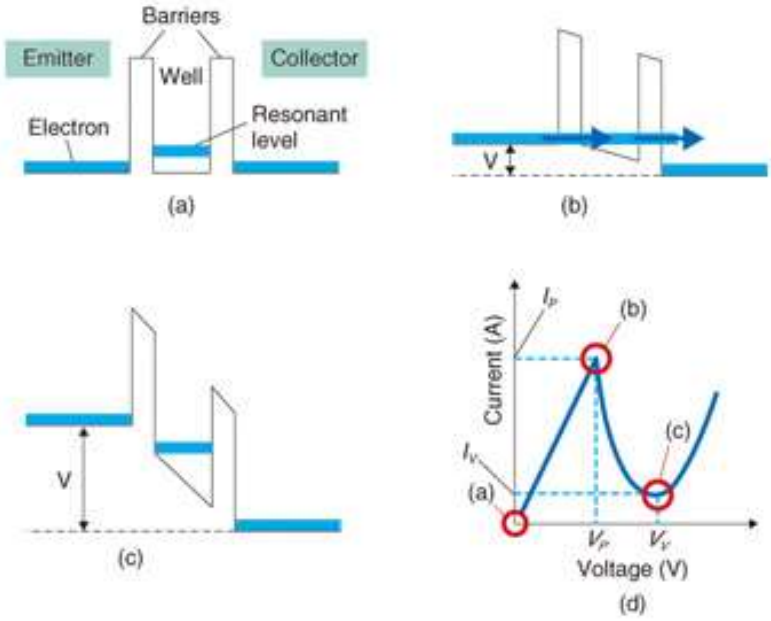

Figure 1-4: a-c) Band diagram of RTD under different bias voltage, d) Typical I-V curve of RTD [49].

1-5 Defects and Carbon derivatives

Defects play an important role in the properties of nano-scale materials like GNRs and CNTs. Physiochemical characteristics of nanostructures may change totally due to accommodation of different kinds of defects [26, 37, 39, 50]. There is no much accurate and quantitative method to distinguish the types of defects that graphene-like materials contain. However, in general, defects within graphene-like structures could be classified in five different groups (Figure 1-5) [26]:

a) Structural defects, reflects the imperfections that markedly distort pristine curvature of hexagonal Carbon lattice. Examples: non-hexagonal rings such as pentagons and heptagons.

b) Bond rotations, caused on the surface, which do not lead to significant structural distortion. Example: 5-7-7-5 pairs surrounded by the hexagonal lattice.

c) Doping, by substituting non-Carbon atoms such as Boron or Nitride in the hexagonal network. Doping increases the surface chemical reactivity due to different atomic numbers of substituted defect atoms.

d) Non-sp2 Carbon defects, includes antidots (vacancies), free trapped atoms, and edges distortion. It has been demonstrated that presence of such defect could significantly change electronic and transport properties of quasi 1D materials alike GNRs and CNTs.

e) Strain (Folding), caused under mechanical deformation in which pristine structure could be stretched, compressed or folded.

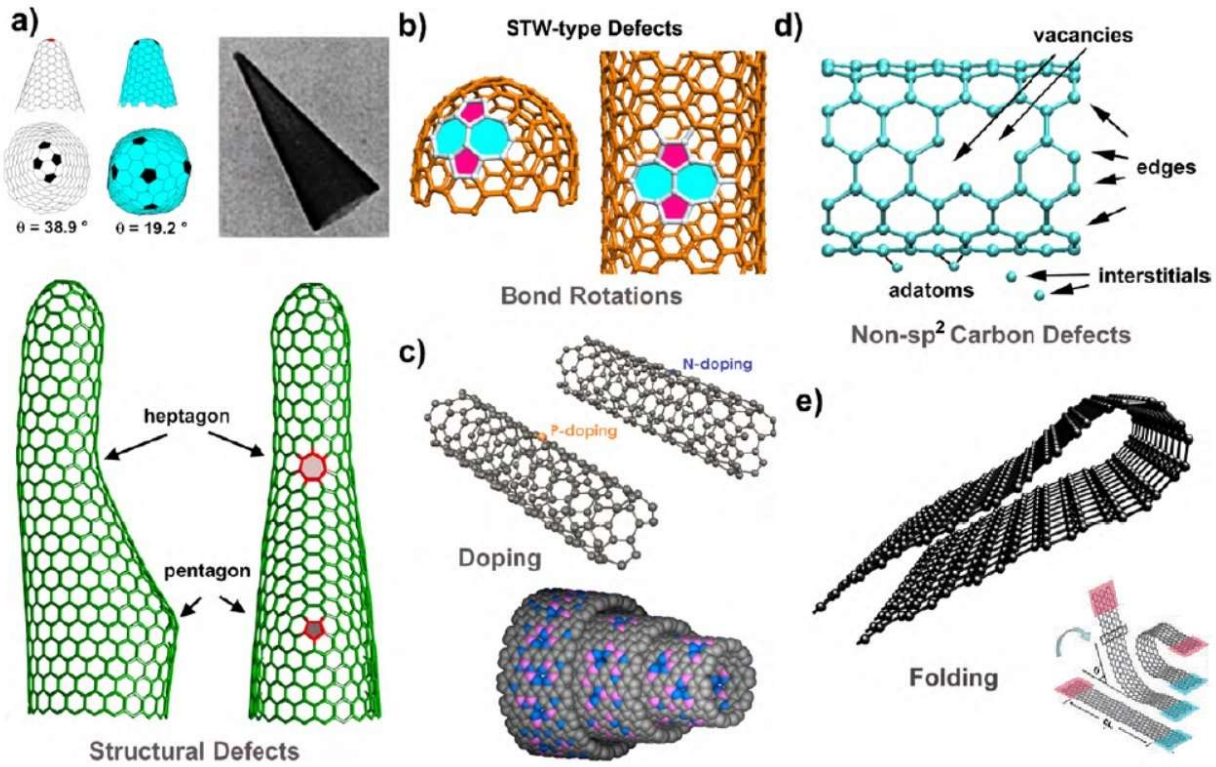

Figure 1-5: Five common kinds of defects, occurring on graphene-like nanostructures [26].

1-6 Motivation and Objectives

So far, the most common defect types in graphene-like structures have been reviewed. As a matter of fact, low dimensional materials have higher surface to volume ratio compared to bulk 3D materials, giving them much higher chemical sensitivity [6, 15]. Being chemically active implies low dimensional materials are more likely of reaction with surrounding and appearance of defects in their bodies. Moreover, any kind of lattice deviation in quasi one-dimensional materials like GNRs and CNTs leads to marked change of quantum confinement and eventually I-V characteristic. There has been huge concern to understand what effects would occur by the presence of defects on nanostructures. Extensive amount of research has been allocated to study impacts of specific profiles of defects on properties of graphene-based nanostructures [26, 34-37, 39, 51, 52].

After discovery of graphene (one atomic thick layer of graphite) in 2004, great amount of attention has been given to realize its potential applications and also robustness against lattice deviation and imperfectness [5, 7, 22, 34, 53-58]. Some of the most frequent kind of defects are antidots (vacancies) and chemical doping. Although variety of study cases regarding antidots, doping, and graphene are observed in the literature [6, 21, 22, 33, 53, 57, 59], however, related works for graphene derivatives such as GNRs and CNTs have not been very frequent and systematic. More specifically, no one has studied what occurs to the electronic and transport properties of GNRs and CNTs if antidot/BN doping topologies are periodically inserted along their length. Using the term periodic enforce some kind of control over substituting defect topologies in pristine lattice. It may be asked then, is there any evidence for such precise control at the nano-scale level and what is the point while defects are considered to happen accidentally and tried to be avoided at the first place.

To date, there are some evidences of precise experimental methods for positioning of topological defects at nano-scale level (Figure 1-6) [29, 60]. Although, these are primary progress, however, remarkable advancement in nanotechnology is not far behind the mind as it is one of the fasted growing fields of research for the time being. Hence, it's quite valuable to conduct theoretical investigations which will come in hand of experimentalist in the future. Keeping in mind that Silicon-based electronics is reaching fundamental limits, importance of discovering novel features of prospective candidates like GNRs/CNTs become double. Moreover, although defects may occur occasionally, however, if we have power to impose them in a controlled way, then defects could be seen as opportunity to manipulate pristine properties and thereby add additional level of tunability and flexibility to the nanostructures. Following such attitude, we'd been motivated to see whether one can design and implement novel electronic devices like RTDs using probable new characteristics of periodic defected structures or not.

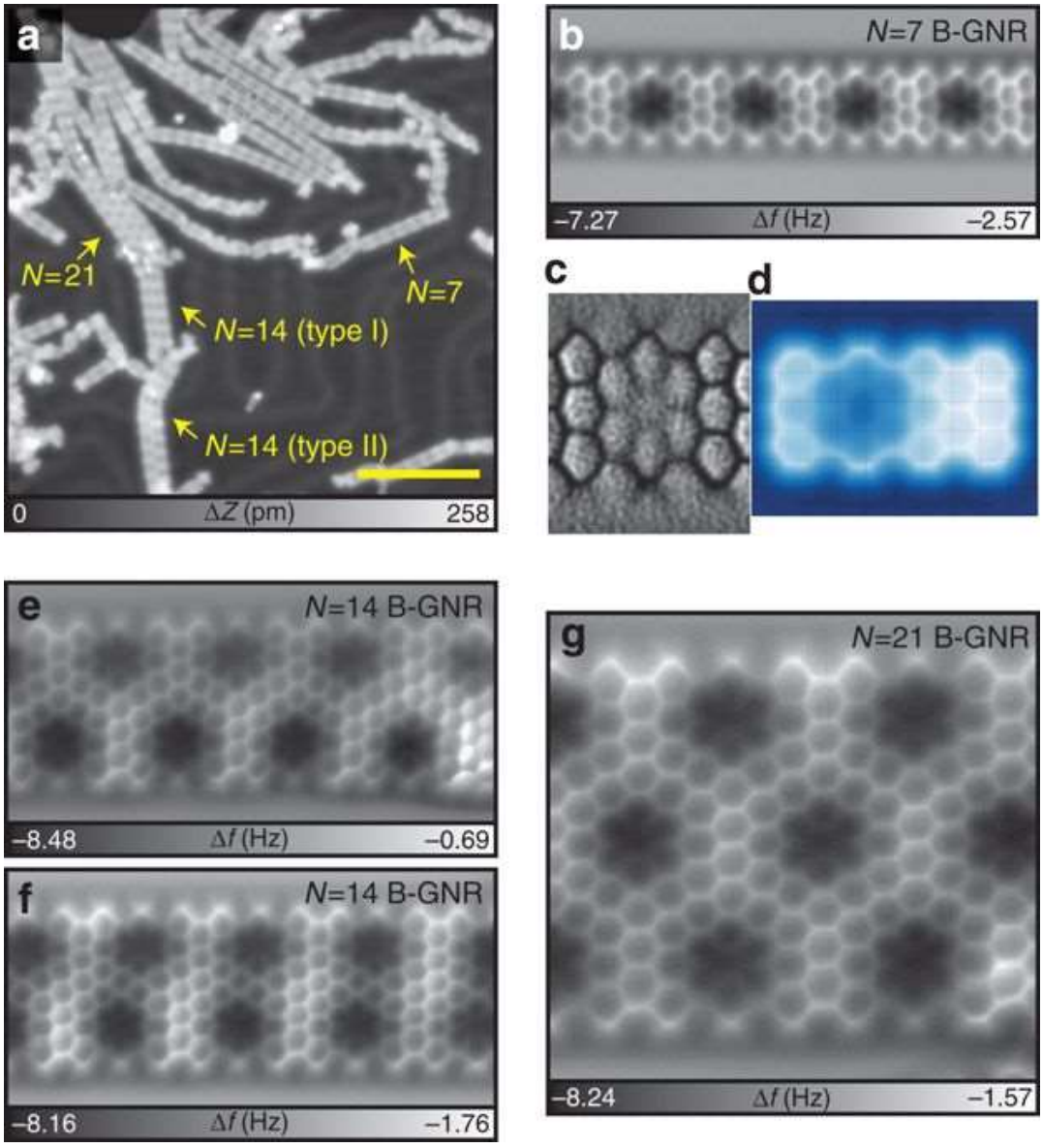

Figure 1-6: STM overview of atomically substitutional BN doping of GNRs [60].

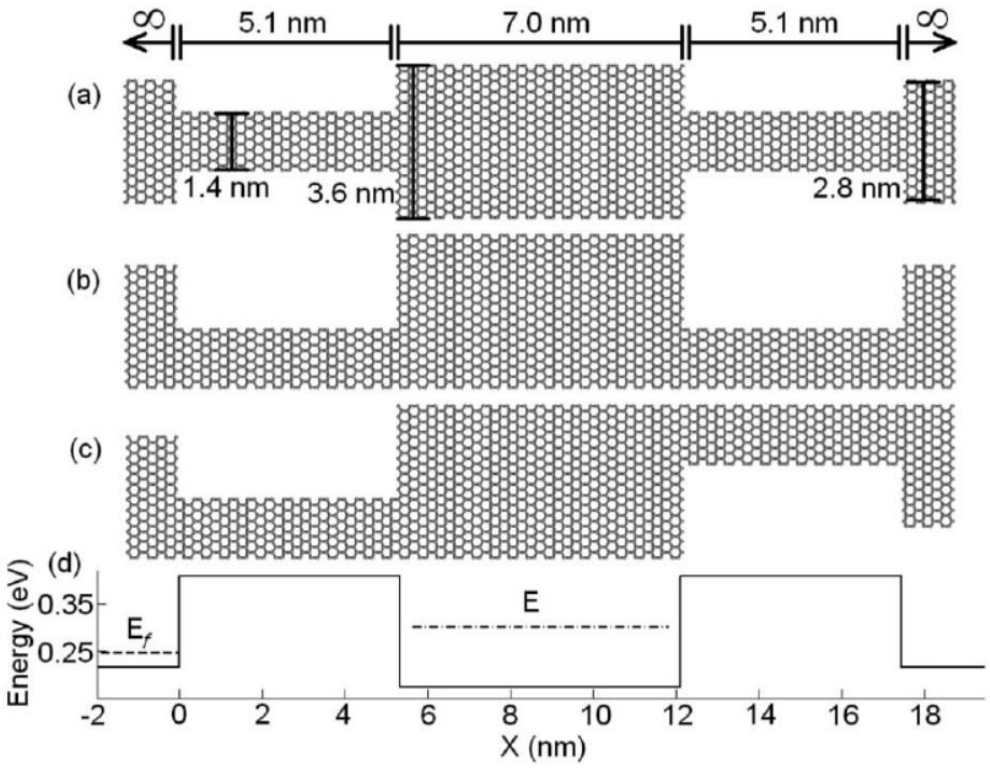

Figure 1-7: a-c) Schematic views of width-modified AGNR RTD. d) corresponding device band diagram [61].

Figure 1-7exhibits the schematic view of width-modified AGNR RTD proposed in [61]. Thinner width of AGNRs (from same family) presents higher band gap level. Using this property, barrier regions are composed of thinner width and corresponding band diagram of device is depicted in Figure 1-7-d. Higher energy level of barriers leads to the formation of DBQW structure and existence of quasi energy states within quantum well. Upon applying bias voltage quasi energy states contribute in conductance via quantum tunneling phenomenon and NDR is resulted in I-V characteristic (RTD device). Now it is inspiring to design novel RTD device in such way that DBQW structure could be shaped by mean of defect-based structure instead of using different widths of AGNRs. The objective then becomes to select some topologies of defects alike hexagons, and next substitute them periodically into the body of GNRs/CNTs. Such modification

in perfect lattice, enforce us to modify TB model since we are dealing with super-structure in which unit cell should contain defect topology. It is expected that each topology represents unique modulated electronic/transport properties. It's also interesting to know how dimensional factors like relative distance between defects may adjust modified properties such as band gap size. It is insightful to discover underlying mechanism and bring insights of how defects influence original behaviors. Afterwards, equipped with defect tuning tool, the target becomes to design defect-based RTD platforms and investigate how device performance can be adjusted.

Another common type of defect is mechanical deformation or in specific format uniaxial strain. Demand for large-area electronic applications such as wearable electronics is growing, meaning more mechanically flexible devices that preserve their performance are demanding [8, 56]. Its known that GNRs can tolerate uniaxial strain up to even 20 percent [62, 63]. Besides, RTD device as a fundamental component of many circuitries have been achieved by mean of GNRs. However, to date, literature lacks proper investigation of how such GNR-based RTD behaves upon mechanical deformation. Indeed, the insights in this regard are brought by deforming two common platforms of GNR RTD devices, width-modified and field-modified. It is interesting to track PVR under different intensity of compressive/tensile strain. Some in-depth analysis regarding local strain, dimensional parameters and corresponding variations in transport properties comprise of transmission, LDOS, and I-V characteristic are also performed.

In summary, our objectives are:

a) Extraction of electronic and transport properties of periodic antidot/ BN doped ZCNTs and comparing efficiency of perfect and defected systems. In depth analysis to discover underlying mechanisms and finding ways to tune system's behavior are also demanded.
b) Design of ZCNT RTD by mean of antidot/BN topologies and investigating performance of such device.
c) Imposing whole-body and local uniaxial strain to width/field modified AGNR RTDs to monitor device performance under mechanical deformation.

1-7 Thesis Outline

In this thesis, chapter 1 reviews some fundamental information regarding GNRs, CNTs, RTDs, defect types for graphene-like material, and also motivation and objective of the thesis. Tight Binding (TB) method coupled with Non-equilibrium Green Function (NEGF) have been derived to discover electronic and transport properties of the systems. Chapter 2 provide details of modeling and how antidots, BN doping, and strain effects are included in calculations. In chapter 3, first, some researches with respect to antidot/BN periodic GNR structures are reviewed. Secondly, results about impacts of periodic antidot/BN topologies on the pristine properties of ZCNTs is presented. In addition, dependency of the new properties on the dimensional parameters of tube is analyzed in depth. Chapter 4 shows how periodic antidot/BN topologies can be utilized to build defect-based RTDs. Using results of subchapter 3-2, novel ZCNT RTD platform by mean of antidot/BN topologies is designed and included in subchapter 4-2. Chapter 5 is allocated to strain and GNRs. Effects of uniaxial strain on the performance of GNRs is recapped from literature and then role of mechanical deformation on the operation of width/field modified AGNR RTDs is examined. Chapter 6 concludes the thesis and suggests potential future researches.

Chapter 2 Modeling

2-1 Tight Binding (TB)

In solid-state physics, the tight-binding model (TB) is an approach to the calculation of electronic band structure using an approximate set of wave functions based upon superposition of wave functions for isolated atoms located at each atomic site [64-67]. The semi-empirical tight binding method is simple and computationally very fast. It therefore tends to be used in calculations of very large systems, with more than around a few thousand atoms in the unit cell. Tight binding is a very effective way to describe motion and energy states of electrons in solids [23, 64, 66, 68-70]. Regarding time-independent form of Schrodinger equation (1), one need to form the Hamiltonian (H) to obtain the wave functions and energy levels of a system. Some methods like Density Functional Theory (DFT), solve the Schrodinger equation analytically to extract the band structure of lattices. Compare to TB, DFT generates more accurate results, however, complexity and lack of flexibility, are the drawbacks of analytical methods [23, 67, 71]. On the other hand, in TB, Schrodinger equation is solved numerically, and Hamiltonian is obtained for the smallest repeatable unit cell by mean of atomic orbital bases. This model based on a critical assumption that potential of lattice is periodical. Also, electron-electron interactions are neglected [23, 64-66].

$$\hat{H} \mid \Psi >= E \mid \Psi > \qquad (1)$$

According to the TB method, the Hamiltonian matrix, *H(k)*, is obtained with consideration of the first and third nearest neighbors' Carbon-Carbon interactions atoms as follows:

$$H(k) = \sum_{m} H_{nm} e^{i\vec{k}\cdot\left(\vec{d}_m - \vec{d}_n\right)} \quad (2)$$

where the index of n is related to the unit cell (for AGNRs) or super unit cell (ASL-AGNRs) which is chosen as the main unit cells in the periodic structure. The summation over m runs for the main unit cell and its neighboring unit cells. As the systems are one-dimensional, the values of m in terms of n can take two values of $m=n-1$ and $m=n+1$ which are related to left and right unit cells of the main unit cell, respectively. The distance between unit cells is denoted by (d_m-d_n) while k is the one-dimensional wave vector. We can introduce a dimensionless phase in terms of k by $K=k(d_m-d_n)$ [$-\pi < K < \pi$] [72].

Solving time-independent Schrodinger Equation for 1-D array of unit cells, we can calculate the band structure by using:

$$H(k) = H_0 + H_L e^{-ika} + H_R e^{+ika} \quad (3)$$

a is the lattice constant and k is the wave vector. H_0 stands for the Hamiltonian of primary unit cell, like the one placed between dark lines in Figure 2-3. H_R, and H_L, specify the connection Hamiltonians between primary unit cell and its right and left neighbor unit cells, respectively. In fact, H_R, and H_L allow us to model the movement of quantum wave to the right and left side of the lattice.

By considering the third nearest neighbor carbon-carbon interactions, more precise results for the electronic band structure of AGNRs can be predicted [65, 72-75]. The on-site and second nearest neighbor interactions are not taken into account in our TB model, because they just shift the electronic band structures respect to the Fermi level [75]. Finally, the electronic band structure can be achieved by finding eigenvalues of the matrix $H(k)$ for each value of k (or K) [72].

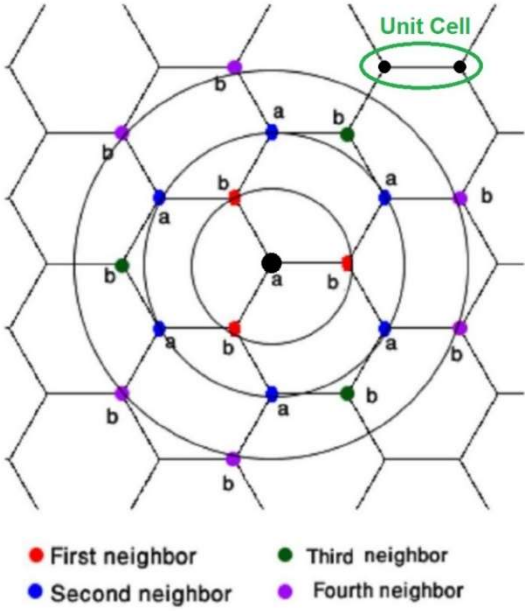

Figure 2-1: Unit cell and neighboring position of atoms in honeycomb structure [76].

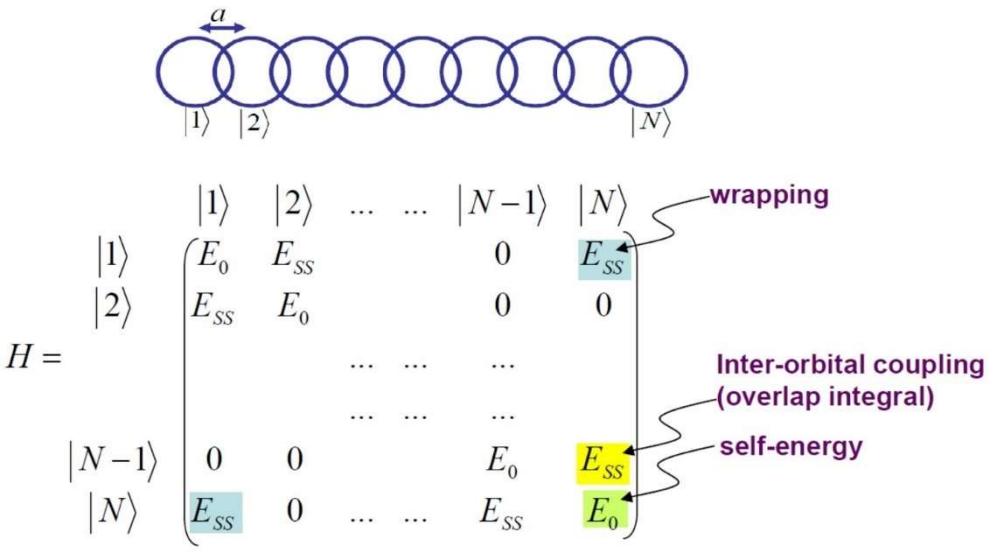

Figure 2-2: Hamiltonian matrix of one-dimensional atomic structure [23].

In the following we solve an example to obtain band structure of 2-AGNR, giving vivid vision of how TB has been implemented in our modeling. 2-AGNR may not exist, but, it's very intuitive case for the sake of an example. First of all, there are some set of assumptions: structure is repetitive and infinite, structure is considered one-dimensional meaning quantum wave just propagate along X (length), atoms at the edges are terminated by Hydrogen atoms avoiding dangling bonds. Lattice constant is set to 1.42 Angstrom and it's the same for whole interior and atoms at the edge regarding Hydrogen saturation assumption. In this example it is assumed that on-site energy of Carbon atoms is zero and merely first nearest neighbor hopping parameter is taken into account which is set to -2.65 eV.

Our job now is to fill out Hamiltonian matrices by orbital atomic bases. In Graphene-based honeycomb structure, P_z orbital is taken into account for purpose of carriers' transmission between Carbon atoms. To keep calculation organized, atoms of unit cells are numbered as shown in Figure 2-3. Since only first nearest hopping parameter is taken into account, then in H_0 matrix, atom number 2 has only connection with atoms 1 and 3 (see the elements of H_0,

Figure 2-4). In the same way, all elements of Hamiltonian matrices are obtained. Having H_0, H_R, and H_L, $H(k)$ can be written as shown in

Figure 2-5, according to the equation (3). Now, in order to obtain band structure (E-K) diagram, k should be discretized and valued between $-\pi/a$ and π/a. Corresponding to each value of k, eigen values of matrix $H(k)$ could be simply extracted, which returns a set of energy values.

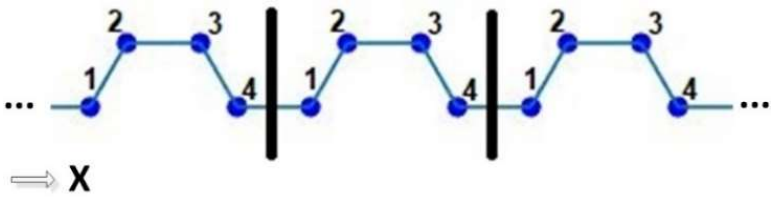

Figure 2-3: Schematic view of 2-AGNR.

Saving these sets of energy values and then drawing them versus *K*, gives the E-*K* diagram. Figure 2-6 shows the corresponding band structure of 2-AGNR. It's noteworthy that while number of atoms in unit cell increases, it is hard to fill out Hamiltonian arrays without having automatic assessment procedure. In this regard, one method could be assigning geometric position to the site of each atom. Next, relative distance between two atoms is calculated and based on that corresponding element of Hamiltonian is valued.

$$H0 = \begin{matrix} 0 & -2.65 & 0 & 0 \\ -2.65 & 0 & -2.65 & 0 \\ 0 & -2.65 & 0 & -2.65 \\ 0 & 0 & -2.65 & 0 \end{matrix}$$

$$HL = \begin{matrix} 0 & 0 & 0 & -2.65 \\ 0 & 0 & 0 & 0 \\ 0 & 0 & 0 & 0 \\ 0 & 0 & 0 & 0 \end{matrix}$$

$$HR = \begin{matrix} 0 & 0 & 0 & 0 \\ 0 & 0 & 0 & 0 \\ 0 & 0 & 0 & 0 \\ -2.65 & 0 & 0 & 0 \end{matrix}$$

Figure 2-4: H_0, H_L, and H_R for TB calculation regarding 2-AGNR.

$$H(k) = \begin{Bmatrix} 0 & -2.65 & 0 & -2.65e^{-ika} \\ -2.65 & 0 & -2.65 & 0 \\ 0 & -2.65 & 0 & -2.65 \\ 2.65e^{+ika} & 0 & -2.65 & 0 \end{Bmatrix}$$

Figure 2-5: *H(k)*, obtained by using *H0*, H_L, and H_R.

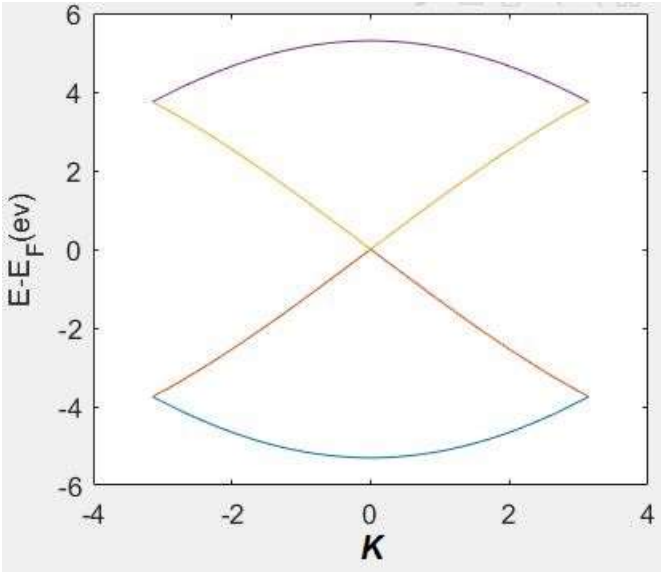

Figure 2-6: Band structure of 2-AGNR.

2-2 Non-Equilibrium Green Function (NEGF)

The non-equilibrium Greens function (NEGF) formalism provides a powerful conceptual and computational framework for treating quantum transport in nanodevices. It goes beyond the Landauer approach for ballistic, non-interacting electronics to include inelastic scattering and strong correlation effects at an atomistic level [77, 78]. Using TB, one can extract electronic properties of infinite lattices. However, once a finite lattice connected to leads (device) is under study, we need a theorem to model transmission and scattering mechanism of electron throughout the device. In this regard, Non-equilibrium Green's function has been widely used to explore transmission probability *T(E)*, local density of states (*LDOS*), and I-V curve of perfect or defected

GNRs and CNTs [23, 38, 77, 79-81]. NEGF provides ideal method for bottom-up device simulation because atomistic description of device allows easy implementation to new systems.

Device, as an open system, in simple picture, is built of channel region connected to source and drain contacts. Most importantly we are interested to know how our device conduct the carriers or in other words, we need to obtain I-V curve of the device. In simple picture, we can attribute fermi level for each contact μ_1 and μ_2. In our modeling we suppose that contacts are semi-infinite

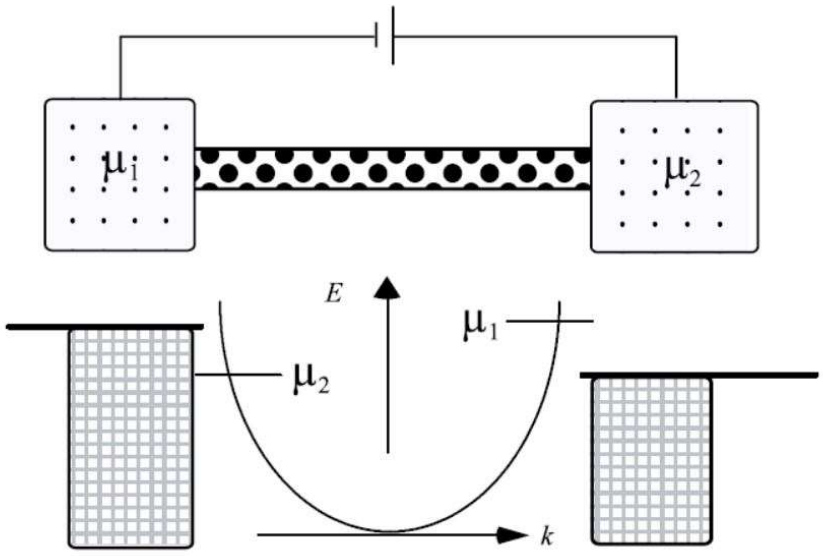

Figure 2-7: Device schematic with fermi levels upon applied bias voltage [78].

from the same material of channel region. Indeed, upon no bias voltage, fermi level is the same all over the device and there is no current flow. But, if voltage is applied to system fermi levels of source and drain is taken to new levels as shown in Figure 2-7. In this case, corresponding fermi functions can be described as below:

$$f_R = 1/(1 + \exp\left(\frac{E-\mu_2}{kT}\right))), \tag{4}$$

$$f_L = 1/(1 + \frac{\exp((E-(\mu_1+V))}{kT})), \tag{5}$$

V is the applied voltage, k is Boltzmann's constant and T is Kelvin's temperature which is set 300 **K** in ours modeling.

If we have the transmission probability of system over energy level nearby fermi level, then current value can be calculated as:

$$I_{LR} = \int_{-\infty}^{\infty} \frac{e}{h} T(E)\,(f_R - f_L)\,dE\ , \tag{6}$$

Notably, in the simulations, equations are solved numerically, hence, we need to discretize the voltage and energy levels. We still need a method to compute Transmission. But, beforehand, we need a technique to couple semi-infinite contacts to the channel to be able to describe the system, this is where NEGF formulism comes in. NEGF uses Green function $G(E)$ and Γ_L and Γ_R (the left and right broadening functions) to calculate Transmission, equations (7) and (8)

$$T\,(\mathrm{E}) = \mathrm{tranc}(\Gamma_L\,\mathrm{G}(\mathrm{E})\Gamma_R\,\mathrm{G}^*(\mathrm{E})), \tag{7}$$

$$\Gamma_{L,R} = i\,[\Sigma_{L,R} - \Sigma^*_{L,R}\,], \tag{8}$$

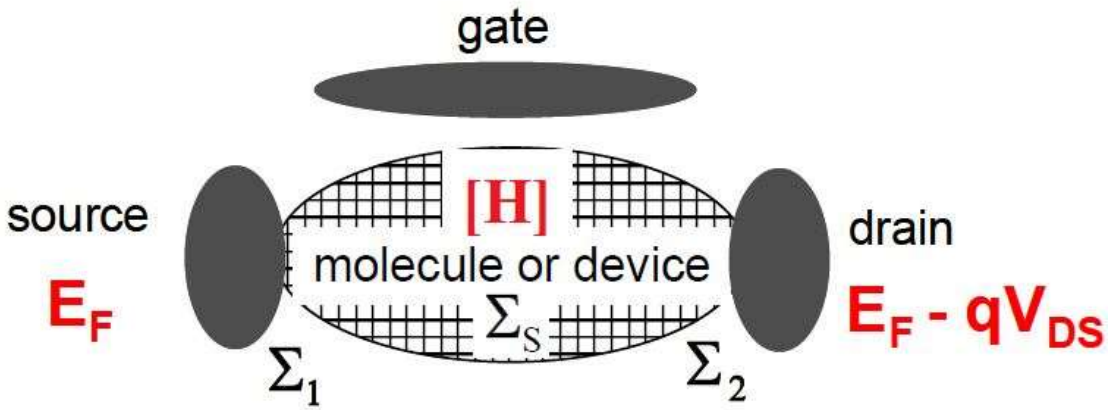

Figure 2-8: The quantities involved in the NEGF formalism [82].

According to NEGF, contacts are coupled with channel via self-energy matrices $\sum_L$ and $\sum_R$. Dissipative processes inside channel such as phonon scattering, or electron-phonon coupling are also modeled by $\sum_S$. In our modeling conductance is supposed to be ballistic and indeed $\sum_S = 0$. Thereby G(E) can be computed according to equation (9)

$$G(\mathrm{E}) = [(\mathrm{E} + \eta\,\mathrm{i}) \times \mathrm{I} - \mathrm{H} - \Sigma_L - \Sigma_R]^{-1}, \tag{9}$$

H is the Hamiltonian of the channel, calculated as explained in TB part. I is the unity matrix with the same size of H, and η is infinitesimally small quantity (1e-4 in our simulation).

In order to calculate Green and broadening functions, we still need to calculate self-energies. Self-energies can be computed according to equation (10), where g is surface Green function obtained through recursive calculations by mean of equation (11). As Figure 2-9 illustrates, τ is the relative connection (Hamiltonian) of the channel region to the surface atoms of contact. Notably τ should be formed in such a way that whole neighboring hopping connections at the surface of channel-contact are taken into account and also dimensions of self-energy matrix matches with dimension of G(E) and rest of formulism.

$$\Sigma = \tau g \tau^{+} \tag{10}$$

$$g = [(E + i\eta) \times I - \alpha - \beta^{+} g \beta]^{-1} \tag{11}$$

Surface green function (g) allows us to involve semi-infinite contacts in the calculation through iterative computations. In order to do that, limited number of atoms (orbital bases) at the channel-contact surface which contain whole neighboring transitions at the surface are selected. Then α becomes the Hamiltonian matrix of those limited number of atoms at the channel with respect to themselves, calculated alike H_0. In this scheme β, represents the relative Hamiltonian matrix of selected atoms at the channel to selected atoms at the contact, calculated alike $H_{L,R}$. Fist, g is given

an initial value and then throughout a loop this value is revaluated via equation (11). Recursive calculation is repeated until difference between new g and g from one step behind becomes negligible.

Also, if we are interested to calculate LDOS, in NEGF it is defined as below

$$LDOS(\mathrm{E},\mathrm{x},\mathrm{y}) = \frac{1}{2\pi} diag\left(\mathrm{G}(\mathrm{E})\Gamma_L\ \mathrm{G}^*(\mathrm{E}) + \mathrm{G}(\mathrm{E})\Gamma_R\ \mathrm{G}^*(\mathrm{E})\right), \tag{12}$$

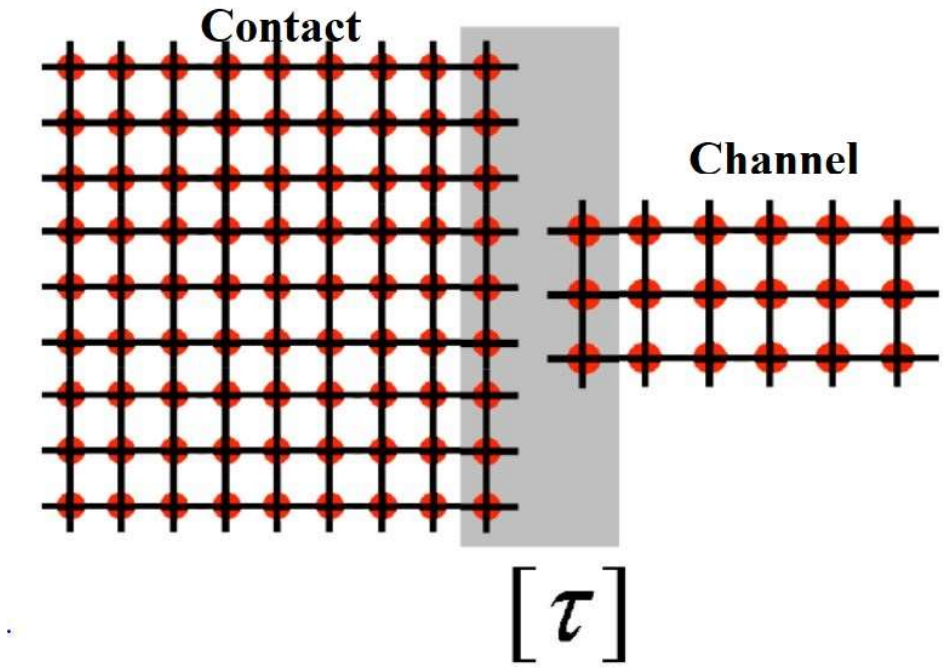

Figure 2-9: To involve semi-infinite contact in the NEGF, limited number of atoms at the channel-contact are chosen and self-energies are computed through iterative technique.

Band structure and transmission probability of an example device (Figure 2-10) have been depicted in Figure 2-11. It can be seen that transmission probability is in agreement with band structure, in which upon existence/removal of a sub-band, transmission increases/decreases over the same range of energy.

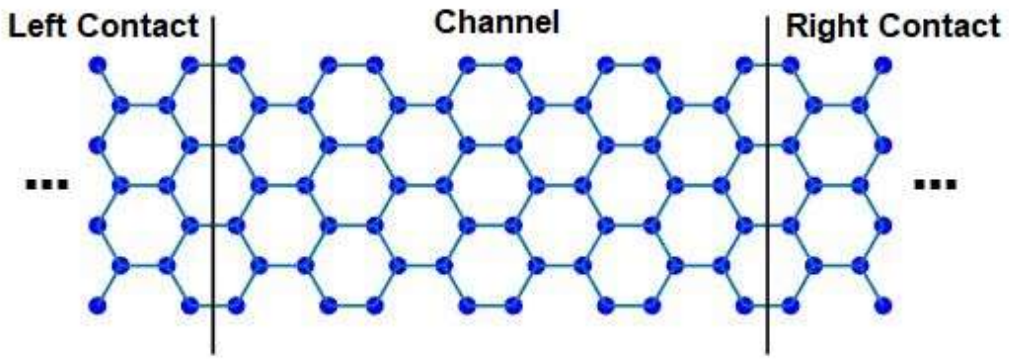

Figure 2-10: Schematic view of a device made of 7-AGNR.

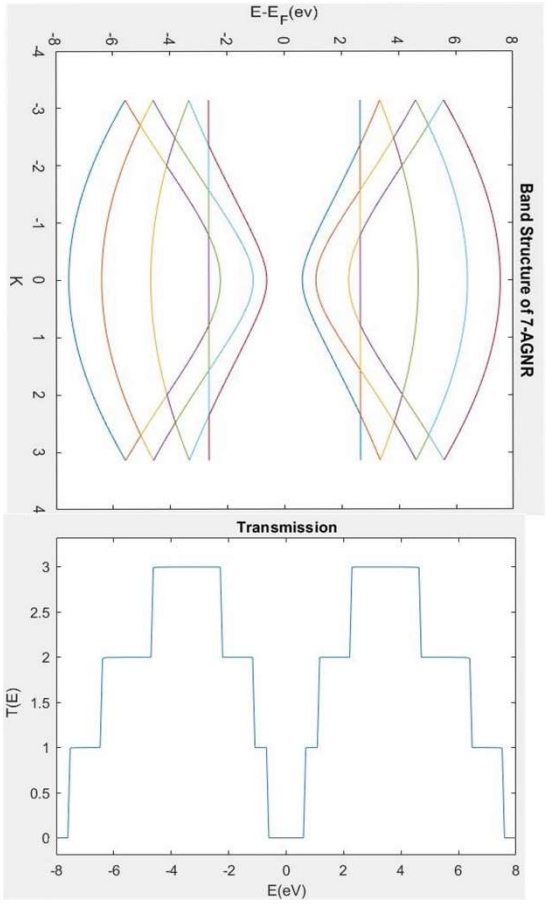

Figure 2-11: Band structure and transmission probability of 7-AGNR device shown in Figure 2-10.

2-3 Antidot and Boron/Nitride Doping

To create antidots, some Carbon atoms are removed from lattice and in case of doping, Boron/Nitride atoms are replaced in honeycomb structure. Figure 3-3 shows some schematic views of defected ACNTs, created by antidot and BN doping topologies. Such manipulated structure is called superlattice. The unit cell, as the smallest repeatable part of lattice, is now the smallest repeatable unit that contains the defect too, as depicted in Figure 3-3 .The corresponding on-site energies of Carbon, Boron, and Nitride atoms and first hopping interaction parameters are set according to Table 2-1 [81, 83]. It's noteworthy that Carbon atoms at the edges of GNR's and nearby vacancies of antidots are passivated by Hydrogen and thereby, C-H terminal is considered. This implies that the Carbon neighbor atoms at the edges have the same bonding distance as interior atoms, meaning hopping interaction parameters are the same everywhere. This assumption is important since it was shown that hopping parameter for edge atoms can increase up to 12% in lack of edge bond relaxation [84].

Table 2-1: Required TB parameters. All numbers are in eV unit.

ε_C	ε_B	ε_N	γ_{CC}	γ_{CB}	γ_{CN}	γ_{BN}
0.00	-2.76	1.64	-2.65	-2.25	-1.70	-2.40

2-4 Uniaxial Strain

Mechanical deformation can be modeled in strain format. There are two types of strain, shear and uniaxial [70, 85]. In this study uniaxial strain is implemented. Uniaxial strain can be induced in

form of stretching the structure (Figure 2-12-c, tensile) or compressing the structure (Figure 2-12-b, compressive). When lattice is deformed under uniaxial strain, location of atoms and length of carbon-carbon bonding alters. Indeed, hopping interaction parameters should be justified regarding new relative positions [86]. In the presence of uniaxial strain, first binding parameter *(ξ_r)* is verified as:

$$\zeta_r = (r_0/r)^2 \zeta_{r0}\left[1/\left(1+\exp(46(r/r_0-1))\right)+(r/r_0)^{4.3}\exp(4.3(1-r/r_0))/\left(1+\exp(46(r/r_0-1))\right)\right], \quad (13)$$

Where r_0 and r are the equilibrium distances between adjacent carbon atoms before and after applying strain, respectively. Using modified first binding parameter, Hamiltonian matrix for strained AGNRs is updated indeed.

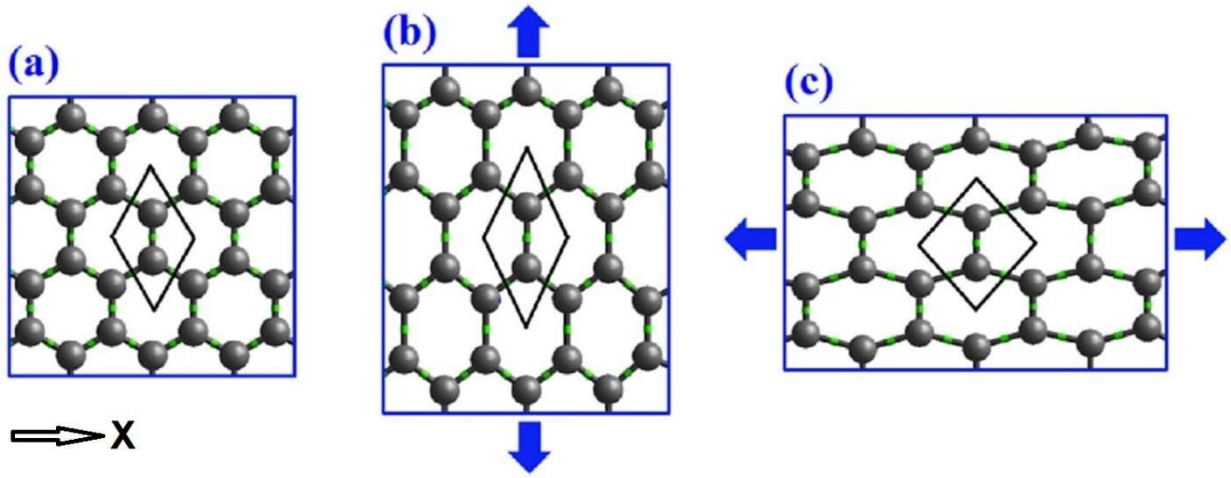

Figure 2-12:a) Unstrained, b) compressed, and c) stretched uniaxial honeycomb structure along X direction [53].

2-5 Conclusion

TB and NEGF theories are used to discover electronic and transport behavior of nanostructures in this thesis, respectively. In chapter 2, fundamentals of these methods were reviewed and details of

implementation on understudy honeycomb structures were elaborated. According to TB, Hamiltonian matrix is formed based on atomic orbital bases. Having Hamiltonian matrix, band structure of periodic system is extracted by computing eigen values over different values of K vector. Green function uses Hamiltonian matrix of device and by iterative self-consistent calculations involves role of contacts, letting us to model how carriers transport through device. The consequences of involving antidots, BN doping, and uniaxial strain to the modeling was also discussed in subchapters 2-3 and 2-4.

Chapter 3 Antidot/Doping and Graphene Allotropes (GNR, CNT)

3-1 Effects of Antidot and BN doping on the performance of GNR's

Although GNRs carry interesting electronic properties, additional flexibility to control fundamental characteristics like bang gap, it's always highly demanded. Thereby, many researches have been allocated to discover how properties of GNRs can be modulated by mean of antidot and/or doping defects [38, 54, 72, 87-92]. Moreover, defects, in particular single/multiple vacancies, may occur in GNR unintentionally. Regarding literature, there are numerous studies subjecting defected GNR under various profiles and conditions [38, 54, 72, 87-92]. This thesis has concentrated on periodical antidot and BN doping defect topologies which are caused intentionally. Hence, some of the most relevant studies are reviewed in the following.

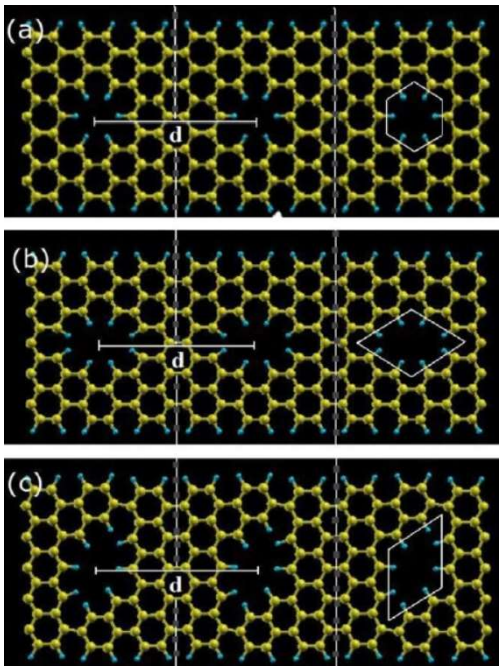

Figure 3-1: Schematic view of antidot periodic structure of AGNR [87].

A periodic structure of antidots on AGNR was introduced in [87] and [93] . Figure 3-1 shows the schematic of three antidot AGNR profiles. Unit cells are marked by dash lines and distance between adjacent defects are specified by *d*. Tian and colleagues found that periodic antidots alters band structure of pristine AGNR and band gap could become either smaller or larger depending on the family of AGNR and also on the proximity of adjacent antidots [93]. Similar results are observed in [87], plus the fact that a series of well-defined gap structures was found in conductance, Figure 3-2. This is function of geometrical structure of super unit cell and their relative distance. Presence of nanoholes within the body of nanoribbons leads to the new quantum confinements, equivalent to introduction of periodic potential barriers [93]. ZGNR is considered metallic under the nonmagnetic state and it preserve its metallic behavior even with the presence of periodic antidots [93].

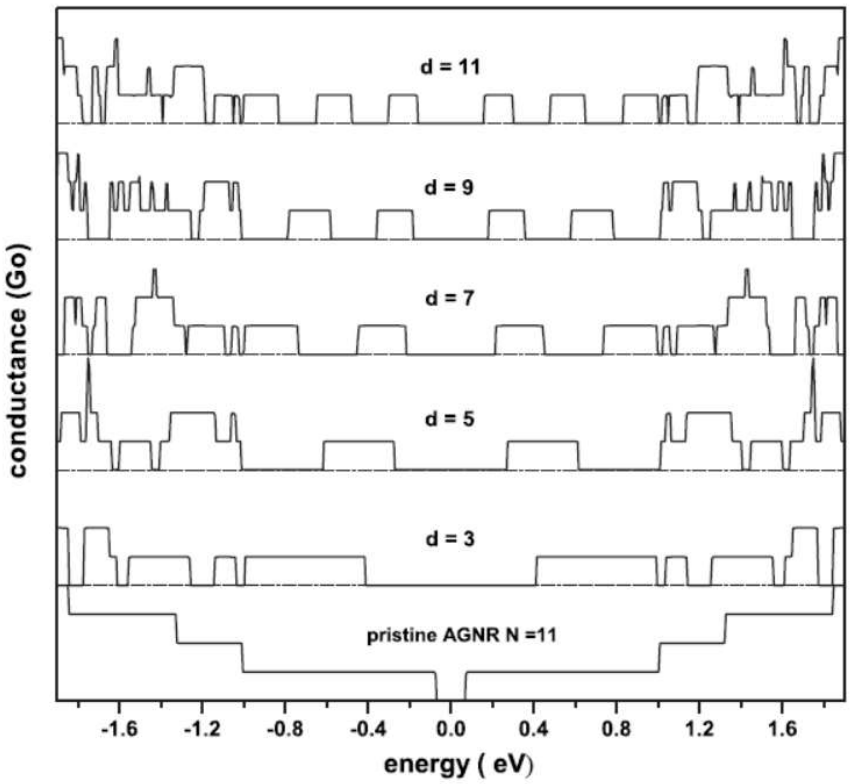

Figure 3-2: Conductance of antidote 11-ANGR as a function of *d*, distance between adjacent antidots [87].

The electronic properties of AGNR defected by Hexagonal antidots and BN doping was investigated in [38]. As illustrated in Figure 3-3 , antidot super lattice (ASL) AGNR and doped super lattice (DSL) AGNR are formed by imposing hexagonal topology to the center of pristine AGNR. Corresponding band structures for 11-AGNR are shown in Figure 3-4. Perfect 11-AGNR contains 0.14 eV band gap, while in spite of hexagonal antidot and BN defects it rises to 0.60 eV and 0.38 eV, respectively. Notably, energy states are rearranged and degeneration breaking occurs due to new quantum confinement. Compared to perfect AGNR, the intensity of variation is stronger in case of antidot compared to BN defects. Probably due to the fact that, antidots as the physical defects result in stronger back scattering mechanism compared to BN chemical doping. The energy band gap of intact and defected AGNR versus widths of ribbons is exhibited in Figure 3-5. It can be seen that, introduction of hexagonal defects to leads to band gap opening for *3P* and 3*P*+2 families of AGNR, whereas band gap decrement happens for 3*P*+1 [38].

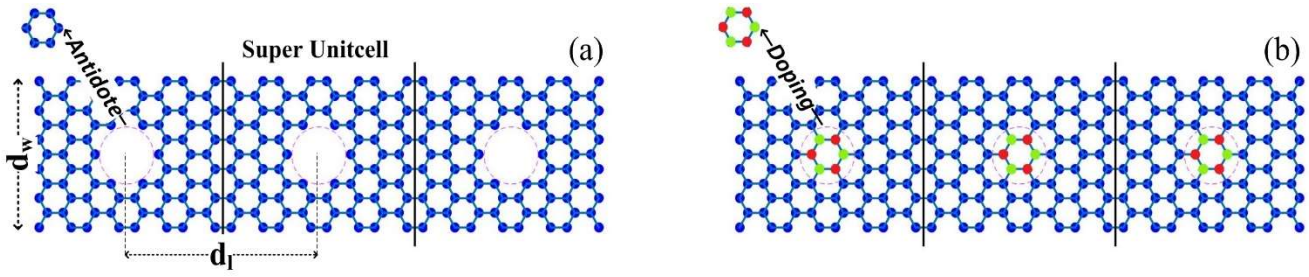

Figure 3-3: a) Antidot superlattice AGNR, b) Doped superlattice AGNR [38].

Corresponding transmission spectrums of AGNRs and defected counterparts are depicted in Figure 3-6 for different widths and families. In general, DSL-AGNRs propose higher transmission ratio, relatively more similar to the original transmission spectrum of perfect AGNR. It was also found that impacts of defects on the electronic and transport properties of AGNR reduce if the distance between defects and width of ribbon increase. As a result, one can implement antidot or BN defects properly to control properties of AGNRs [38].

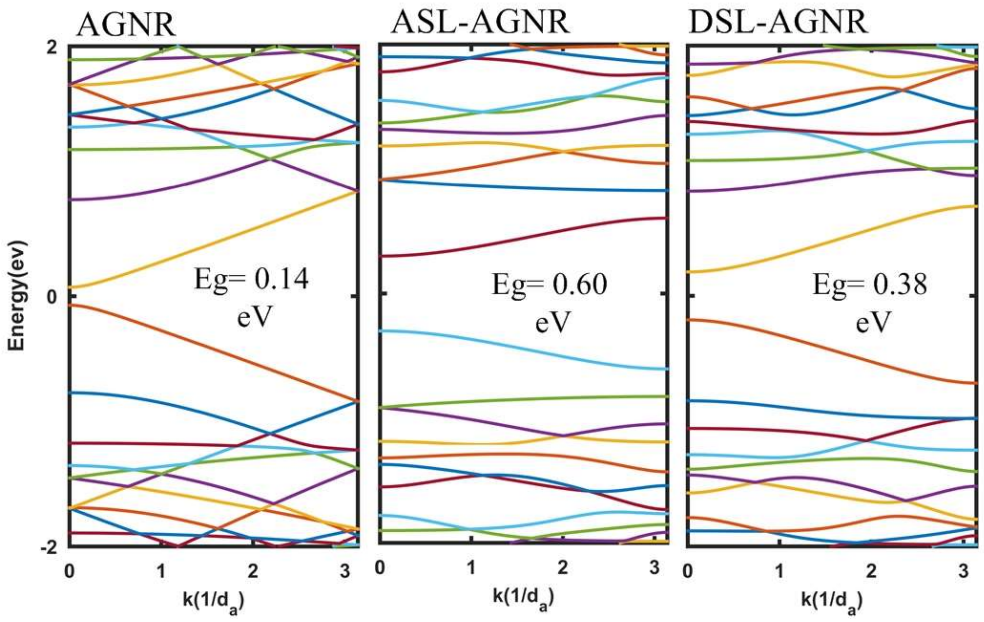

Figure 3-4: Electronic band structure of perfect AGNR and defected AGNR [38].

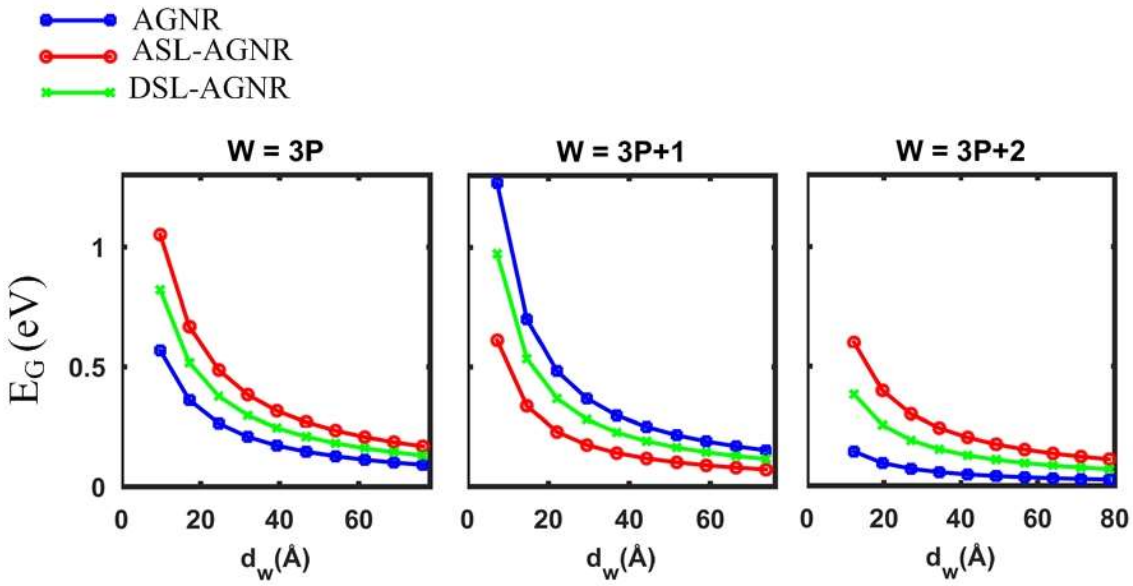

Figure 3-5: Energy band gap of perfect AGNR and defected AGNR [38].

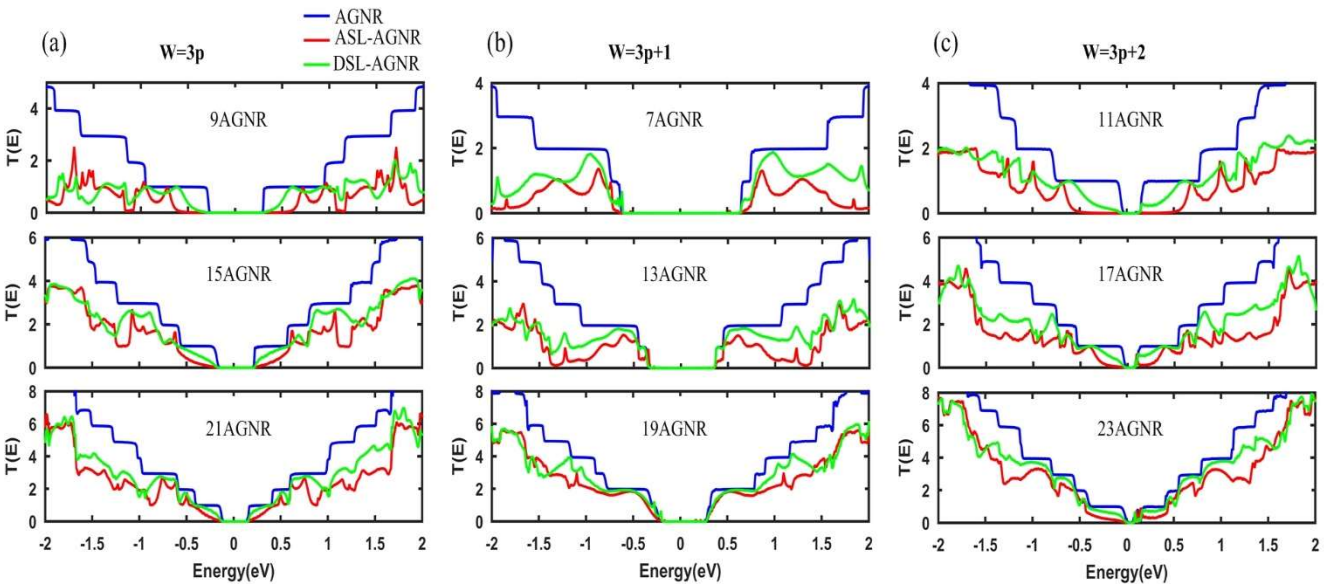

Figure 3-6: Transmission probability of perfect AGNR and defected AGNR [38].

3-2 Effects of Antidot and BN doping on the performance of CNT's

3-2-1 Prologue

Electronic properties of CNTs are specified by their radius and chirality [2, 42, 43]. Based on these geometrical factors, CNTs demonstrate various electrical conductivity behavior, from metallic to semiconducting. Since CNTs have exhibited novel electronic and transport properties, they have been studied for a wide range of application including nano-electronic devices and chemical sensors [2, 30, 94, 95].

However, experimental observations show that the properties of CNTs vary with the addition of defects [35, 37, 50, 51, 58, 96]. The presence of defects such as vacancies or adsorption of molecules influence physical and chemical characteristics of CNTs. For instance, it was studied that the presence of single vacancy or even small vacancy clusters can reduce the tensile strength

and critical strain of tubes [36, 51, 97, 98]. Operation mechanism of nano-electronic devices and sensors underlies on the electronic properties such as band gap size which could markedly change if defects are caused at the body of CNTs [34, 35]. CNTs can be considered as the quasi one-dimensional nanostructures and therefore small and even limited number of topological defects or molecule adsorbates can cause remarkable variations in their properties. Indeed, it is critical to explore how topological defects impact the characteristics of CNTs. A number of studies were conducted in this regard [34-37, 39, 51, 52, 98, 99] and, in particular, Charlier [35] reported that defects such as pentagons or heptagons vacancies or dopant can modify the electronic properties of CNTs. It was discussed that defects can be proposed as an interesting way to tailor intrinsic properties of tubes and thereby building novel nano-devices. In other research, it was studied that adsorption of single molecules like NO2, NH2, H, COOH, OH by metallic CNT, leads to suppression of one of two available transport channel around Fermi level [98]. It was also shown that arbitrary number of molecules could be adsorbed on the CNT sidewall while full open channel transport is preserved. This depends on the sub-lattice of adsorption and relative positions of molecules.

Electronic and transport properties of Armchair CNT's (ACNT's) upon the presence of periodic bi-site perturbation was investigated by Hashemi and colleagues [100]. It was demonstrated that by the repetition of small Hydrogen clusters on ACNT, it turns from metallic to semiconducting. It was shown that, the strength of variations depends on number, strength, and distance of defect clusters along the CNT.

Despite theoretical studies about the role of patterned defects in the body of nanostructures alike AGNR, this question may come to mind whether there is any possibility to create such patterned defects in a controlled way or not? Although it is quite imaginable that technological advancements will reach the point to conveniently examine such theoretical researches, however, to date, there are some evidences of precise controlled techniques of doping and causing vacancies [29, 54, 60, 101]. Kawai and colleagues demonstrated atomically substitution mechanisms of boron doping atoms in GNRs with the widths of N=7,14, and 21 [60]. In other work, it was shown how individual

vacancies in CNTs can be caused by mean of 1 $\mathring{A}$ diameter electron beam, meaning that it is possible to impose controlled atomic-scale topological defects to the nanostructure systems [101].

In this sub-chapter, two different topologies of antidot and BN doping are imposed throughout the length of zigzag Carbon nanotubes (ZCNTs) periodically. Using Tight Binding (TB) model combined with non-equilibrium Green's function (NEGF) model, electronic and transport properties of these modulated ZCNTs are explored. It is found that, creation of periodical defects changes electronic and transport properties of perfect CNTs in which the extent of variation depends on some factors such as: the shape of topologies, kind of defects, and dimensional parameters. Role of each of these parameters are examined and analyzed. Furthermore, based on the obtained results new platforms of ZCNT resonant tunneling diode (RTD) by mean of periodic defects are proposed. The analysis in depth shows that expected behavior of RTD device such as negative differential resistance (NDR) and resonance in transmission spectra are verified for such RTD platforms.

3-2-2 Periodically defected ZCNT platform

Electronic properties of single wall CNTs (SWCNTs) including band gap size depend on the diameter of tube (radius) and the way it is folded (chirality) [30, 35, 42]. Chirality of CNTs is identified by two integer numbers *(n,m)*. Depending on the relative value of *n* and *m*, CNTs have different band gap size and electronic characteristics. Technically, CNTs with m=0 are so-called ZCNTs and the armchair CNTs (ACNT) are attributed to those ones with n=m.

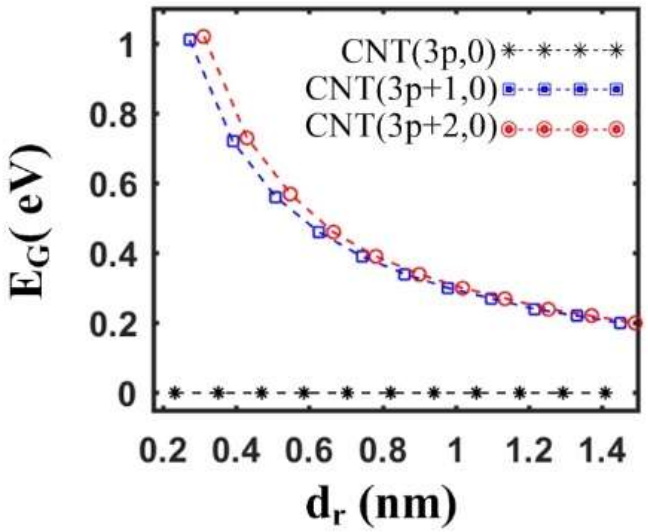

Figure 3-7: Band gap of ZCNTs versus radius.

In the present work, ZCNTs are considered. Figure 3-7 shows the band gap size of ZCNTs with different values of n versus different radius (d_r), ranging from smaller than 0.3 nm to over 1.4 nm. The ZCNTs can be classified in three categories, namely n=3p, n=3p+1, and n=3p+2 while p is an integer number. According to this classification, the category n=3p is metallic and has no band gap size. Two other categories have remarkable band gap size and while larger diameter of them are selected their band gap size declines toward zero value. Although there is no much difference between categories n=3p+1 and n=3p+2 in terms of band gap size, it will be shown that this classification brings some insights where new electronic and transport properties of defected ZCNTs are calculated.

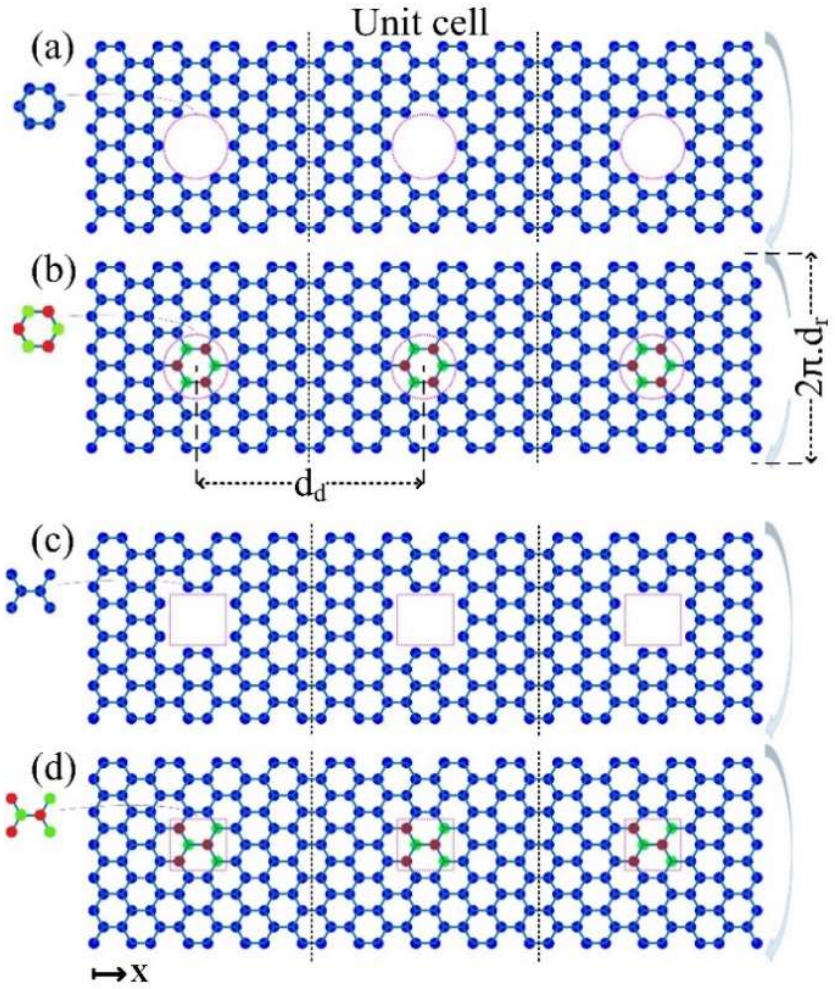

Figure 3-8: Schematic view of defected ZCNTs (6,0). (a) Antidot ZCNT topology 1, (b) BN doping ZCNT topology 1, (c) antidot ZCNT topology 2, (d) BN doping ZCNT topology 2.

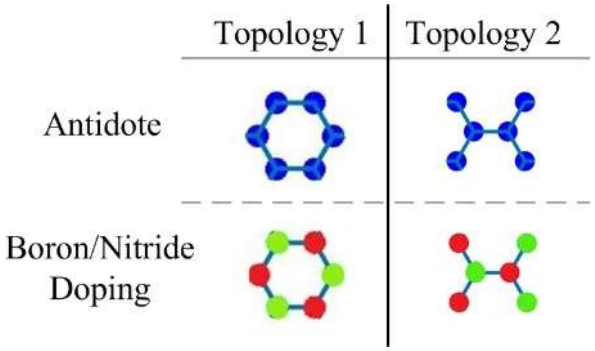

Figure 3-9: Different topologies and kinds of defects. Blue, red, and green circles represent Carbon, Nitride, and Boron atoms, respectively.

Schematic view of defected ZCNTs (6,0) are illustrated in Figure 3-8. Two types of topologies and two kind of defects (antidot (physical) and BN doping (chemical)) are implemented. Defects are imposed throughout the length of tubes in a periodical format. For the sake of convenient illustration, unwrapped views of tubes are drawn. Noteworthy, tubes are infinite, however, in the figure just three unit cells of each case are shown. The radius of tubes and the distance between adjacent defects are denoted by d_r and d_d, respectively. Super unit cell of periodically defected tubes can be identified as the one specified between dotted black lines in Figure 3-8.

3-2-3 Electronic and Transport Properties of Defected ZCNTs

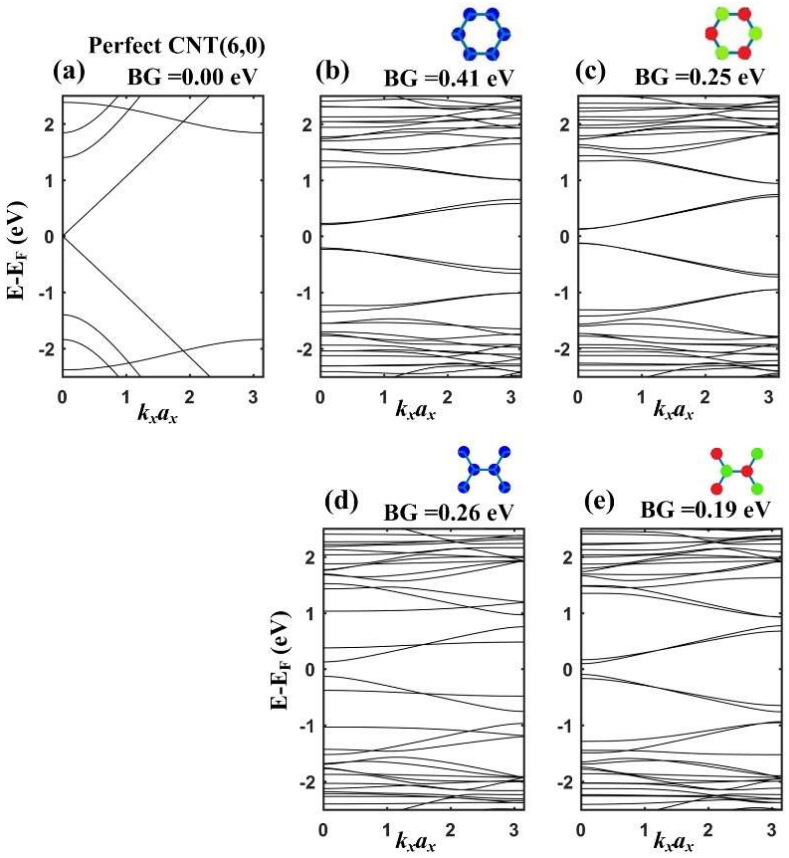

Figure 3-10: (a) Band structure of perfect CNT (6, 0) and (b-e) band structures of defected CNTs.

Properties of CNTs are sensitive to the presence of defects because of their quasi one-dimensional nature [35, 37, 51, 99]. Indeed, it is predicted that, if defects could be created along the length of tubes in a controlled pattern, new tunable electronic properties would be resulted.

The band structure of perfect and defected tubes *(n=6, m=0)* are represented in . Radius of tubes *(d_r)* and distance between defects *(d_d)* are 0.23 and 0.17 nm, respectively. One can notice that perfect ZCNT(6,0) is gapless as illustrated in -a, however, the presence of defects changes the pristine band structure and thereby a modified band gap size is achieved. Considerably, metallic characteristic of perfect ZCNT(6,0) turns to semiconducting in all cases, although the obtained band gap sizes are at different levels depending on the topology and kind of defects. Therefore, the band gap size of ZCNTs can be tuned if proper topology and defects with specified dimensions are introduced into the tubes.

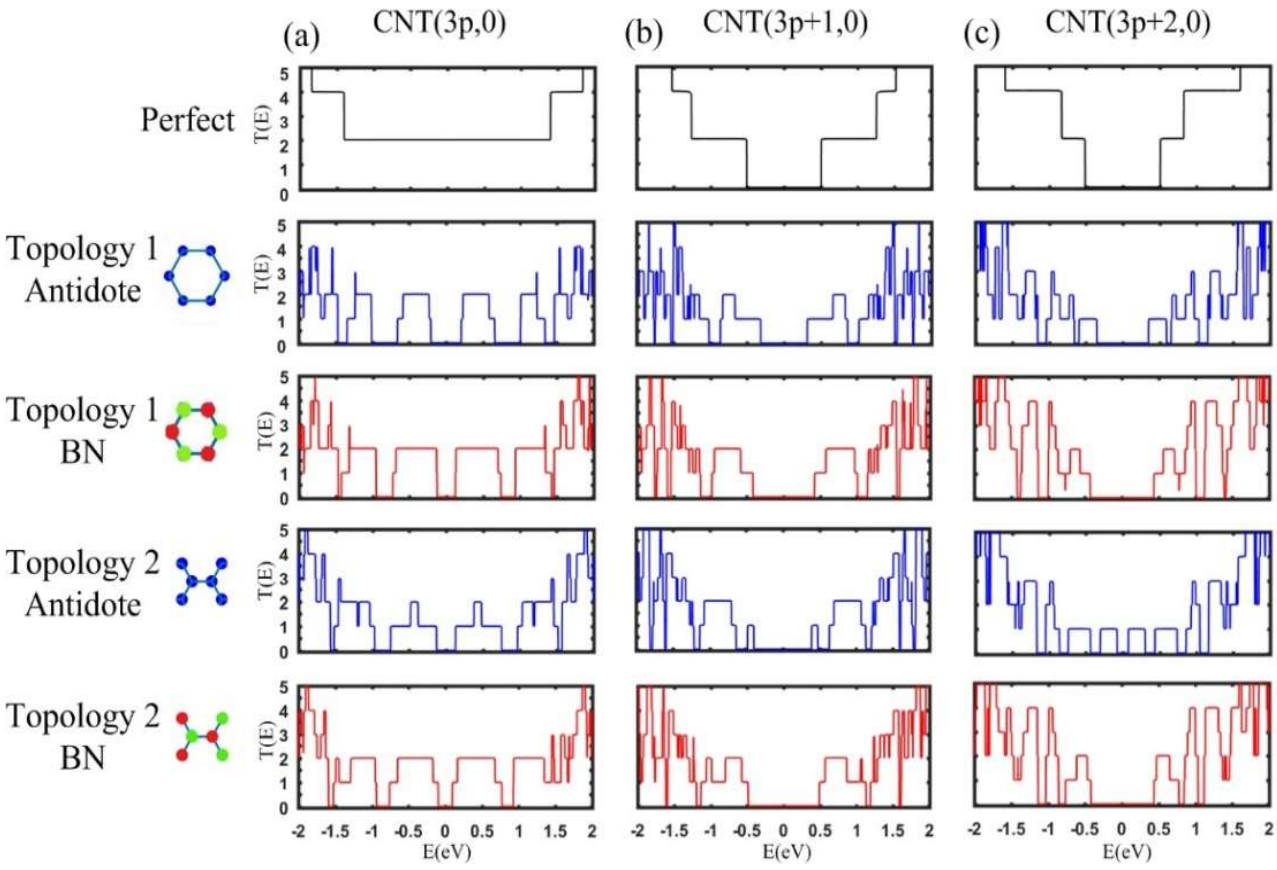

Figure 3-11: Transmission probabilities of perfect and defected ZCNTs.

In addition, transmission probability and local density of states (LDOSs) of perfect and defected ZCNTs are displayed in

Figure 3-11 and Figure 3-12, respectively. Corresponding diagrams for different topologies and kinds of defects are presented in these figures. For all cases dd is 0.17 nm and radii of the categories 3p (ZCNT(6,0)), 3p+1 (ZCNT(7,0)), and 3p+2 (ZCNT(8,0)) are set to 0.23 nm, 0.27 nm, and 0.31 nm, respectively.

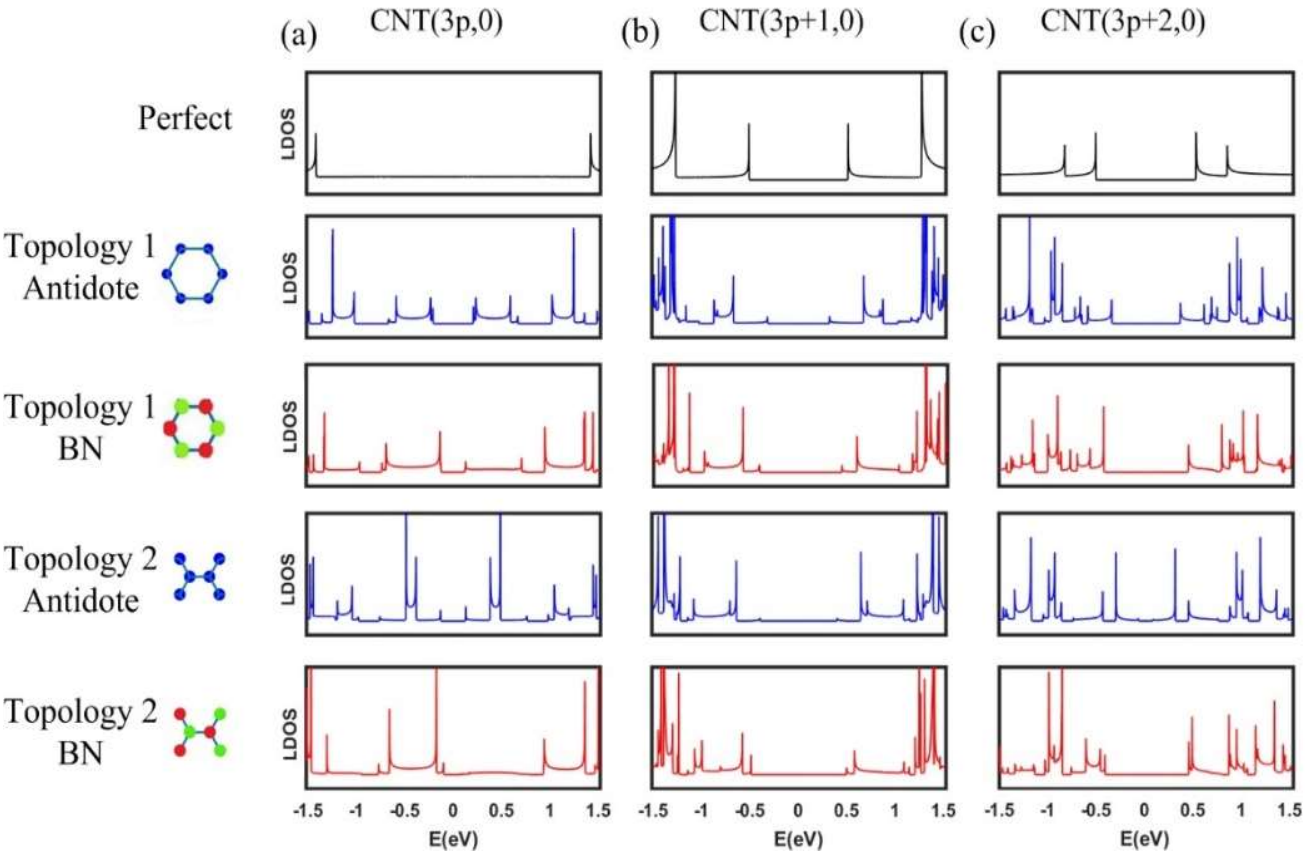

Figure 3-12: Local density of states (LDOSs) of perfect and defected ZCNTs.

Presence of defects in the ZCNTs, impacts on the properties of wave function in the structure, leading to the alternation of whole energy band structure, as demonstrated in . Transmission probability and LDOSs diagrams of defected ZCNTs indicate the same results. Regarding

Figure 3-11 and Figure 3-12, one can observe apparition of the energy gaps and also available electronic states in defected tubes. In fact, introducing defects to ZCNTs modulate the quantum confinement of tubes and, indeed, the energy dispersion of the systems changes completely. Upon the presence of defects, mini bands and mini gaps appear in the transmission probability diagrams, especially for low energies around the Fermi level. In other words, transmission is suppressed for some energy regions and localized energy states occur. These consequences are pretty similar to the case of multi barrier systems in which quantum interference mechanisms lead to the apparition of mini bands and mini gaps through the transmission spectra. Thus, defects in ZCNTs could be considered equivalent to the introduction of periodic potential barriers.

Imposing defects and, in particular, antidot topologies to GNRs also results in new quantum confinement and thereby new electronic and transport properties are achieved [72, 87, 92, 93]. However, as investigated before, the novel obtained properties depend on the geometry of defects and also the edge (zigzag or armchair) of GNRs. Actually, the quantum confinement of defected GNRs is the function of edge shape of ribbon and also the shape of defects [87, 93]. In this scheme, there is no such edges for ZCNTs, hence, it could be expressed that introducing defects to ZCNTs is more effective way of band gap tuning compared to the case of GNRs.

3-2-4 Band Gap Size of Defected ZCNTs as a Function of Tube's Radius

In this part, defects are introduced onto different categories of ZCNT while radius of tubes (d_r) are scaled to different values. Using TB model, the band gap sizes of perfect and defected tubes are

calculated and compared, as shown in Figure 3-13. Band gap sizes of perfect, antidot, and BN doped CNTs are depicted by black dashed lines, square blue dashed lines, and circle red dashed lines, respectively. Also, the distance between adjacent defects is kept constant in all cases, which is equal to 0.17 nm.

It is evident from Figure 3-13 that the perfect *3p* category of ZCNT is metallic, but introducing defects, either antidot or BN, results in remarkable band gap opening. It demonstrates that metallic behavior of ZCNTs are converted to semiconducting having via using either antidot or BN doped periodical defects. Considering categories $3p+1$ and $3p+2$, either antidot or BN doping of topology 1 leads to decrement in the band gap size (with increasing radius d_r), whereas topology 2 causes distinct results to some extent. Category $3p+2$ experiences reduction in its band gap size for both antidot and BN doping of topology 2, but reduction level for antidot is more intense and tubes are converted to semi-metal. It is noticeable that the defects of topology 2 cause small changes in the band gap size of category $3p+1$, almost in all cases.

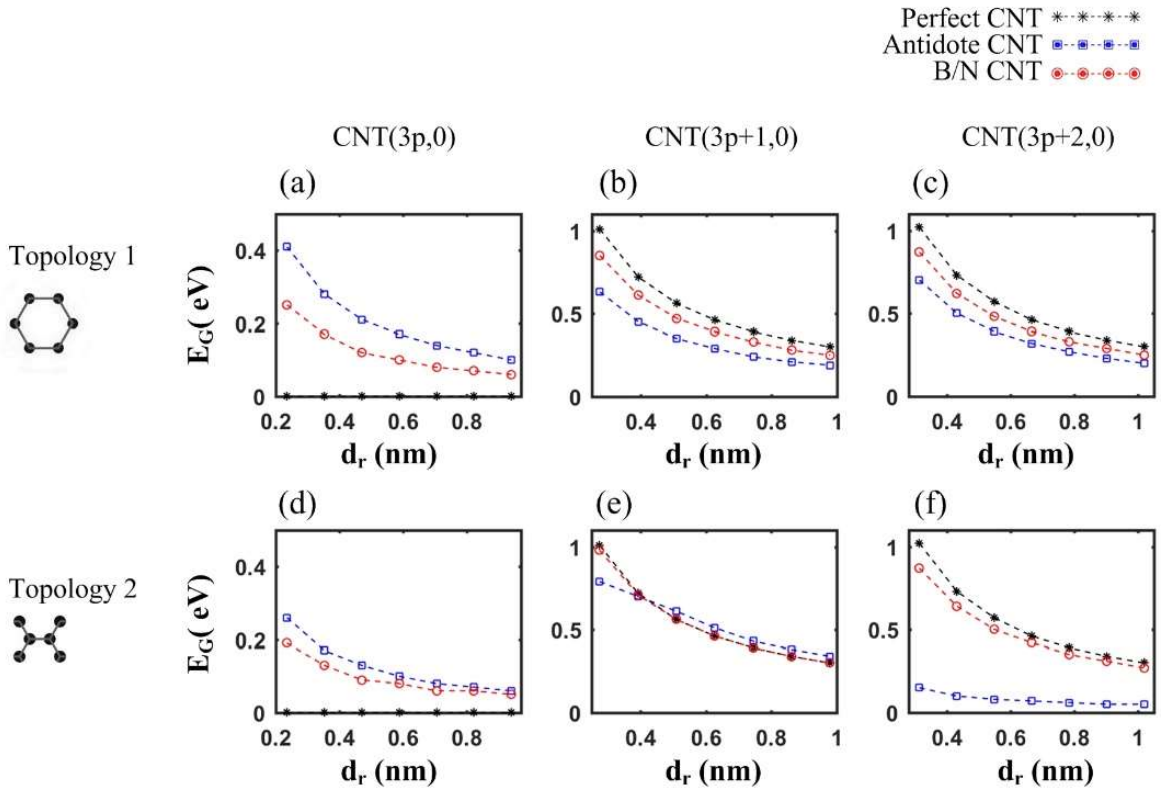

Figure 3-13: Band gap size of different topologies and categories of ZCNTs versus radii (d_r).

In general, as the diameter (radius) of tubes grows, the difference between the intrinsic and defected band gap size of ZCNTs reduces and the effects of defects are diminished. This implies that ZCNTs with larger sizes are less sensitive to the appearance of defects in their structure. Lastly, it is notable that, antidot defects have more intense impacts on the band gap size of ZCNTs compared to that of BN doped defects.

3-2-5 Band Gap Size of Defected ZCNTs as a Function of Defects' Distance

Like previous part, the antidot and BN doping topologies 1 and 2 are imposed to three categories of ZCNTs while distance between adjacent defects *(d_d)* is scaled between 0.8 and 8.5 nm. Band gap size of perfect and defected tubes versus d_d are plotted in Figure 3-14. The radius sizes of categories 3*p* (ZCNT(6,0)), 3*p*+1 (ZCNT(7,0)), and 3*p*+2 (ZCNT(8,0)) for these simulations are 0.23 nm, 0.27 nm, and 0.31 nm, respectively.

Considering Category 3*p*, presence of defects results in the band gap opening, however, antidot defects have stronger effects and higher band gap size is fulfilled. For categories 3*p*+1 and 3*p*+2, decrement in terms of band gap size is observed regardless of topology (1 or 2) and kind of defects. In general, BN doping of defects affects intrinsic band gap size of perfect ZCNT in shallower degrees. In addition, the relative difference between band gap sizes of perfect and defected tubes is larger when the defects are closer to each other along the tube's length.

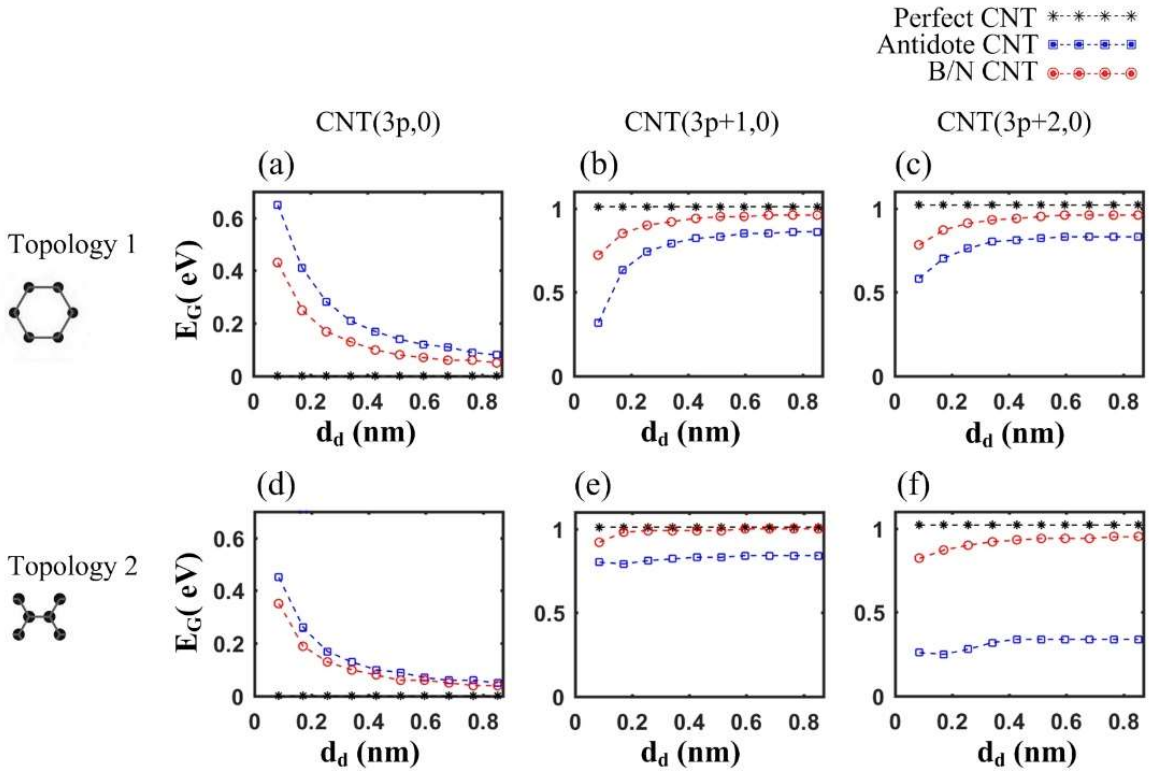

Figure 3-14: Band gap size of different topologies and categories of ZCNTs versus distance between adjacent defects (d_d).

3-3 Conclusion

It was reviewed that introducing both topologies of antidotes and BN doping atoms to the middle of AGNRs lead to the formation of new quantum confinements. In general, electronic structure, in particular band gap size, and transport properties of periodic doped AGNR is relatively closer to that of pristine AGNR, compared to periodic antidot AGNR. It was also reported that if dimensions of defected AGNRs (d_w and d_l) are increased, the quantum confinements of defected AGNRs become more similar to quantum confinements of pristine AGNRs. As a result, if the dimensions of ribbons are enhanced, the effects of defects on the electronic properties of AGNRs disappear gradually.

In addition, electronic and transport properties of periodically defected ZCNTs were investigated in subchapter 3-2. Our calculations showed that electronic and transport properties of ZCNTs alter markedly upon the presence of both antidote and BN doping. When defects are placed throughout tubes in periodical format, they could be considered as the potential barriers leading to the new quantum confinement. Consequently, a number of mini bands and mini gaps appear in the transmission spectra, which are mostly near the Fermi energy level. In other words, conductive channels contributing to transmission are suppressed in some energy levels.

Furthermore, defects in ZCNTs results in rearrangement of energy states and thereby new band gap sizes are achieved. While defects are imposed to ZCNTs, metallic category of ZCNTs ($3p$) turns to semiconducting and band gap opening happens. On the contrary, for the two other categories ($3p+1$ and $3p+2$), with increasing radii of ZCNTs, decrement in terms of band gap size occurs in most of the cases. In general, BN doping defects change intrinsic band gap size of perfect ZCNTs in shallower degrees in comparison with antidot defects. Moreover, the impacts of defects diminish by increasing tube radius and the secondary band gap sizes become closer to that of defect-free ZCNTs.

Chapter 4 GNR/CNT RTD devices made of Antidot/doping defects

4-1 GNR RTD device by mean of antidots and/or BN doping

Design of RTD device by mean of GNRs, have been subject of many investigations in recent years [61, 81, 102-109]. AGNRs contain width tunable band gap, which makes them ideal for building DBQW structure by using thinner ribbons at the barrier regions. Taking this advantage, width-modified AGNR RTDs have been designed and studied in [61, 105]. Some studies revealed that special formats of BN doping can lead to appearance of NDR behavior on AGNRs as well.

As discussed on section (3-1), imposing hexagonal antidot/BN defects to the AGNR results in the new quantum confinement, rearrangement of sub-bands, and importantly band gap variation [38, 72]. This implies that upon selecting proper defect geometry and dimensions, electronic properties of pristine AGNR can be modulated in very good extend. This feature has been utilized in [81] to design defect-based AGNR RTD device, shown in Figure 4-1. Barrier regions are made of defected ribbons, while other parts remain intact. Such platforms lead to the formation of DBQW structure due to modified band energy of barrier regions.

Figure 4-2 illustrates transmission probability and I-V characteristic of all three hexagonal antidot, hexagonal BN and, compound defect AGNR RTD platforms. NDR behavior is recorded for all cases, but with different intensity. BN doping presents the slightest performance regarding the fact that BN doping has least effect on the original band structure of AGNRs [81].

The role of dimensional parameters including lengths of channel (d_{ch}), barriers (d_b), and distance between antidots (d_a) on the performance of antidot AGNR RTD was investigated in-depth. While dimensional factors manifest direct impact on the V_{Peak} and I_{Peak}, noticeably PVR rises over increasing d_{ch}, and d_b [81].

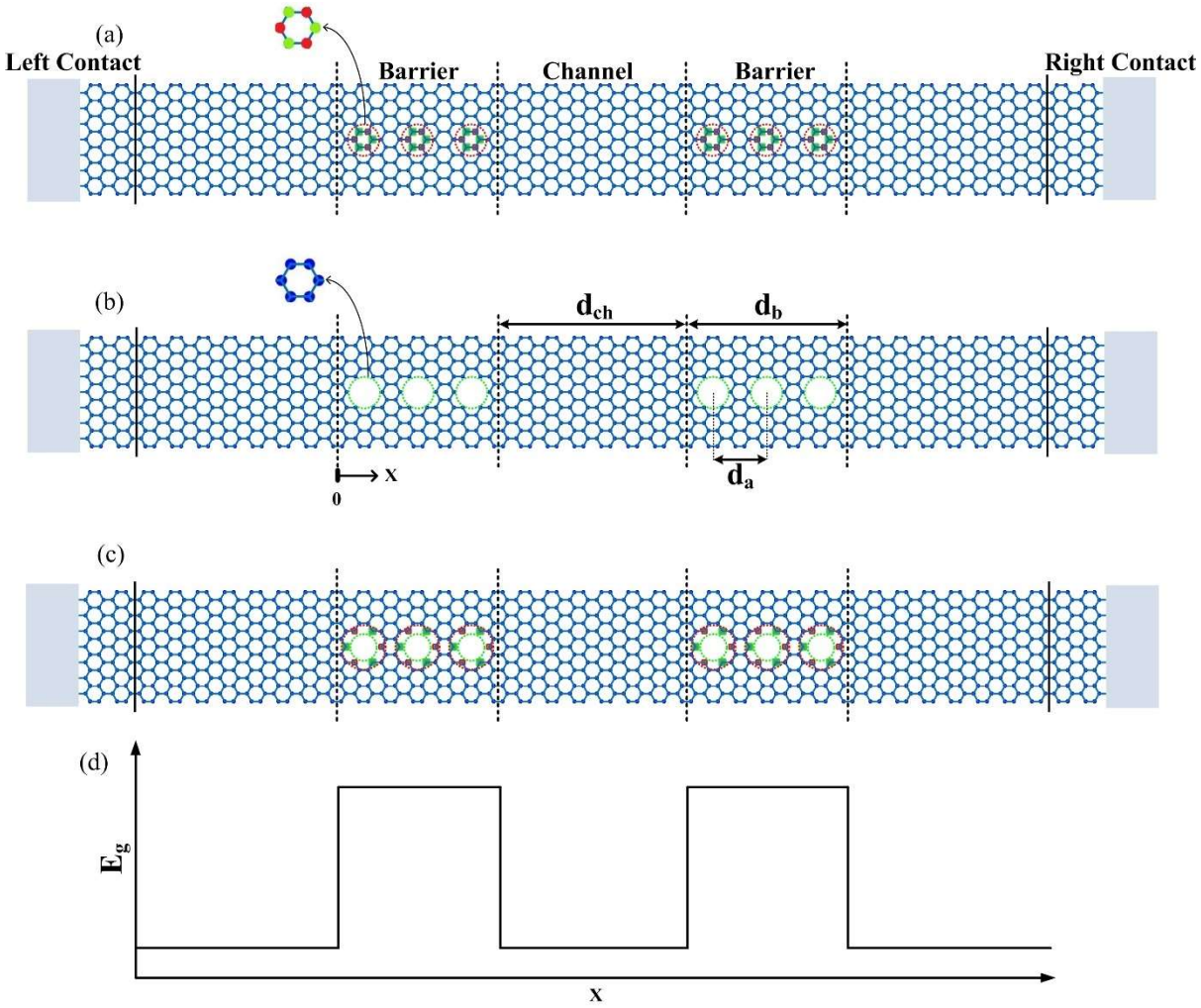

Figure 4-1: AGNR RTD by mean of a) BN doping, b) antidot, and c) compound defects [81].

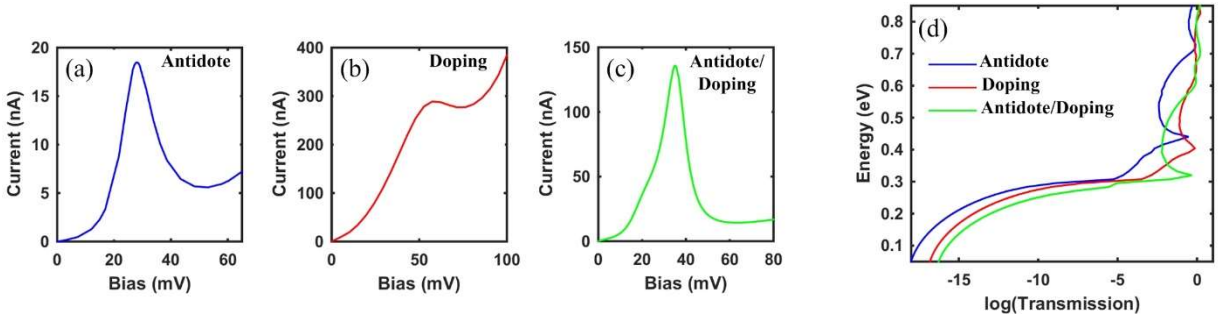

Figure 4-2: I-V characteristics and transmission probability of defect-based AGNR RTD [81].

4-2 CNT RTD device by mean of antidots and/or BN doping

4-2-1 ZCNT RTD by mean of patterned defects

So far, it has been demonstrated that electronic properties, in particular the band gap size, of ZCNTs are modified if patterned defects are caused in the body of tubes. This implies that patterned defects can be utilized to manipulate intrinsic electronic properties in such a way that novel platforms of electronic devices could be achieved. In this part, patterned defects are implemented to design defect-based platform of ZCNT RTDs.

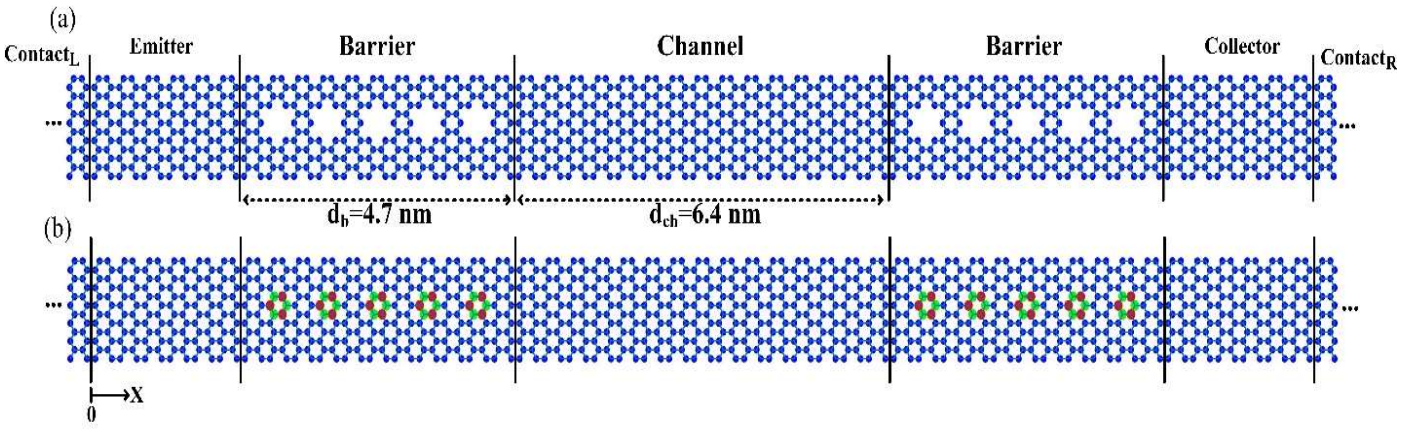

Figure 4-3: Defect-based ZCNT RTD platforms.

Figure 4-3 exhibits two samples of defect-based ZCNT RTD, a) antidot ZCNT(6,0) RTD, and b) BN ZCNT(6,0) RTD. As shown, hexagonal topology of antidot (Figure 4-3-a) and BN doping (Figure 4-3-b) are imposed to the barrier regions while other regions are made of perfect ZCNT (6,0). ZCNT(6,0) is metallic with no band gap size, but upon the presence of periodic hexagonal antidote and BN doping, its properties turn into semiconducting with a significant band gap, as illustrated previously. Indeed, such platforms of Figure 4-3 could result in the formation of double

barrier quantum well (DBQW) and apparition of quantized energy states within quantum well (channel).

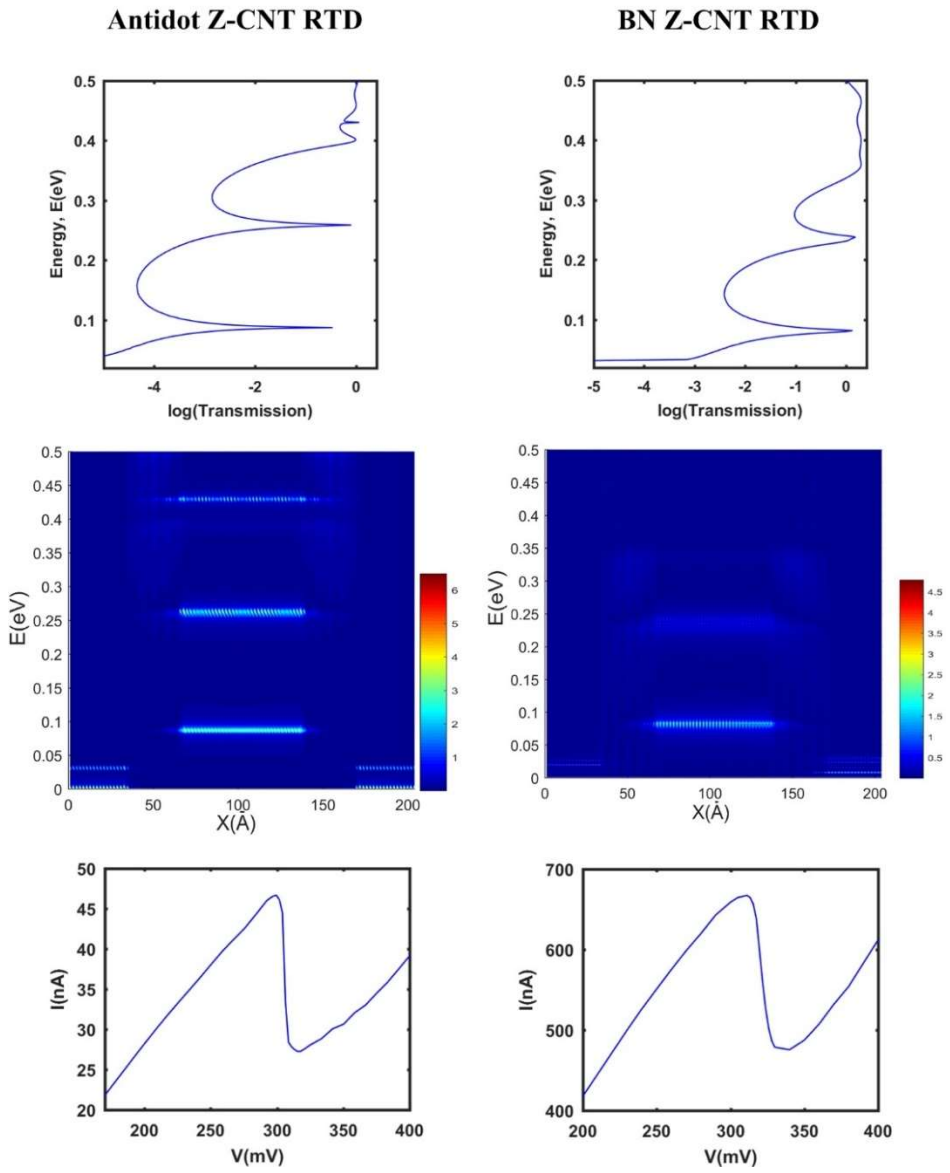

Figure 4-4: Transmission probability, LDOSy(E,x) (blue plots), and I-V characteristics of antidot ZCNT(6,0) RTD (left column) and BN ZCNT(6,0) RTD (right column).

Transmission probability, LDOSy(E,x) which sums LDOSy(E,y,x) over y-axis, and I-V characteristics of antidot ZCNT(6,0) RTD and BN ZCNT(6,0) RTD are evaluated via NEGF method and are exhibited in Figure 4-4. The transmission probability for both platforms resonates in which first and second peaks are quite apparent. However, the resonances of transmission probability for antidot ZCNT(6,0) RTD are more intense which can be attributed to stronger back scattering effect of antidots compared to that of BN doping atoms. Regarding LDOSy(E,x) plots (blue plots), one can see that quantized energy states at the same energy of transmission peaks occurs within the channel region. This picture is in agreement with DBQW structure in which quantized energy state within the quantum well contribute to highest transmission due to tunneling phenomenon.

Once bias voltage is applied to the understudy platforms, NDR behavior, which is expected from a RTD device, is obtained, (as shown in Figure 4-4). The first peak and valley points for both platforms happens within a very narrow voltage difference. Plus, peak to valley ratio (PVR) stands at 1.67 and 1.48 for antidot ZCNT(6,0) RTD and BN ZCNT(6,0) RTD, respectively. These values are close and thus, it would be concluded that both platforms lead to more and less similar performance, although it should be noticed that current level of BN ZCNT(6,0) RTD is more than one order of magnitude higher than antidot ZCNT(6,0) RTD.

4-3 Conclusion

It was reviewed that how AGNR RTD can be established by mean of antidote and BN doping topologies. Modulated structures for creating AGNR-RTD were formed by inserting antidote, BN doping, and combination of antidote and BN doping at the middle of pristine AGNRs without varying the width of ribbons. I-V curves showed NDR property for all types of modulated AGNR-RTDs and in-depth study revealed efficiency of such device is function of dimensional parameters, as well as, type of defect and utilized topology.

Furthermore, using the point that intrinsic properties of ZCNT can be tuned upon the presence of periodic defects (subchapter 3-2), new platforms of defect-based ZCNT RTD were designed and their performances were evaluated (subchapter 4-2). Resonances in transmission probability and formation of quantized energy states for both antidot ZCNT(6,0) RTD and BN ZCNT(6,0) RTD were recorded. Plus, NDR behavior was observed when bias voltage was applied to such devices. As a result, it was demonstrated that patterned defects can be utilized to design novel electronic devices.

Chapter 5 Uniaxial Strain and Graphene Nanoribbon

5-1 Effects of Uniaxial Strain on the performance of GNR's

Silicon electronic industry has used strain deformation extensively to empower and control performance of electronic devices [110-112]. While Silicon has been used for decades successfully, there is great willingness to move toward alternative low dimensional materials which propose interesting properties in variety of aspects [5, 6, 11, 13, 21, 22, 30, 31, 94]. Two dimensional materials like graphene and $MoSe_2$ and quasi one-dimensional structures like GNR and CNT have shown great potential for making next generation electronic, optoelectronic devices and sensors [21, 22, 30, 31, 113]. Hence, study of strain effects on the performance of low dimensional materials like graphene and GNR have been the subject of many theoretical and experimental researches [33, 56, 114-116].

To build low dimensional device or sensor, the ability to tune the electronic and transport properties of such materials is crucial. There are possible means to achieve this, comprise of electric field [86], chemical doping [60, 96], antidot patterning [81, 91, 92] and so on. One possibility is imposing strain to the device, which can be performed locally or over whole device [59, 86, 115, 117, 118]. Notably, mechanical deformation is not always caused intentionally. If graphene or GNR are grown on substrates with a different constant, this may cause some mechanical deviations which could be modeled as a form of strain [119, 120]. Even there is no lattice mismatch issue, strain still may happen along the edges [57, 121].

Graphene has no band gap and studies shows that graphene's band gap stays close to zero even if strain as large as 20% is introduced to it [62, 63, 85]. However, electronic structure of GNR is markedly modulated with strain [62, 106, 115, 116, 122, 123]. In fact, strain could be considered

as an effective way to tailor electronic properties of GNRs and tune fundamental characteristics like band gap.

According to literature, two types of strain are usually the matter of attention, uniaxial strain and shear strain [62, 124-126]. Figure 5-1 illustrates a schematic view of the mechanical deformation that each of these strain types represents. Most of studies have been dedicated to the uniaxial strain and shear strain is rarely discussed. Most probably because uniaxial strain is more likely to happen and perhaps easier to execute in the case of intentional deformation. In this thesis, uniaxial strain is taken into account and ignore shear one. Uniaxial strain involves two situations. While structure is stretched, called tensile strain, and where structure is compressed (compressive strain). Upon applying strain, the relative positions of carbon atom in honeycomb structure change. The relative variation in bonding distance is considered as the intensity of strain, expressed in percentage, $\varepsilon = (\Delta L/L) \times 100\%$, where L is the initial bonding length and ΔL the difference in bonding length caused by strain. Figure 5-2 shows how tensile and compressive uniaxial strain deform GNRs. Details of modeling are described in chapter 2-4.

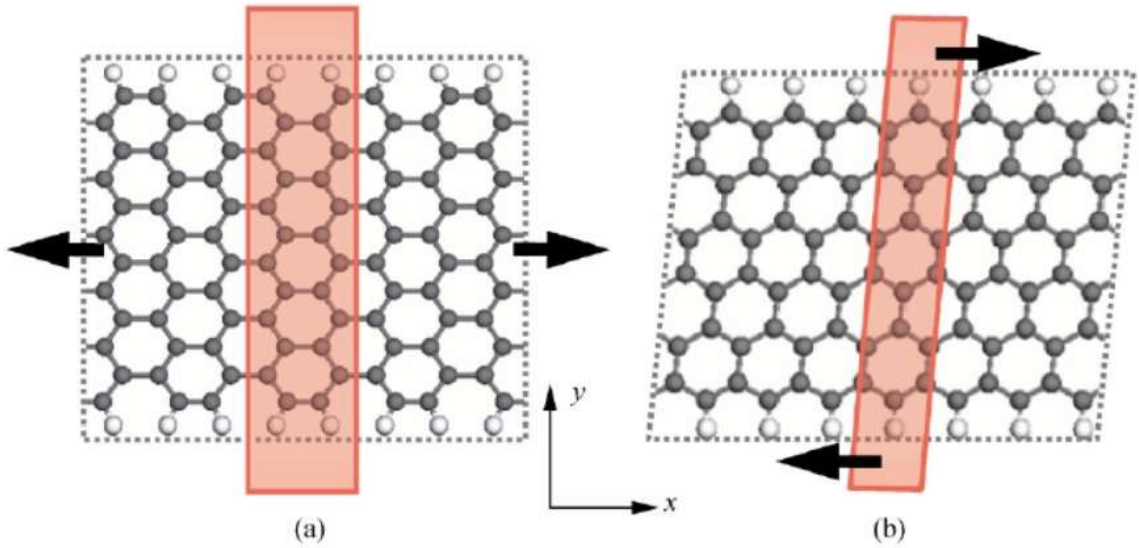

Figure 5-1: Schematic views of GNRs under strain. a) 12-AGNR under 10% uniaxial strain b) 6-. . .ZGNR under 10% shear strain [62].

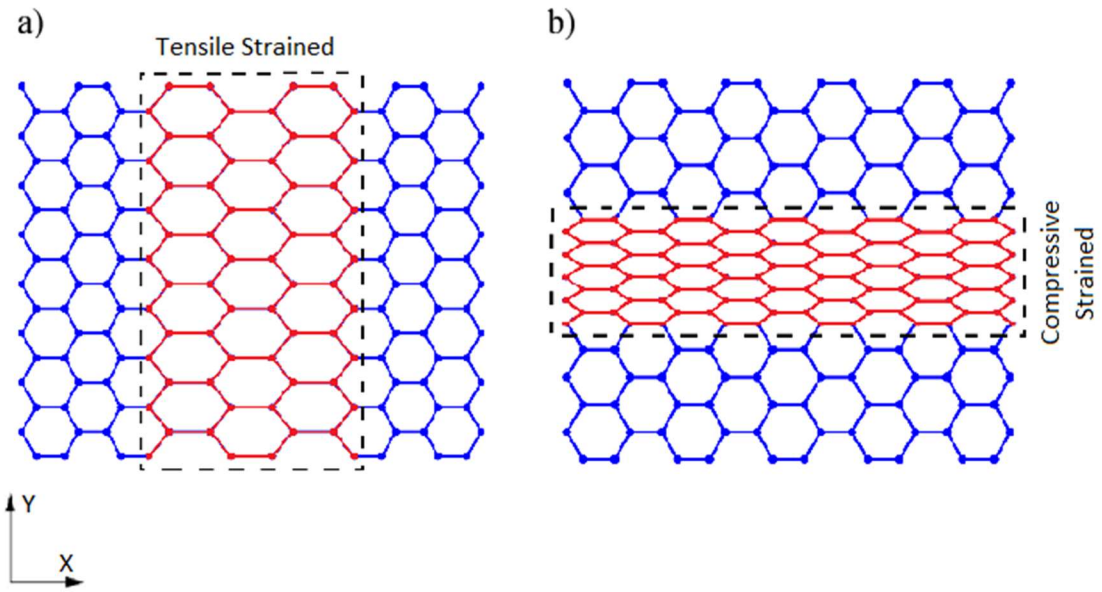

Figure 5-2: Uniaxial strained GNRs. a) tensile strain along X direction, b) Compressive strain along Y direction [127].

It is well known that band gap of AGNRs can be divided in three groups with respect to the ribbon width i.e., $N = 3P$, $3P+1$, and $3P+2$, where P is a positive integer. If AGNR goes under uniaxial strain, electronic structure and conductivity alter significantly [62, 124-126]. Regarding band structure, some bands shift toward the Fermi level, while some others move the other way [62]. Importantly, bang gap of AGNRs is modified in a periodic zigzag pattern as exhibited in Figure 5-3. One can notice that there are distinct phases corresponding to three groups of $N = 3P$, $3P+1$, and $3P+2$. It can be seen from Figure 5-3-b that effects of uniaxial strain reduces when width of ribbon is magnified. This is in agreement with analysis of strained graphene, where strain has no impact on the band gap size. Figure 5-4 gives more comprehensive picture in hand. This figure depicts band gap of different widths (2 to 10 nm) of AGNR for strain intensity of -15% to +15%. In general, band gap is periodically dependent of strain strength and inversely proportional to the ribbon's width [125].

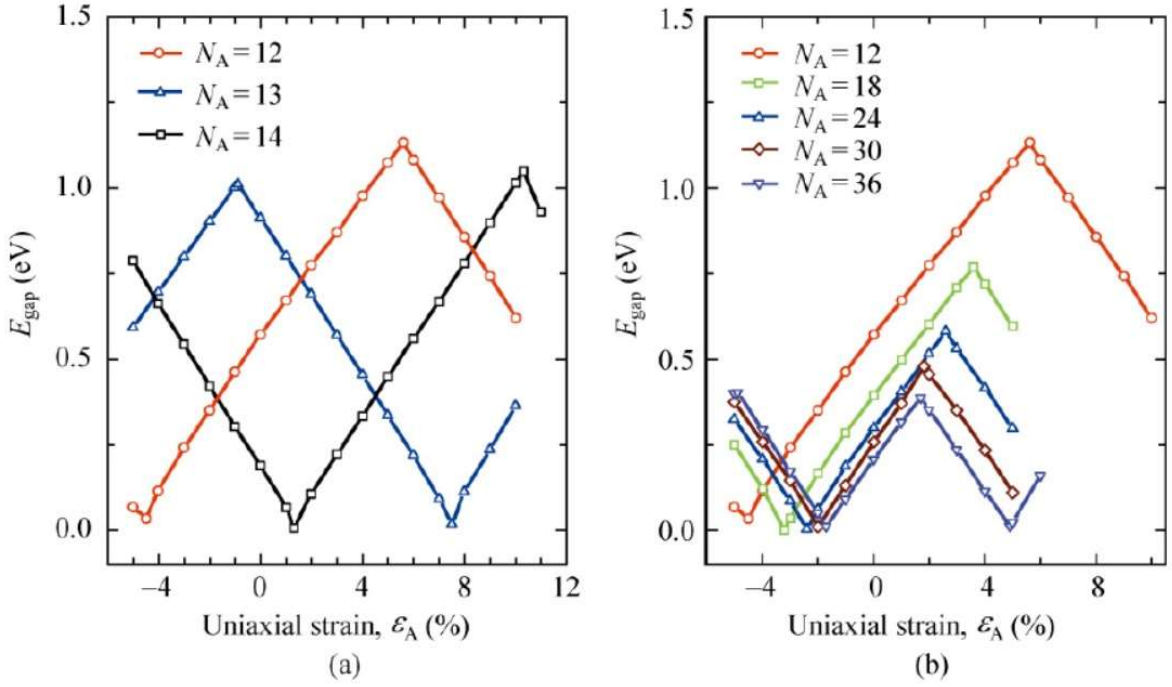

Figure 5-3: Energy band gap of strained AGNR, a) for widths of 12, 13, and 14, b) group of *3P* [62].

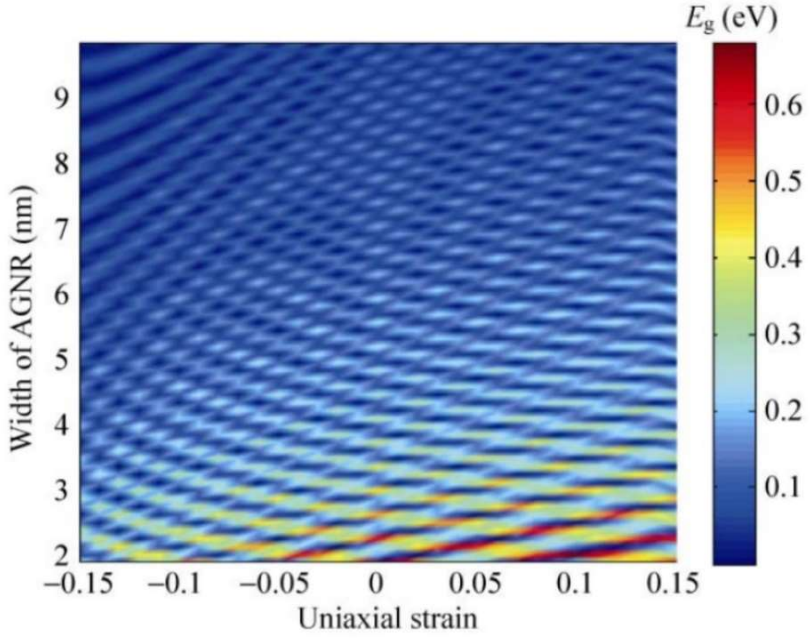

Figure 5-4: Band gap of AGNR, scaled from 2 to 10 nm width and strain strength of -15% to 15% [125].

In contrast with AGNR, ZGNR does not carry any bang gap unless spin polarization is taken into calculation [62]. Studies reveal uniaxial strain does not open band gap in ZGNR while spin polarization is not considered. However, imposing uniaxial strain to spin polarized ZGNR may lead to slight increment of band gap and rearrangement of energy bands [62], as shown in Figure 5-5. As a result, ZGNRs contain half-metallicity characteristic which has potential applications in spintronic [90, 128].

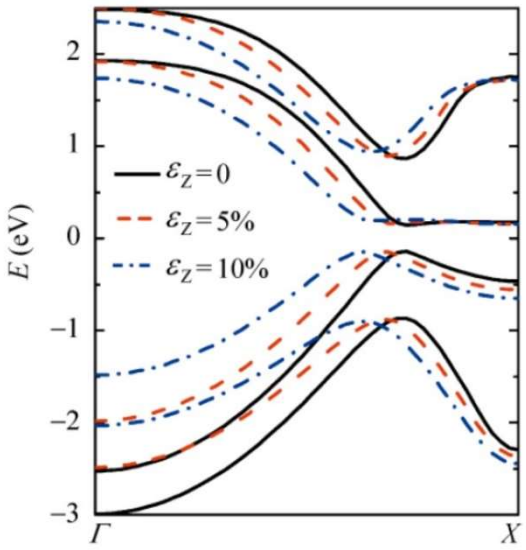

Figure 5-5: Slight band gap opening of spin polarized ZGNR upon applied uniaxial strain [62].

5-2 GNR RTD devices and strain deformation

5-2-1 Prologue

Extraordinary features of low dimensional structures have attracted much attention and they are considered as the very promising candidates for the next generation nano-electronic devices [11, 12]. In particular, graphene-based electronic devices have been the subject of many theoretical and experimental research [22, 31, 91, 129]. Among derivatives of graphene, armchair graphene

nanoribbon (AGNR) has demonstrated interesting electronic properties such as width-tunable band gap. There are three families of AGNR according to the band gap of ribbons and in all three families, band gap is inversely proportional to the width of ribbons [41, 72].

GNR's have a number of advantageous over conventional 3D semiconductors [22, 61, 81, 103]. Most of the state of art double barrier RTD devices are made of heterojunctions of different materials. Hence, the expected performance of 3D RTD device is degraded due to interface quality issues including dislocations and mismatched lattice [81, 103]. In contrast, AGNR RTD devices alike two understudy platforms of this study, are constructed by a single material, avoiding any interface problem. Furthermore, operation mechanism of 3D semiconductor devices is based on the bulk characteristics which cannot be preserved regarding size shrinking trend of electronic industry. On the other hand, length of AGNR RTD's stand at few nm's which make them promising candidates for the future electronic devices. However, in terms of PVR, AGNR based-RTD's do not certainly propose better or comparable efficiency. PVR of AGNR RTD's highly depends on the device design, ranging from few units to few hundreds [59, 86, 103, 106]. Importantly, AGNR's have shape-dependent band gap size. Hence, electrical and transport characteristics of AGNR's could be adjusted by cutting the ribbon in proper width [103]. This feature provides much better control mechanism over PVR value compared to conventional 3D devices. Taking this advantage, a number of AGNR based nano-electronic devices have been designed including AGNR resonant tunneling diodes (RTDs) [61, 81, 130].

To date, a number of methods have been implemented to design RTD device which are based on AGNR structure [61, 81, 123]. As a conventional technique, the barrier regions of RTD device are imposed to the external electric field by using a gate terminal [131, 132]. This leads to the formation of double barrier quantum well (DBQW) and apparition of quasi energy states within the quantum well. If a bias voltage is applied to such device, due to quantum tunneling phenomenon, negative differential resistance (NDR) appears in the I-V characteristic which fulfills the requirement of RTD device. In another method, AGNR RTDs can be designed if the barrier regions are composed of smaller widths compared to the channel and other parts [61, 105]. In this

platform, barrier regions have higher band gap and, therefore, DBQW and NDR property are achieved as well.

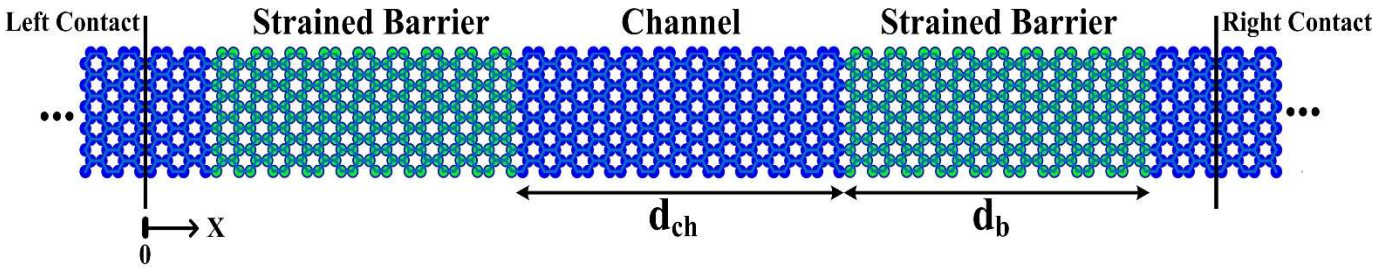

Figure 5-6: Schematic view of SI-12AGNR RTD [106].

Regarding current technologies, nano-scale structures including graphene-based devices cannot be fabricated as perfect as they are designed in theoretical studies [32, 133]. Hence, some investigations have been conducted to understand how mechanical imperfections such as edge-roughness can influence the performance of such devices [134, 135]. Also, nano-scale devices may go under strain, or in other words, they could be mechanically stretched out or compressed in. This may happen while stretchable substrate is utilized [56, 136] or due to real working conditions [119]. Indeed, it is insightful to understand what impacts strain could have on the performance and properties of nano-scale devices, as it has been done in some research [33, 114, 117, 118, 126]. The effects of uniaxial strain on the GNR field effect transistor and resonant tunneling transistor were studied in [137] and [116], respectively. It was reported that applying proper uniaxial strain can enhance band gap and electron effective mass of graphene nanoribbons (GNRs). Thus, imposing uniaxial strain can be considered as a method to adjust the performance of AGNR field effect transistors [137]. Moreover, in some works [106, 123], uniaxial strain has been used to achieve NDR property. H. Fang and colleagues investigated the transport properties of GNR's under tensile strain, It was found that, NDR effect is merely gained for AGNR(3p-1) which becomes stronger and then disappears over increasing intensity of tensile strain [123]. Strain-

induced platform of AGNR RTD by mean of local strain was introduced in [106]. As shown in Figure 5-6, barrier regions are deformed under uniaxial tensile strain whereas other parts are kept intact. Such platform leads to the formation of DBQW due to higher band gap of strained barriers. As a result, NDR behavior is attained in the I-V characteristic which is determined to be function of strain intensity. It was found that there is a direct relation between PVR and intensity of strain in which PVR grows proportionally upon increment of ε from 1% to 5% (refer to Figure 5-7).

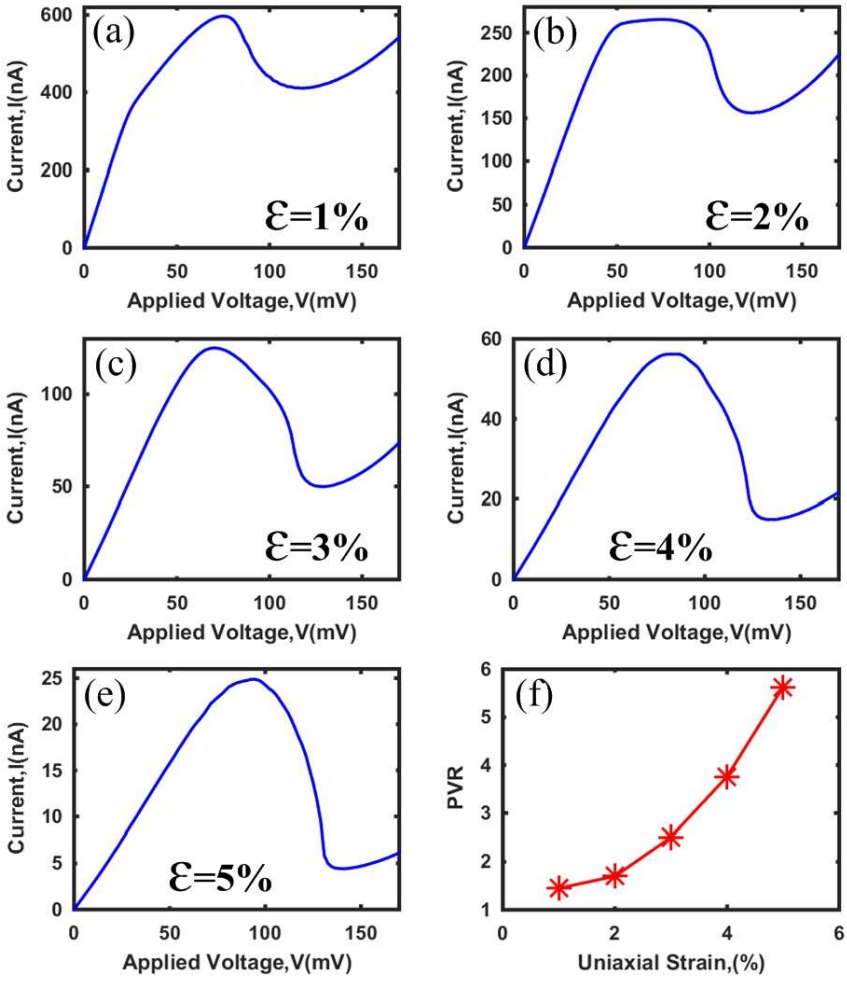

Figure 5-7: (a-e) I-V characteristics of SI-12-AGNR RTD under different strain percentage (ε). (f) PVR value versus strain percentage (ε) [106].

In this sub-chapter, computational study to reveal what impacts uniaxial strain would have on the performance of AGNR RTDs is performed. To achieve this goal, two different platforms of AGNR RTDs are chosen and studied. These platforms are named as width-modified AGNR RTD and field-modified AGNR RTD. Tensile and compressive uniaxial strains are introduced into the devices and corresponding properties of RTD device comprise of peak to valley ratio (PVR), transmission peak points, and current-voltage data are extracted and analyzed. Furthermore, impacts of local strain on the channel and barrier regions are extracted and compared with whole-body strained device. Finally, performance of device is monitored and analyzed while width of the device is scaled to different values.

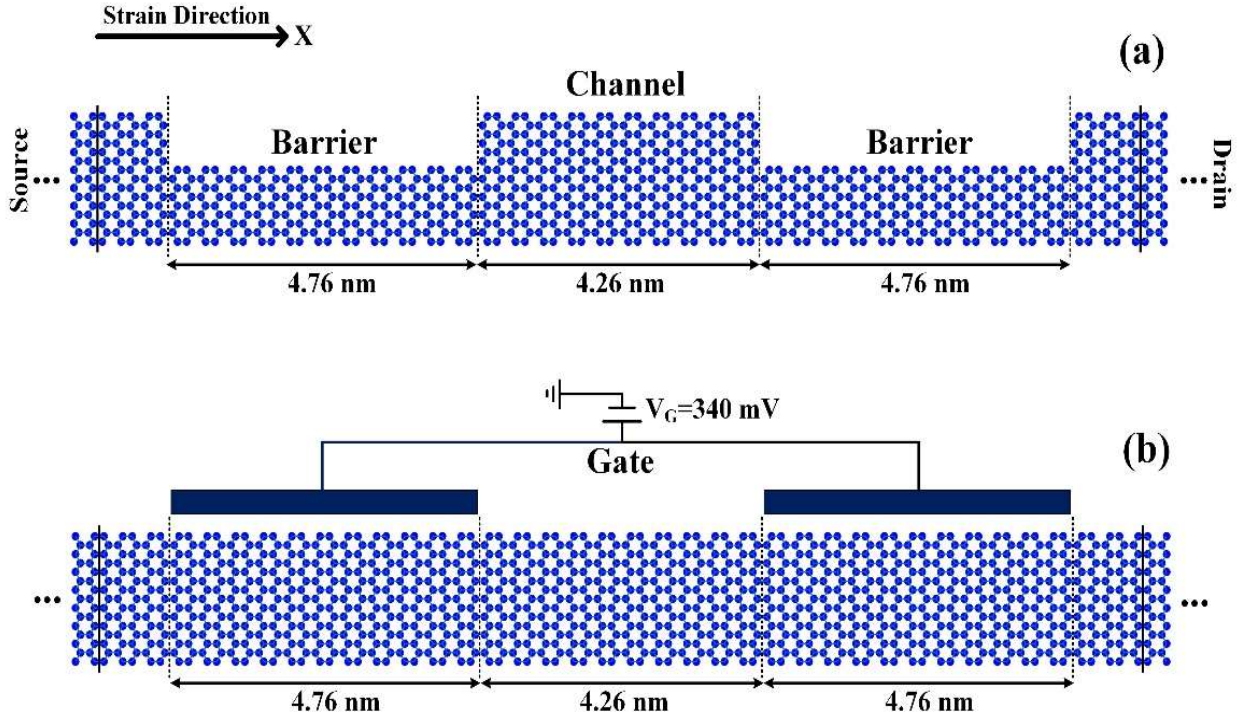

Figure 5-8: AGNR RTD platforms. (a) Width-modified 15-AGNR RTD. (b) Field-modified 15-AGNR RTD.

5-2-2 Operation Mechanism of AGNR RTD under Uniaxial Strain

The width-modified 15-AGNR RTDs and field-modified 15-AGNR RTD (platforms shown in Figure 5-8) are subjected to the uniaxial strain which is induced over the whole body of device in the X direction. Strain proportion is chosen from -2% compressive to +2% tensile with steps of 1 percent. A bias voltage is applied to the contacts and, corresponding transmission probabilities, I-V characteristics, and $LDOS_y(E,x)$ (colored plots) are illustrated in Figure 5-9 and Figure 5-10. Also, performances of both RTD platforms are compared and summarized in Figure 5-12 and Table 5-1.

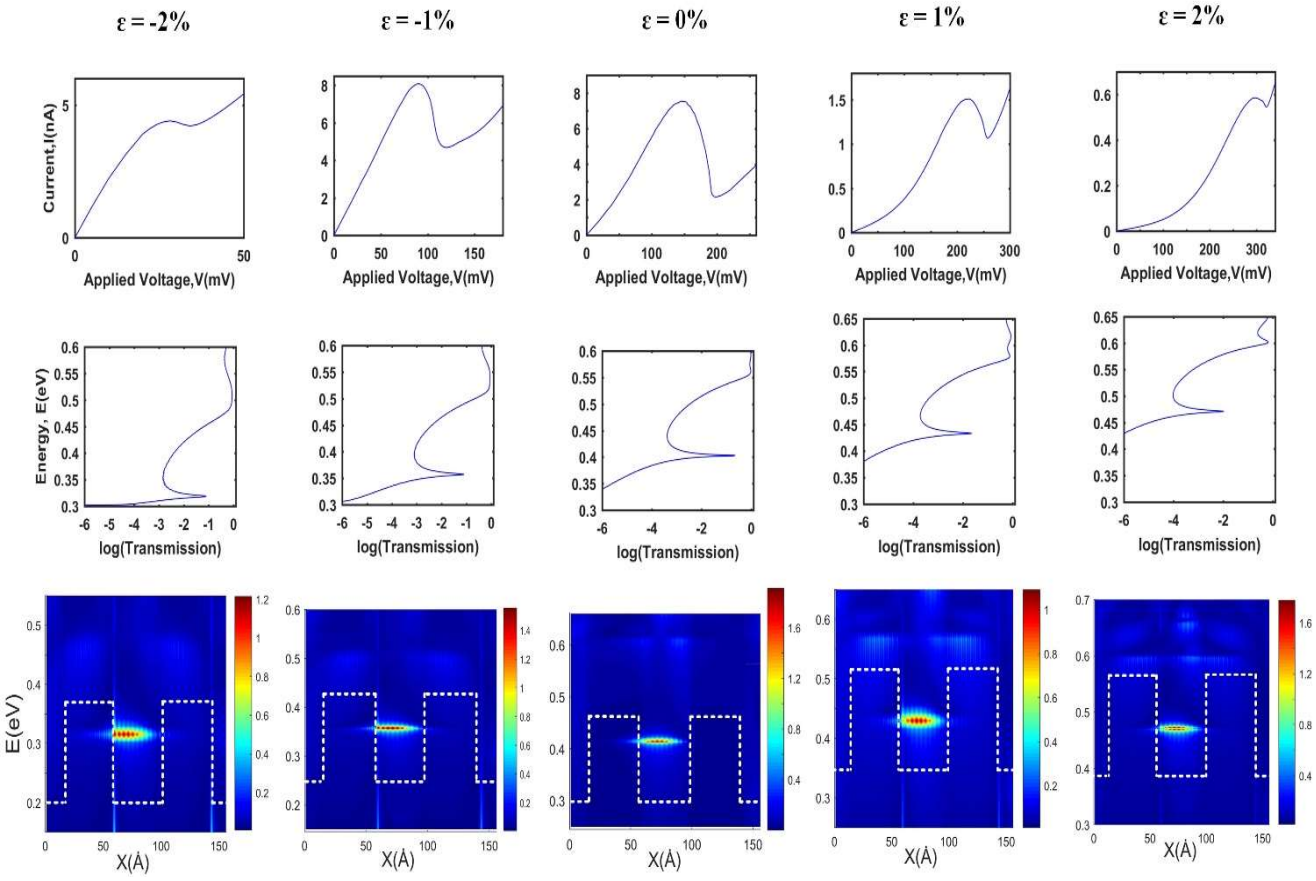

Figure 5-9: I-V characteristic (first row), transmission probability (second row), and $LDOS_y(E,x)$ (third row) of width-modified 15-AGNR RTD under different strain percentages.

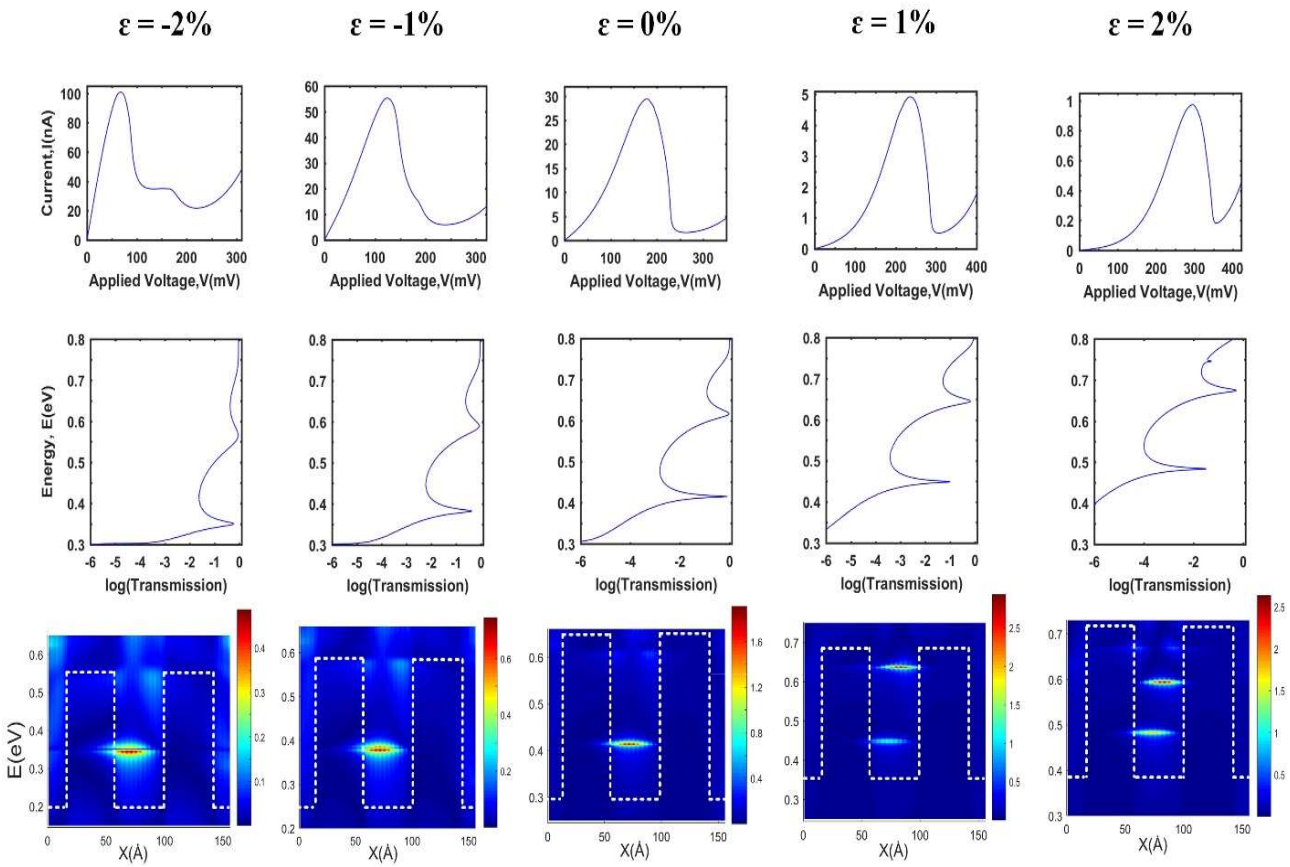

Figure 5-10: I-V characteristic (first row), transmission probability (second row), and $LDOS_y(E,x)$ (third row) of field-modified 15-AGNR RTD under different strain percentages.

Figure 5-11 shows the band diagram of both platforms along the length of device. Regarding conduction band edges, one can notice that DBQW occurs for both platforms. First quasi energy state within quantum well contributes to the tunneling phenomenon and indeed NDR behavior in I-V curve. Upon tensile/compressive uniaxial strain, conduction band edges and quasi energy states experience increase/decrease in their levels. As exhibited in Figure 5-9 and Figure 5-10, when there is no strain (ε = 0%), the first quasi-state energy (hot color dash line in blue plots of LDOS) is appeared around 0.4 eV for both types of RTD devices. As a result, the first peak of transmission happens in the same energy and, due to resonance in transmission probability, NDR behavior is clearly observable in I-V curve.

It is very interesting that, while device goes under strain, the first quasi-state moves toward higher energy for tensile strain and toward lower energy for compressive strain. The similar scenario occurs for the position of first transmission peaks. Transition of first transmission peak is reflected in voltage peak point (V_{Peak}) of I-V curve. The V_{Peak} drifts from 28.08 mV to 296.77 mV when ε swipes from -2% to + 2%, in case of width modified 15-AGNR RTD and from 68.48 mV to 294.73 mV for field-modified 15-AGNR RTD (Figure 5-12 and Table 5-1). It is informative that quantum confinement (level of first quasi-state) and V_{Peak} demonstrate linear dependency on the mechanical deformation.

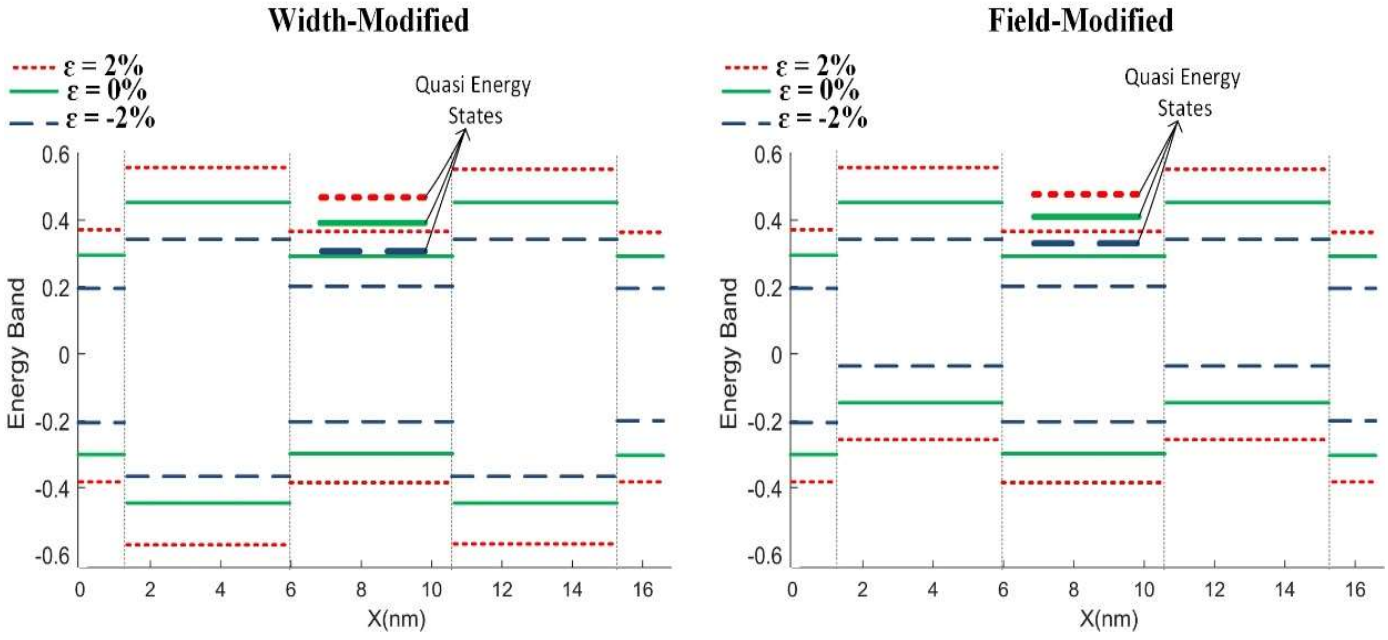

Figure 5-11: Band diagram of width/Field modified AGNR RTD.

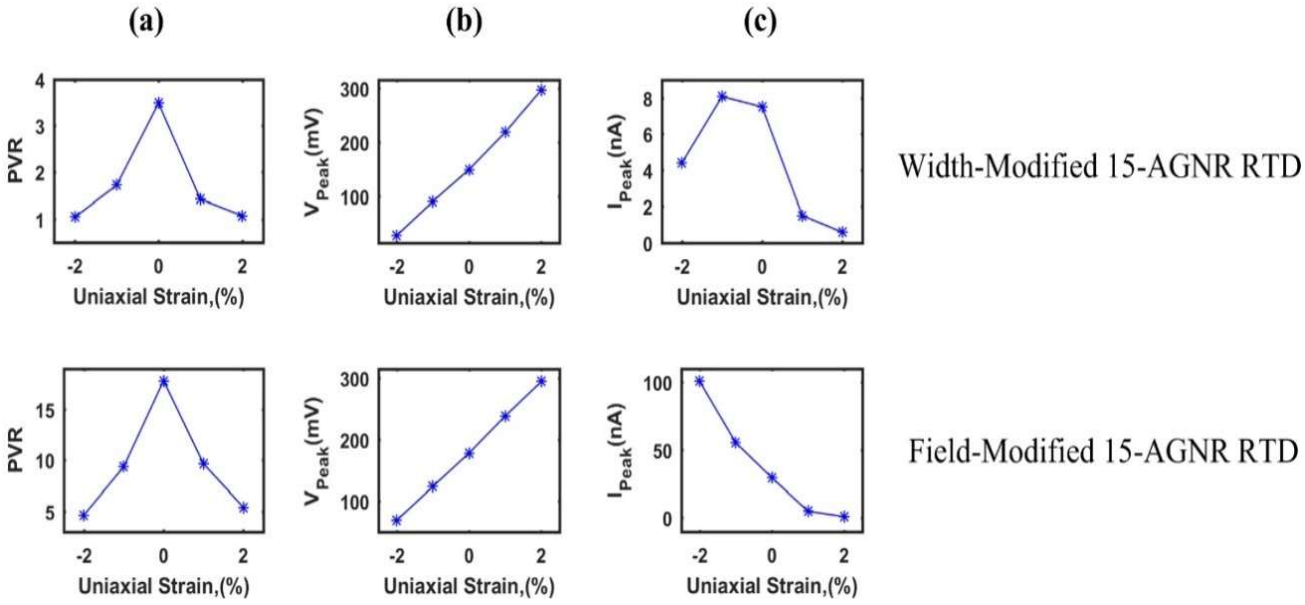

Figure 5-12: (a) PVR, (b) V_{Peak} and (c) I_{Peak} of width/field modified 15-AGNR RTDs as a function of strain percentage.

There are three factors that determine the first resonance of RTD device. The value of transmission in first peak (tail of first peak), how much transmission falls after first peak (dip intensity), and the proximity of first and second transmission peaks. The first transmission tail indicates how much I_{Peak} can grow. Dip intensity shows how much current level can continue falling (negative resistance area) before transmission rises again due to the second peak. Regarding transmission probability diagrams, one can notice that the relative proximity of first and second peaks stays almost same in all strained/unstrained cases. However, once uniaxial strain is applied, dip intensity with respect to tail of first peak, is always less than unstrained case. As a result, current of strain-induced devices cannot drops as much as unstrained devices, meaning PVR value reduces if whole body of device goes under strain. For example, PVR for unstrained width-modified 15-AGNR RTD stands at the value of 3.49, but it reaches to 1.04 and 1.07 for ε = -2% and +2 % respectively (Figure 5-12 and Table 5-1). This manifests that, uniaxial strain as a form of mechanical deformation can deeply influence quantum confinement of AGNR RTD device in such a way that expected performance would be totally damaged.

Table 5-1: Performance of width/field modified 15-AGNR RTD under different strain percentage.

	Width-Modified 15-AGNR RTD					Field-Modified 15-AGNR RTD				
ε(%)	PVR	V_{Peak}(mV)	V_{Valley}(mV)	I_{Peak}(nA)	I_{Valley}(nA)	PVR	V_{Peak}(mV)	V_{Valley}(mV)	I_{Peak}(nA)	I_{Valley}(nA)
-2	1.04	28.08	34.14	4.40	4.21	4.62	68.48	224.56	100.82	21.82
-1	1.72	90.71	119.03	8.08	4.69	9.34	123.28	238.30	55.36	5.93
0	3.49	149.32	199.81	7.51	2.15	17.83	177.65	260.41	29.42	1.65
1	1.42	218.26	258.47	1.50	1.06	9.65	238.23	306.87	4.92	0.51
2	1.07	296.77	321.13	0.58	0.54	5.39	294.73	357.48	0.97	0.18

5-2-3 Performance of AGNR RTD with Strained Barrier regions

Study of local strain effects would bring new insights and give some tools to control performance of a device in a desired way. Moreover, local strain can be employed to create novel devices and sensors [59, 85, 106, 115]. For instance, in [106], stain induced (SI) AGNR RTD was designed. It was shown not only RTD device can be attained by local strain on barrier regions of AGNR, but also performance of such device can be adjusted by the intensity of imposed mechanical deformation (strain).

In this part, only barrier regions go under strain, whereas other parts of device are kept unchanged. 15-AGNR RTD is used and two barriers are subjected to uniaxial strain of ε=-2%, -1%, 0%, +1%, and +2%. The I-V characteristics and transmission probability of the field-modified 15-AGNR-RTD with strained barriers are exhibited in Figure 5-13. One can notice that, the first transmission peak of all cases (from ε=-2% to ε=+2%) occurs at almost the same level of energy (around E=0.42 eV). This is reflected in I-V characteristics, where V_{Peak} does not drift much. Noticeably, this behavior proposes different picture compared to the situation of whole-body strained device (as discussed in part 3.A), where first transmission peak and hence V_{Peak} explicitly drift as a function of imposed strain.

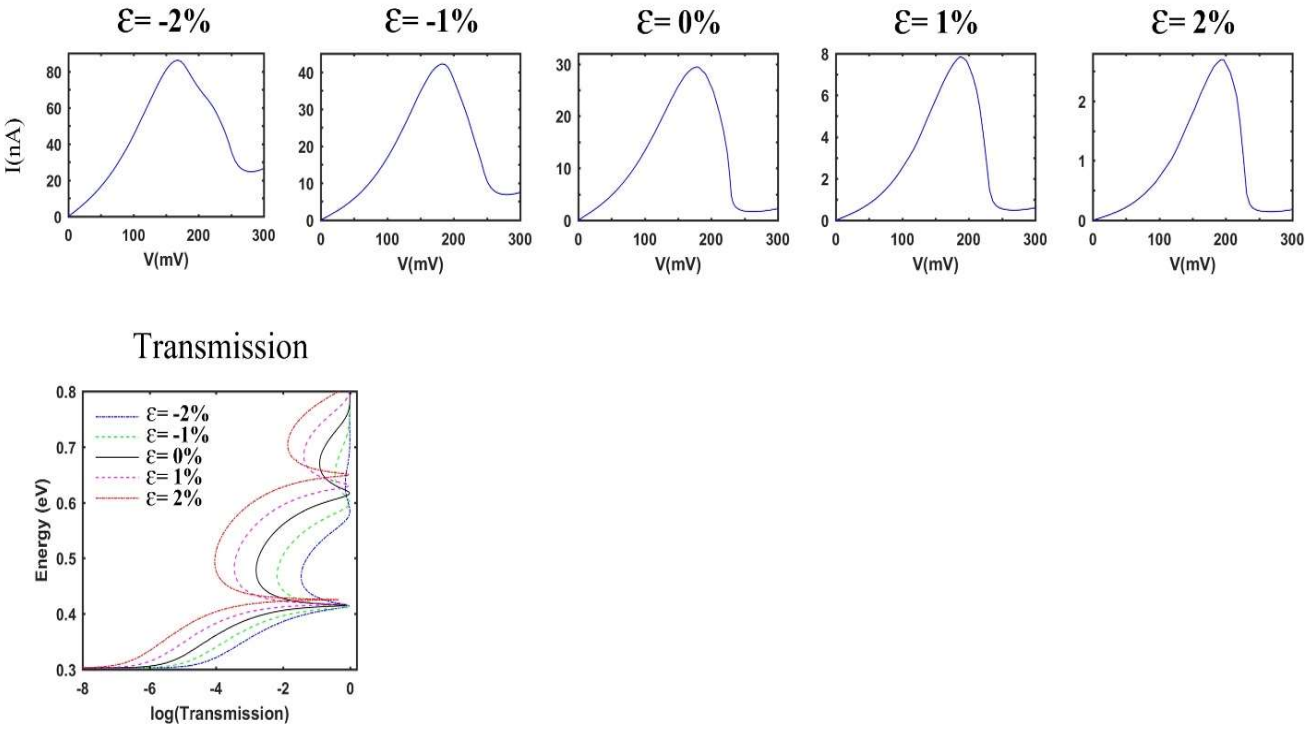

Figure 5-13: I-V characteristic and transmission probability of field-modified 15-AGNR RTD while barrier regions are under strain effect.

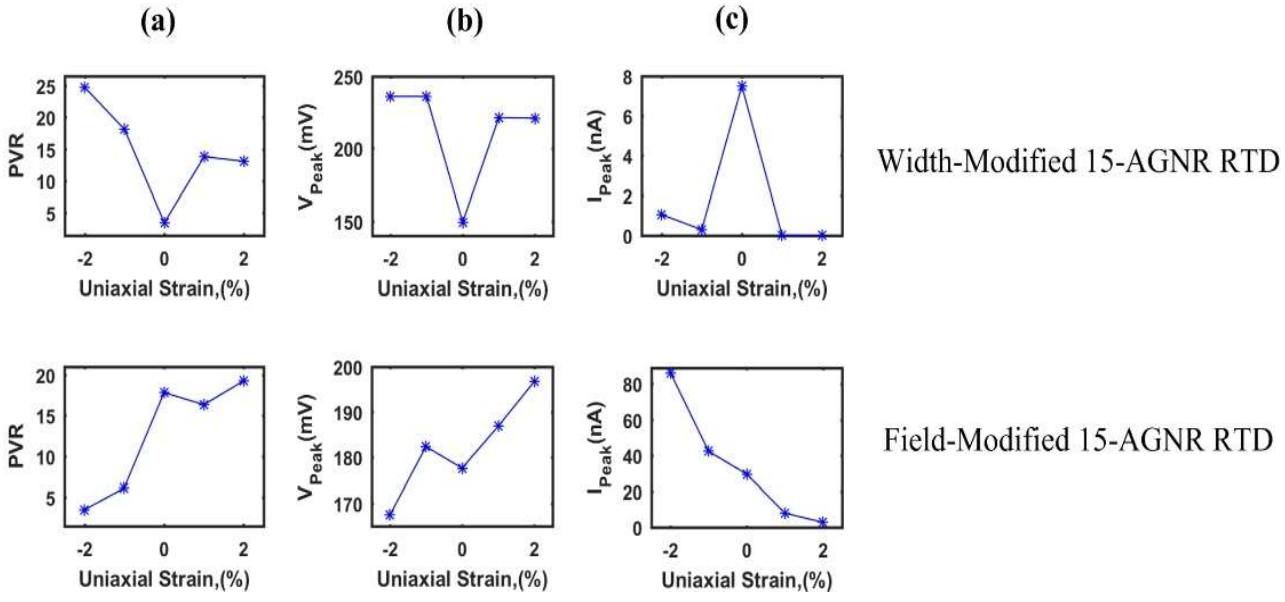

Figure 5-14: (a) PVR, (b) V_{Peak} and (c) I_{Peak} of width/field modified 15-AGNR RTDs while strain effect is confined to the barrier regions.

Details of operation mechanisms of width/field modified 15-AGNR RTD are illustrated in Figure 5-14 and Table 5-2. It can be seen that both compressive and tensile strains on the width-modified 15-AGNR RTD improve the PVR criterion. This improvement could be even up to 7 times more at ε=-2% (24.7/3.49≈7, refer to Table 5-2). Compared to the whole-body strained device, this enhancement of PVR shows that the uniaxial strain has not necessarily destructive consequences for the efficiency of device.

In case of field-modified 15-AGNR RTD, while compressive strain is induced to the barriers, second peak become closer to the first peak and there is shallower dip, leading to weaker PVR. In contrast, upon tensile strain opposite behavior occurs and higher PVR is fulfilled.

Therefore, one can conclude that the impact of imposing uniaxial strain to the AGNR RTD device has dependency on the type of strain (tensile or compressive) and also on those regions of device that go under strain (location of strain).

Table 5-2: Performance of width/field modified 15-AGNR RTD when only barrier regions are under strain.

	Width-Modified 15-AGNR RTD					Field-Modified 15-AGNR RTD				
ε(%)	PVR	$V_{Peak(mV)}$	$V_{Valley(mV)}$	$I_{Peak(nA)}$	$I_{Valley(nA)}$	PVR	$V_{Peak(mV)}$	$V_{Valley(mV)}$	$I_{Peak(nA)}$	$I_{Valley(nA)}$
-2	24.76	236.12	309.68	1.04	0.042	3.49	167.38	280.34	86.26	24.67
-1	18.12	236.10	310.53	0.29	0.016	6.13	182.37	280.35	42.21	6.88
0	3.49	149.32	199.81	7.51	2.15	17.83	177.65	260.41	29.42	1.65
1	13.81	221.45	260.72	18.51×10^{-3}	1.34×10^{-3}	16.35	186.92	265.62	7.85	0.48
2	13.08	221.02	255.89	4.58×10^{-3}	0.35×10^{-3}	19.28	196.83	265.57	2.70	0.14

5-2-4 Performance of AGNR RTD with Strained Channel region

To deepen our understanding about local strain effects, it is interesting to investigate how behavior of AGNR RTD may vary if uniaxial strain is merely induced to the channel region.

Figure 5-15 shows corresponding I-V characteristics and transmission probability of field-modified 15-AGNR RTD while only channel is under strain. It can be seen that first and second transmission peaks of transmission probability drift to higher energies as strain changes from ε=-2% compressive to ε=+2% tensile. Therefore, V_{Peak} moves from 78.11mV to 286.51 mV (Table 5-3). Also, I_{Peak} decreases for both tensile and compressive strains. Further examinations were conducted in case of width-modified 15-AGNR RTD and corresponding results are summarized in Figure 5-16 and Table 5-3. Although roughly the same patterns of V_{Peak} and I_{Peak} are observed, PVR exhibits different behavior. For field-modified 15-AGNR RTD, PVR is degraded if channel region of device is under either compressive or tensile strain. In contrast, the PVR of width-modified 15-AGNR RTD enhances under both compressive and tensile strains. Noteworthy, this increment is more intense by compressive deformation compared to tensile one.

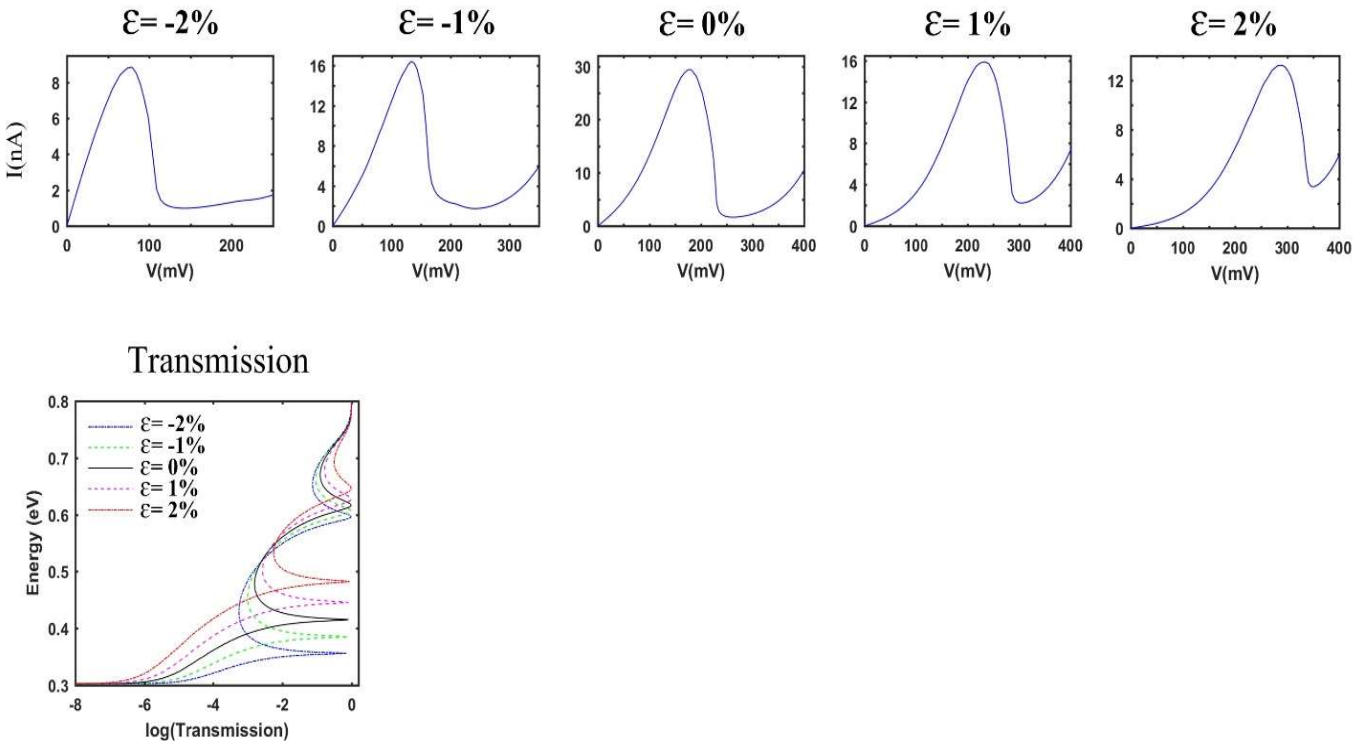

Figure 5-15: I-V characteristic and transmission probability of field-modified 15-AGNR RTD when only channel region is strained.

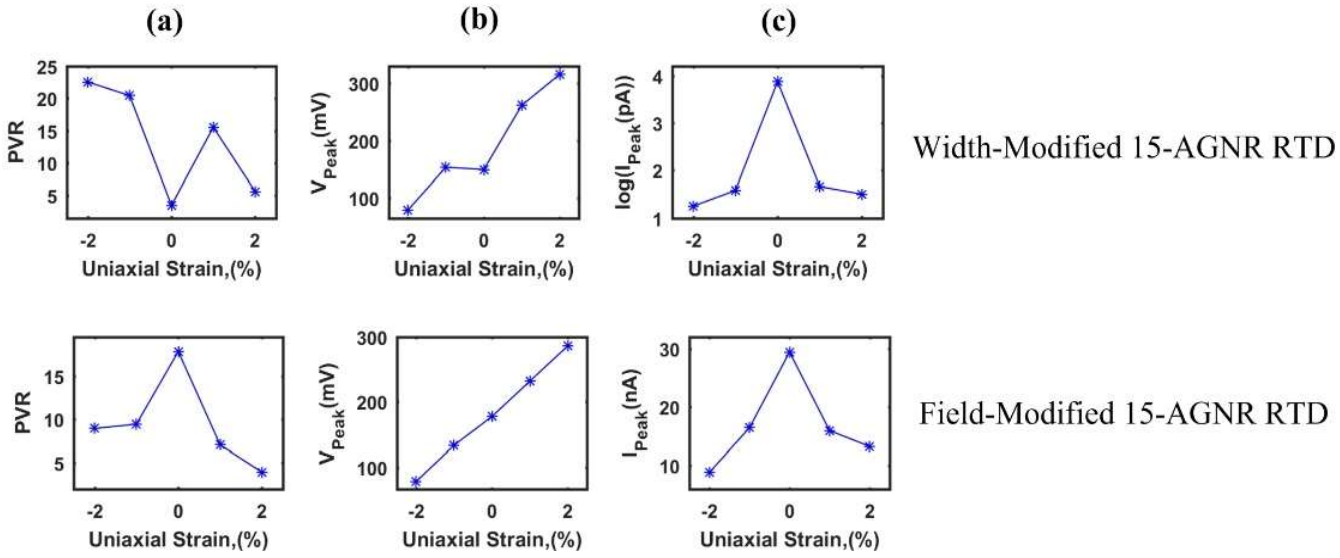

Figure 5-16: (a) PVR, (b) V_{Peak} and (c) I_{Peak} of width/field modified 15-AGNR RTDs while strain effect is confined to the channel region.

Table 5-3: Performance of width/field modified 15-AGNR RTD when only channel region is under strain.

	Width-Modified 15-AGNR RTD					Field-Modified 15-AGNR RTD				
ε(%)	PVR	$V_{Peak(mV)}$	$V_{Valley(mV)}$	$I_{Peak(pA)}$	$I_{Valley(pA)}$	PVR	$V_{Peak(mV)}$	$V_{Valley(mV)}$	$I_{Peak(nA)}$	$I_{Valley(nA)}$
-2	22.57	79.11	158.13	18.06	0.80	8.93	78.11	143.32	8.85	0.99
-1	20.45	153.29	251.90	38.45	1.88	9.43	133.47	2.42	16.42	1.74
0	3.49	149.32	199.81	7514.26	2153.08	17.83	177.65	260.41	29.42	1.65
1	15.53	261.84	325.9	46.28	2.98	7.05	232.25	311.14	15.93	2.26
2	5.62	316.17	380.33	32.15	5.72	3.93	286.51	350.68	13.23	3.37

5-2-5 Performance of Strain Induced AGNR RTD versus Width Scaling

So far, the behavior of two platforms of AGNR RTD devices under whole-body and local uniaxial strains has been examined, however, the width of device in all studies was constant (15AGNR). In this part, it is investigated how performance of strained AGNR RTD's varies while the width

of device is tuned. Here, 12, 15, and 18 AGNR's are utilized to design three profiles of field-modified AGNR RTD's, as illustrated in Figure 5-17. All these three ribbons are from the same family of AGNR's (3P). Same gate voltage is applied to the barrier regions (V_G=340mV) and lengths of channel and barrier parts are all the same, (4.76 nm and 4.26 nm respectively). Compressive (ε=-2%) or tensile (ε=+2%) strain is imposed throughout whole body of device and, corresponding I-V characteristics and transmission probability are depicted in Figure 5-18. Furthermore, Figure 5-19 and Table 5-4 present performances of unstrained/strained field-modified AGNR RTD's.

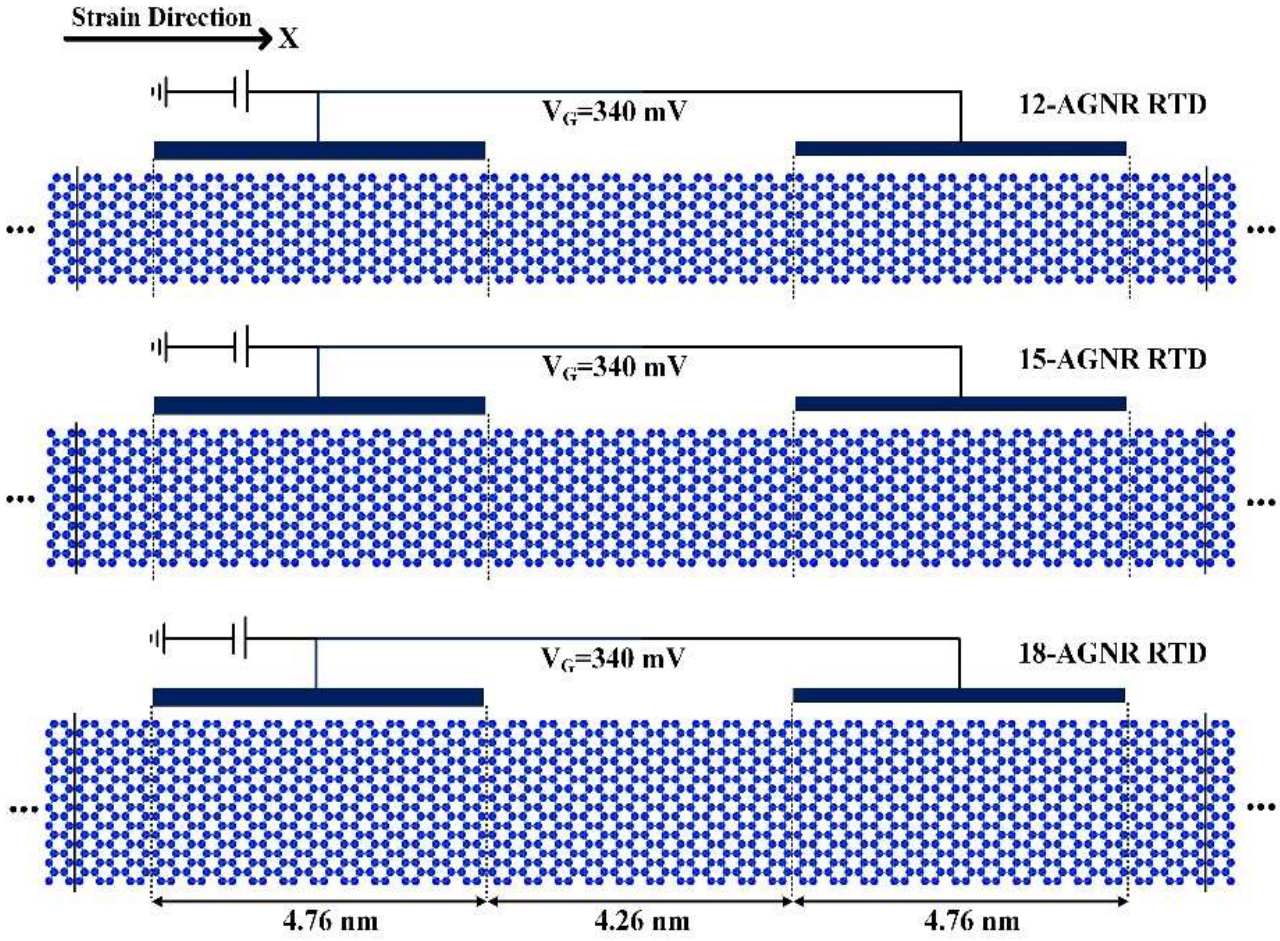

Figure 5-17: Platforms of field-modified AGNR RTDs with different widths.

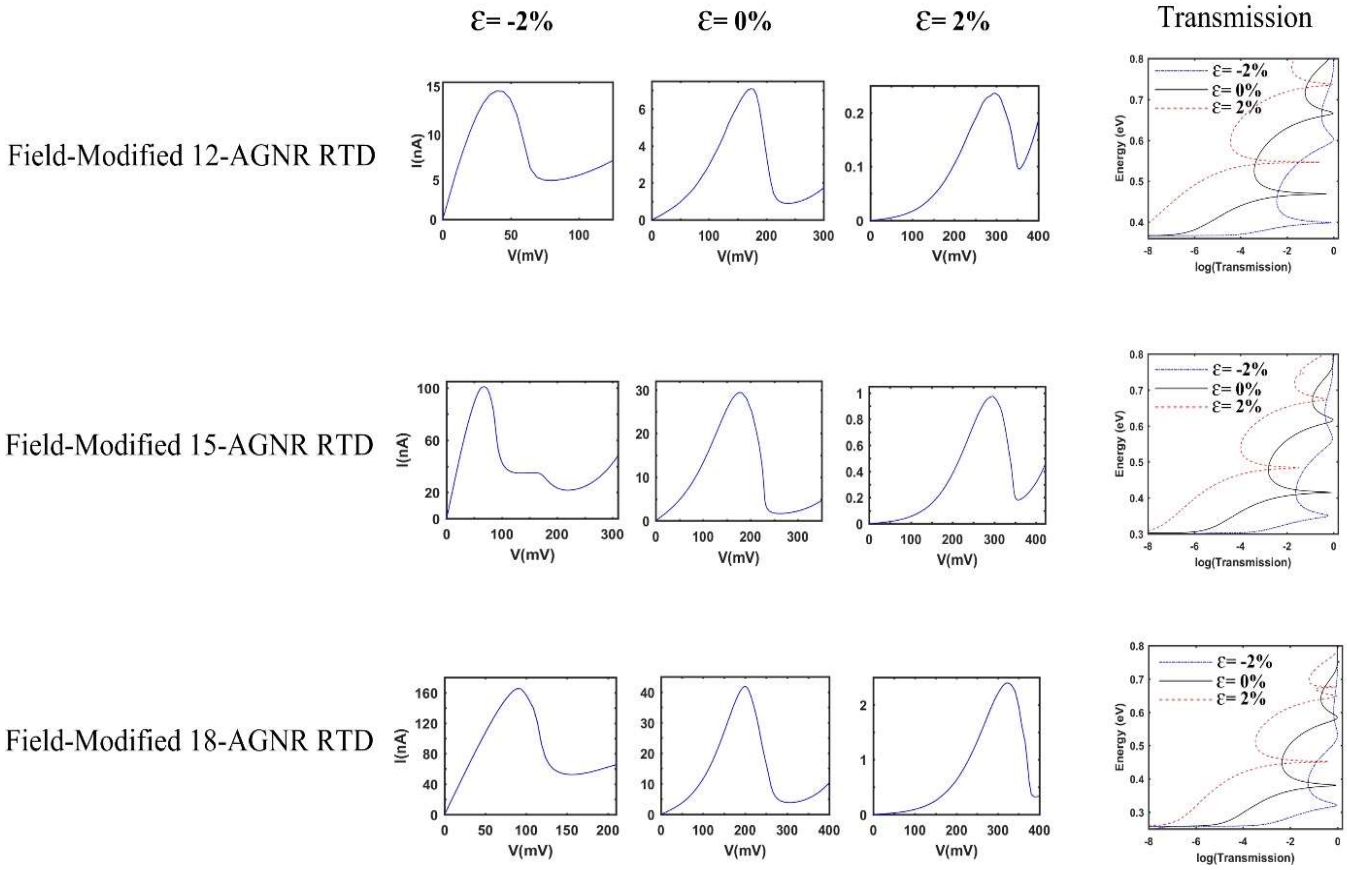

Figure 5-18: I-V characteristic and transmission probability of field-modified 12/15/18-AGNR RTD for strain proportion of -2%, 0%, and +2%.

It can be seen that as tensile strain is employed, first transmission peak and indeed V_{Peak} shift toward higher energy, compared to unstrained situation. For compressive strain opposite effect is monitored. These effects are true for all three different widths and could be generalized for an arbitrary width of ribbons. In terms of I_{Peak}, tensile strain reduces the current value, while compressive strain enhances it. This could be counted as a general rule when strain deformation occurs throughout whole body of field-modified AGNR RTD's. Regarding PVR, no matter tensile or compressive strain is applied, performance of device always degrades. However, it is important to notice that degradation of PVR occurs in different degrees. For instance, compressive -2%

imposed on 15-AGNR RTD leads to reduction of PVR from 17.83 (unstrained) to 4.62 (17.83/4.62≈ 3.86 times less), whereas 18-AGNR RTD with +2% tensile strain shows a decrement of PVR from 10.72 to 7.50 (10.72/7.50≈1.43 times less).

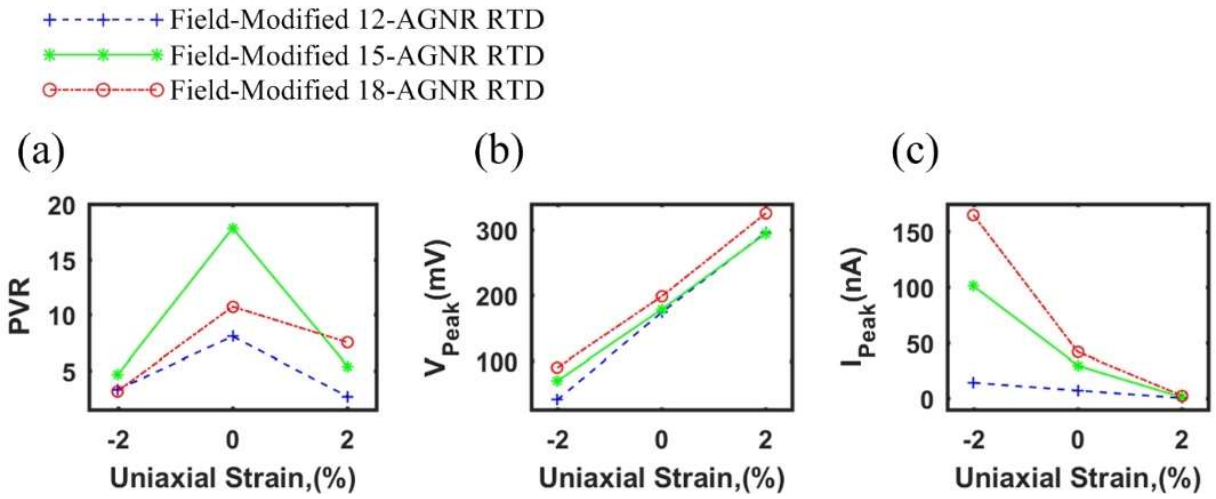

Figure 5-19: (a) PVR, (b) V_{Peak} and (c) I_{Peak} of field-modified 12/15/18-AGNR RTD.

Table 5-4: Performance of field-modified AGNR RTD at different widths.

	ε(%)	PVR	V_{Peak}(mV)	V_{Valley}(mV)	I_{Peak}(nA)	I_{Valley}(nA)
SI 12-AGNR RTD	-2	3.30	39.62	79.11	14.02	4.25
	0	8.04	172.91	237.14	7.08	0.88
	2	2.67	296.36	355.62	0.24	0.09
SI 15-AGNR RTD	-2	4.62	68.48	224.56	100.82	21.82
	0	17.83	177.65	260.41	29.42	1.65
	2	5.39	294.73	357.48	0.97	0.18
SI 18-AGNR RTD	-2	3.15	88.89	158.1	165.35	52.53
	0	10.72	197.65	306.22	41.47	3.87
	2	7.50	325.90	390.18	2.40	0.32

5-3 Conclusion

Effects of uniaxial strain on the GNRs and relative strain-based AGNR RTD was recapped from literature. It was found that AGNR-based RTD can be achieved if uniaxial strain is introduced to the barrier regions of device. It was shown that by intensifying strain from 1% to 5%, PVR grows from 1.45 to 5.63 proportionally, which manifests there is direct link between PVR and strain percentage (ε).

Regarding subchapter 5-2, effects of whole-body and local uniaxial strain on the performance of width/field modified 15-AGNR RTDs were investigated in this chapter. It has been found that if strain is imposed throughout whole body of device, energy level of first quasi-state within DBQW and first transmission peak change, depend on the type (compressive or tensile) and intensity of applied strain. The more the device is mechanically compressed (stretched), the more the first quasi-state and transmission peak shift toward lower (higher) energies.

If whole body of width/field modified AGNR RTD go under uniaxial strain, PVR always reduces compared to unstrained device and it could be even fully damaged if mechanical deformation is intense enough.

On the other hand, local strain could be either destructive or constructive in terms of PVR, depending on the type of strain and utilized platform of RTD. For instance, while strain is merely introduced to the barriers or only to the channel region of width-modified 15-AGNR RTD, PVR always grow, for both compressive and tensile strains. In strained barrier case, PVR increases from 3.49 (unstrained) to 24.76 for $\varepsilon = -2\%$ (refer to Table II), revealing a growth rate more than 7 times. In contrast, PVR of field-modified 15-AGNR RTD degrades in cases of compressed barriers/channel or stretched channel.

Chapter 6 Conclusion

In summary, the case study here has shown that periodic antidot/BN topologies can be induced to GNRs and ZCNTs to effectively tune the pristine electronic and transport properties. Such periodical defects along the length of structure could be considered equivalent of multi potential barriers which lead to new quantum confinement, degeneration breaking, rearrangement of sub band arrays, and modification of band gap. Regarding GNRs, ZGNR is less influenced by topological defects, compared to AGNR. Metallic behavior of ZGNR is preserved although its weakened. In contrast, either band gap opening or closing may occur for AGNR and ZCNT depending on the shape of utilized defect topology and family of ribbon/tube. Noteworthy, antidots, as the physical defects, always enforce stronger consequences in the electronic and transport properties, compared to that of BN doping as the chemical defect. In addition, new properties of defected systems are function of dimensional parameters. As a general rule, if relative distance between defects (antidot/BN doping atoms) or width/radius of GNR/CNT increases, new properties become closer to the pristine ones.

While periodic antidot/BN-doped structures provide new flexibility to tune pristine properties, this advantage was used to design defect based RTD platforms. Formation of DBQW structure and NDR behavior was proved by computing transmission, LDOS, and I-V curve of both defected AGNR RTD and ZCNT RTD.

Performance of width/field modified AGNR RTD under uniaxial strain was also studied. It was found that upon strong enough whole-body strain, RTD functioning can be fully destroyed. It occurs for both compressive and tensile strain. Role of dimensional factors on this mechanism and impacts of local strain on the channel and barrier regions was also investigated. Our analysis reveals that AGNR RTD performance varies markedly upon mechanical deformation which could be promising in design of motion-based sensors or could be considered very negative in design of large area flexible electronics, where efficiency robustness against motions is critical.

Contribution

In order to examine our objectives, first, fundamentals of TB and NEGF models were programmed in MATLAB software and well-known characteristics of GNRs, CNTs, and RTDs were regenerated and verified. Established reliable simulation environment, extra features comprise of topological defects and uniaxial strain were adopted to the modeling. Eventually, developed MATLAB simulator is capable of defining arbitrary number of antidots, BN doping topologies, and strain deformation at desired positions. One only needs to define the desired platform and set out system's inputs and outputs parameters, whereas, whole electronic/transport processes are derived automatically with no need of recoding.

Having such simulation tool in hand, the research objectives in terms of periodic defected CNTs and also design of defect-based CNT RTD were performed. Moreover, performance of width/field modified AGNR RTDs were monitored under different scenarios of uniaxial mechanical deformation. Results of this thesis were published in two credible journal papers and presented in ICNN 2019.

- *M Zoghi, MZ Kabir "Effects of uniaxial strain on the performance of armchair graphene nanoribbon resonant tunneling diode" Semiconductor Science and Technology (IOP) , May 2019, Volume 34, Issue 5, Page 055012*
- *M Zoghi, AY Goharrizi, SM Mirjalili, MZ Kabir " Electronic and transport properties of zigzag carbon nanotubes with the presence of periodical antidot and boron/nitride doping defects" Semiconductor Science and Technology (IOP) , May 2018, Volume 33, Issue 6, Page 065015*
- *M Zoghi, MZ Kabir "Performance of Armchair Graphene Nanoribbon Resonant Tunneling Diode Under Uniaxial Strain" 21st International Conference on Nanoscience and Nanotechnology (ICNN2019), June 2019, Toronto*

Potential future study

a) Investigation of local uniaxial and shear strain on the performance of CNTs. To date, no study of local strain, neither uniaxial nor shear have been conducted about CNTs. Indeed, one can design scenarios to impose local strain to the CNTs and investigates consequences in the electronic and transport properties.

b) Design strain-based CNT RTD platform and discovering role of strain intensity and dimensional paraments on the performance of such device. Strain-based GNR RTD have been designed and studied regarding the fact that electronic properties of GNR can be tuned under strain. Thereby, it is imaginable that one could tune pristine properties of CNTs and use it to come up with strain-based CNT RTD.

c) Design and study of multibarrier GNR/CNT RTD by mean of defects. Double barriers GNT/RTDs have been the subjects of many studies, however, much less attention has been paid to multibarrier cases. Having more barrier and channel regions of RTD device may result in higher degrees of tunability and even better efficiency.

d) Regenerating chapters 3 to 5 for bilayer and multilayer GNRs/CNTs and comparing results with case of monolayer. Chemical bonding of inter-layers atoms and staking format of layers add complexity to the system. One can manipulate staking layers in such way that novel performance could be gained. For instance, having second layer in GNRs, antidot/doping topologies can be substituted in variety of patterns. One layer with antidots, the other with doping. Or, antidots of layers on top of each other creating wholes with bonding rearrangements at the edges.

References

[1] S. H. Chae and Y. H. J. N. C. Lee, "Carbon nanotubes and graphene towards soft electronics," vol. 1, no. 1, p. 15, 2014.

[2] M. F. De Volder, S. H. Tawfick, R. H. Baughman, and A. J. Hart, "Carbon nanotubes: present and future commercial applications," *science,* vol. 339, no. 6119, pp. 535-539, 2013.

[3] M. J. N. Schulz, "The end of the road for silicon?," vol. 399, no. 6738, p. 729, 1999.

[4] A. Lidow, "Is it the End of the Road for Silicon in Power Conversion?," in *2011 IEEE Bipolar/BiCMOS Circuits and Technology Meeting*, 2011, pp. 119-124: IEEE.

[5] A. K. Geim and K. S. Novoselov, "The rise of graphene," *Nature materials,* vol. 6, no. 3, pp. 183-191, 2007.

[6] A. C. Ferrari *et al.*, "Science and technology roadmap for graphene, related two-dimensional crystals, and hybrid systems," vol. 7, no. 11, pp. 4598-4810, 2015.

[7] J. K. Wassei and R. B. J. M. t. Kaner, "Graphene, a promising transparent conductor," vol. 13, no. 3, pp. 52-59, 2010.

[8] D. Akinwande, N. Petrone, and J. Hone, "Two-dimensional flexible nanoelectronics," *Nature communications,* vol. 5, p. 5678, 2014.

[9] V. K. Sangwan and M. C. J. A. r. o. p. c. Hersam, "Electronic transport in two-dimensional materials," vol. 69, pp. 299-325, 2018.

[10] Q. H. Wang, K. Kalantar-Zadeh, A. Kis, J. N. Coleman, and M. S. J. N. n. Strano, "Electronics and optoelectronics of two-dimensional transition metal dichalcogenides," vol. 7, no. 11, p. 699, 2012.

[11] G. Fiori *et al.*, "Electronics based on two-dimensional materials," *Nature nanotechnology,* vol. 9, no. 10, pp. 768-779, 2014.

[12] S. Z. Butler *et al.*, "Progress, challenges, and opportunities in two-dimensional materials beyond graphene," *ACS nano,* vol. 7, no. 4, pp. 2898-2926, 2013.

[13] G. R. Bhimanapati *et al.*, "Recent advances in two-dimensional materials beyond graphene," vol. 9, no. 12, pp. 11509-11539, 2015.

[14] A. Neto and K. J. M. E. Novoselov, "Two-dimensional crystals: beyond graphene," vol. 1, no. 1, pp. 10-17, 2011.

[15] A. B. J. J. o. M. R. Kaul, "Two-dimensional layered materials: Structure, properties, and prospects for device applications," vol. 29, no. 3, pp. 348-361, 2014.

[16] F. Schwierz, J. Pezoldt, and R. J. N. Granzner, "Two-dimensional materials and their prospects in transistor electronics," vol. 7, no. 18, pp. 8261-8283, 2015.

[17] D. Chimene, D. L. Alge, and A. K. J. A. m. Gaharwar, "Two-dimensional nanomaterials for biomedical applications: emerging trends and future prospects," vol. 27, no. 45, pp. 7261-7284, 2015.

[18] Y. Liu, X. Duan, Y. Huang, and X. J. C. S. R. Duan, "Two-dimensional transistors beyond graphene and TMDCs," vol. 47, no. 16, pp. 6388-6409, 2018.

[19] J. W. J. S. S. May, "Platinum surface LEED rings," vol. 17, pp. 267-270, 1969.

[20] J. A. Wilson and A. J. A. i. P. Yoffe, "The transition metal dichalcogenides discussion and interpretation of the observed optical, electrical and structural properties," vol. 18, no. 73, pp. 193-335, 1969.

[21] K. S. Novoselov, V. Fal, L. Colombo, P. Gellert, M. Schwab, and K. Kim, "A roadmap for graphene," *nature,* vol. 490, no. 7419, pp. 192-200, 2012.
[22] A. K. Geim, "Graphene: status and prospects," *science,* vol. 324, no. 5934, pp. 1530-1534, 2009.
[23] S. Datta, *Quantum transport: atom to transistor*. Cambridge university press, 2005.
[24] N. Tagmatarchis, *Advances in carbon nanomaterials: Science and applications*. CRC Press, 2012.
[25] M. Haselman and S. J. P. o. t. I. Hauck, "The future of integrated circuits: A survey of nanoelectronics," vol. 98, no. 1, pp. 11-38, 2009.
[26] M. Terrones *et al.*, "Graphene and graphite nanoribbons: Morphology, properties, synthesis, defects and applications," vol. 5, no. 4, pp. 351-372, 2010.
[27] L. Xie *et al.*, "Graphene nanoribbons from unzipped carbon nanotubes: atomic structures, Raman spectroscopy, and electrical properties," vol. 133, no. 27, pp. 10394-10397, 2011.
[28] Y. Gogotsi, *Nanomaterials handbook*. CRC press, 2006.
[29] S. Schofield *et al.*, "Atomically precise placement of single dopants in Si," *Physical review letters,* vol. 91, no. 13, p. 136104, 2003.
[30] C. Wang, K. Takei, T. Takahashi, and A. Javey, "Carbon nanotube electronics–moving forward," *Chemical Society Reviews,* vol. 42, no. 7, pp. 2592-2609, 2013.
[31] A. Safari, P. Hosseiniun, I. Rahbari, and M. R. Kalhor, "Graphene based electronic device," *World Acad. Sci. Eng. Technol. Int. J. Electr. Comput. Energ. Electron. Commun. Eng,* vol. 8, no. 8, pp. 1232-1237, 2014.
[32] X. Jia, J. Campos-Delgado, M. Terrones, V. Meunier, and M. S. Dresselhaus, "Graphene edges: a review of their fabrication and characterization," *Nanoscale,* vol. 3, no. 1, pp. 86-95, 2011.
[33] V. H. Nguyen, H.-V. Nguyen, and P. Dollfus, "Improved performance of graphene transistors by strain engineering," *Nanotechnology,* vol. 25, no. 16, p. 165201, 2014.
[34] M. Dresselhaus, A. Jorio, A. Souza Filho, and R. Saito, "Defect characterization in graphene and carbon nanotubes using Raman spectroscopy," *Philosophical Transactions of the Royal Society of London A: Mathematical, Physical and Engineering Sciences,* vol. 368, no. 1932, pp. 5355-5377, 2010.
[35] J.-C. Charlier, "Defects in carbon nanotubes," *Accounts of chemical research,* vol. 35, no. 12, pp. 1063-1069, 2002.
[36] S. Zhang *et al.*, "Mechanics of defects in carbon nanotubes: atomistic and multiscale simulations," *Physical Review B,* vol. 71, no. 11, p. 115403, 2005.
[37] S. L. Mielke *et al.*, "The role of vacancy defects and holes in the fracture of carbon nanotubes," *Chemical Physics Letters,* vol. 390, no. 4, pp. 413-420, 2004.
[38] M. Zoghi and A. Y. Goharrizi, "The electronic properties of armchair graphene nanoribbons defected by hexagonal antidotes and Boron/Nitride atoms," in *Electrical Engineering (ICEE), 2017 Iranian Conference on*, 2017, pp. 355-359: IEEE.
[39] J. Kotakoski, A. Krasheninnikov, and K. Nordlund, "Energetics, structure, and long-range interaction of vacancy-type defects in carbon nanotubes: Atomistic simulations," *Physical Review B,* vol. 74, no. 24, p. 245420, 2006.
[40] E. Kan, Z. Li, and J. Yang, "Graphene nanoribbons: Geometric, electronic, and magnetic properties," in *Physics and Applications of Graphene-theory*: IntechOpen, 2011.
[41] A. Rozhkov, S. Savel'ev, and F. Nori, "Electronic properties of armchair graphene nanoribbons," *Physical Review B,* vol. 79, no. 12, p. 125420, 2009.

[42] M. S. Dresselhaus, G. Dresselhaus, P. Eklund, and A. Rao, "Carbon nanotubes," in *The Physics of Fullerene-Based and Fullerene-Related Materials*: Springer, 2000, pp. 331-379.
[43] T. W. Odom, J.-L. Huang, P. Kim, and C. M. Lieber, "Structure and electronic properties of carbon nanotubes," ed: ACS Publications, 2000.
[44] B. J. R. Attaf, W. A. P.-A. i. M. S. Innovation in Carbon Nanotube-Based Composites, and Applications, "An Eco-approach to boost the sustainability of carbon nanotube-based composite products," pp. 1-14.
[45] L. L. Chang, L. Esaki, and R. Tsu, "Resonant tunneling in semiconductor double barriers," *Applied Physics Letters,* vol. 24, no. 12, pp. 593-595, 1974.
[46] F. Capasso, K. Mohammed, and A. Y. Cho, "Resonant tunneling through double barriers, perpendicular quantum transport phenomena in superlattices, and their device applications," in *Electronic Structure of Semiconductor Heterojunctions*: Springer, 1988, pp. 99-115.
[47] J. J. U. o. R. Ling, Rochester, NY, "Resonant tunneling diodes: Theory of operation and applications," vol. 14627, 1998.
[48] W. Prost, "Resonant tunnelling diodes for digital circuit applications," in *Advanced Semiconductor Devices and Microsystems, 2002. The Fourth International Conference on*, 2002, pp. 115-124: IEEE.
[49] H. Sugiyama, S. Suzuki, and M. J. N. T. R. Asada, "Room-temperature resonant-tunneling-diode terahertz oscillator based on precisely controlled semiconductor epitaxial growth technology," vol. 9, no. 1, 2011.
[50] M. B. Nardelli, J.-L. Fattebert, D. Orlikowski, C. Roland, Q. Zhao, and J. Bernholc, "Mechanical properties, defects and electronic behavior of carbon nanotubes," *Carbon,* vol. 38, no. 11, pp. 1703-1711, 2000.
[51] M. Sammalkorpi, A. Krasheninnikov, A. Kuronen, K. Nordlund, and K. Kaski, "Mechanical properties of carbon nanotubes with vacancies and related defects," *Physical Review B,* vol. 70, no. 24, p. 245416, 2004.
[52] H. J. Choi, J. Ihm, S. G. Louie, and M. L. Cohen, "Defects, quasibound states, and quantum conductance in metallic carbon nanotubes," *Physical Review Letters,* vol. 84, no. 13, p. 2917, 2000.
[53] S. Kundalwal, S. Meguid, and G. J. C. Weng, "Strain gradient polarization in graphene," vol. 117, pp. 462-472, 2017.
[54] J. Velasco Jr *et al.*, "Nanoscale control of rewriteable doping patterns in pristine graphene/boron nitride heterostructures," *Nano letters,* vol. 16, no. 3, pp. 1620-1625, 2016.
[55] O. Hod and G. E. Scuseria, "Electromechanical properties of suspended graphene nanoribbons," *Nano letters,* vol. 9, no. 7, pp. 2619-2622, 2009.
[56] T. Yu, Z. Ni, C. Du, Y. You, Y. Wang, and Z. Shen, "Raman mapping investigation of graphene on transparent flexible substrate: the strain effect," *The Journal of Physical Chemistry C,* vol. 112, no. 33, pp. 12602-12605, 2008.
[57] S. J. P. R. B. Jun, "Density-functional study of edge stress in graphene," vol. 78, no. 7, p. 073405, 2008.
[58] R. G. Amorim, A. Fazzio, A. Antonelli, F. D. Novaes, and A. J. da Silva, "Divacancies in graphene and carbon nanotubes," *Nano Letters,* vol. 7, no. 8, pp. 2459-2462, 2007.

[59] M. C. Nguyen, V.-H. Nguyen, J. Saint-Martin, and P. Dollfus, "Strong negative differential resistance in graphene devices with local strain," in *Computational Electronics (IWCE), 2015 International Workshop on*, 2015, pp. 1-3: IEEE.
[60] S. Kawai *et al.*, "Atomically controlled substitutional boron-doping of graphene nanoribbons," *Nature communications,* vol. 6, 2015.
[61] H. Teong, K.-T. Lam, S. B. Khalid, and G. Liang, "Shape effects in graphene nanoribbon resonant tunneling diodes: A computational study," *Journal of Applied Physics,* vol. 105, no. 8, p. 084317, 2009.
[62] Y. Li, X. Jiang, Z. Liu, and Z. J. N. R. Liu, "Strain effects in graphene and graphene nanoribbons: the underlying mechanism," vol. 3, no. 8, pp. 545-556, 2010.
[63] G. Gui, J. Li, and J. J. P. R. B. Zhong, "Band structure engineering of graphene by strain: first-principles calculations," vol. 78, no. 7, p. 075435, 2008.
[64] S. Schulz and G. J. P. R. B. Czycholl, "Tight-binding model for semiconductor nanostructures," vol. 72, no. 16, p. 165317, 2005.
[65] S. Reich, J. Maultzsch, C. Thomsen, and P. Ordejon, "Tight-binding description of graphene," *Physical Review B,* vol. 66, no. 3, p. 035412, 2002.
[66] W. A. J. S. s. Harrison, "Tight-binding methods," vol. 299, pp. 298-310, 1994.
[67] W. M. C. Foulkes and R. J. P. r. B. Haydock, "Tight-binding models and density-functional theory," vol. 39, no. 17, p. 12520, 1989.
[68] D. Gunlycke and C. J. P. R. B. White, "Tight-binding energy dispersions of armchair-edge graphene nanostrips," vol. 77, no. 11, p. 115116, 2008.
[69] R. J. M. P. L. B. Kundu, "Tight-binding parameters for graphene," vol. 25, no. 03, pp. 163-173, 2011.
[70] V. M. Pereira, A. C. Neto, and N. J. P. R. B. Peres, "Tight-binding approach to uniaxial strain in graphene," vol. 80, no. 4, p. 045401, 2009.
[71] N. Marks, N. Cooper, D. McKenzie, D. McCulloch, P. Bath, and S. J. P. R. B. Russo, "Comparison of density-functional, tight-binding, and empirical methods for the simulation of amorphous carbon," vol. 65, no. 7, p. 075411, 2002.
[72] M. Zoghi, A. Y. Goharrizi, and M. Saremi, "Band Gap Tuning of Armchair Graphene Nanoribbons by Using Antidotes," *Journal of Electronic Materials,* vol. 46, no. 1, pp. 340-346, 2017.
[73] A. Yazdanpanah, M. Pourfath, M. Fathipour, H. Kosina, and S. Selberherr, "A numerical study of line-edge roughness scattering in graphene nanoribbons," *IEEE Transactions on Electron Devices,* vol. 59, no. 2, pp. 433-440, 2012.
[74] D. Gunlycke and C. White, "Tight-binding energy dispersions of armchair-edge graphene nanostrips," *Physical Review B,* vol. 77, no. 11, p. 115116, 2008.
[75] C. T. White, J. Li, D. Gunlycke, and J. W. Mintmire, "Hidden one-electron interactions in carbon nanotubes revealed in graphene nanostrips," *Nano letters,* vol. 7, no. 3, pp. 825-830, 2007.
[76] A. Bahari, "An alternative approach to the problem of CNT electron energy band structure," in *Electronic Properties of Carbon Nanotubes*: IntechOpen, 2011.
[77] N. Neophytou, S. Ahmed, and G. Klimeck, "Non-equilibrium Green's function (NEGF) simulation of metallic carbon nanotubes including vacancy defects," *Journal of Computational Electronics,* vol. 6, no. 1, pp. 317-320, 2007.
[78] S. J. S. Datta and microstructures, "Nanoscale device modeling: the Green's function method," vol. 28, no. 4, pp. 253-278, 2000.

[79] G. Abadir, K. Walus, and D. Pulfrey, "Basis-set choice for DFT/NEGF simulations of carbon nanotubes," *Journal of computational electronics,* vol. 8, no. 1, pp. 1-9, 2009.
[80] S. Aravind, S. Shravan, S. Shrijan, R. V. Sanjeev, and B. B. T. Sundari, "Simulation of carbon nanotube field effect transistors using NEGF," in *IOP Conference Series: Materials Science and Engineering*, 2016, vol. 149, no. 1, p. 012183: IOP Publishing.
[81] A. Y. Goharrizi, M. Zoghi, and M. Saremi, "Armchair Graphene Nanoribbon Resonant Tunneling Diodes Using Antidote and BN Doping," *IEEE Transactions on Electron Devices,* vol. 63, no. 9, pp. 3761-3768, 2016.
[82] J. Guo and M. Lundstrom, "Device simulation of SWNT-FETs," in *Carbon nanotube electronics*: Springer, 2009, pp. 107-131.
[83] R. Zhao, J. Wang, M. Yang, Z. Liu, and Z. Liu, "BN-embedded graphene with a ubiquitous gap opening," *The Journal of Physical Chemistry C,* vol. 116, no. 39, pp. 21098-21103, 2012.
[84] Y.-W. Son, M. L. Cohen, and S. G. Louie, "Energy gaps in graphene nanoribbons," *Physical review letters,* vol. 97, no. 21, p. 216803, 2006.
[85] V. M. Pereira and A. C. Neto, "Strain engineering of graphene's electronic structure," *Physical Review Letters,* vol. 103, no. 4, p. 046801, 2009.
[86] K. Khaliji, M. Noei, S. M. Tabatabaei, M. Pourfath, M. Fathipour, and Y. Abdi, "Tunable bandgap in bilayer armchair graphene nanoribbons: concurrent influence of electric field and uniaxial strain," *IEEE Transactions on Electron Devices,* vol. 60, no. 8, pp. 2464-2470, 2013.
[87] L. Rosales, M. Pacheco, Z. Barticevic, A. León, A. Latgé, and P. Orellana, "Transport properties of antidot superlattices of graphene nanoribbons," *Physical Review B,* vol. 80, no. 7, p. 073402, 2009.
[88] C. Leon, M. Costa, L. Chico, and A. J. S. r. Latgé, "Interface effects in hybrid hBN-graphene nanoribbons," vol. 9, no. 1, p. 3508, 2019.
[89] E. Gracia-Espino, H. R. Barzegar, and A. J. A. O. Zettl, "Coronene-Based Graphene Nanoribbons Insulated by Boron Nitride Nanotubes: Electronic Properties of the Hybrid Structure," vol. 3, no. 10, pp. 12930-12935, 2018.
[90] F. Zheng *et al.*, "Half metallicity along the edge of zigzag boron nitride nanoribbons," vol. 78, no. 20, p. 205415, 2008.
[91] P. Palla, A. S. Ethiraj, and J. Raina, "Resonant tunneling diode based on band gap engineered graphene antidot structures," in *AIP Conference Proceedings*, 2016, vol. 1724, no. 1, p. 020069: AIP Publishing.
[92] Y.-T. Zhang, Q.-M. Li, Y.-C. Li, Y.-Y. Zhang, and F. Zhai, "Band structures and transport properties of zigzag graphene nanoribbons with antidot arrays," *Journal of Physics: Condensed Matter,* vol. 22, no. 31, p. 315304, 2010.
[93] W. Tian, Y. Zeng, and Z. Zhang, "Electronic properties of graphene nanoribbons with periodically hexagonal nanoholes," *Journal of Applied Physics,* vol. 114, no. 7, p. 074307, 2013.
[94] Y. Che, H. Chen, H. Gui, J. Liu, B. Liu, and C. Zhou, "Review of carbon nanotube nanoelectronics and macroelectronics," *Semiconductor Science and Technology,* vol. 29, no. 7, p. 073001, 2014.
[95] J. Kong *et al.*, "Nanotube molecular wires as chemical sensors," *science,* vol. 287, no. 5453, pp. 622-625, 2000.

[96] P. Ayala, R. Arenal, M. Rümmeli, A. Rubio, and T. Pichler, "The doping of carbon nanotubes with nitrogen and their potential applications," *Carbon,* vol. 48, no. 3, pp. 575-586, 2010.
[97] T. Dumitrica, M. Hua, and B. I. Yakobson, "Symmetry-, time-, and temperature-dependent strength of carbon nanotubes," *Proceedings of the National Academy of Sciences,* vol. 103, no. 16, pp. 6105-6109, 2006.
[98] J. M. García-Lastra, K. S. Thygesen, M. Strange, and Á. Rubio, "Conductance of sidewall-functionalized carbon nanotubes: universal dependence on adsorption sites," *Physical review letters,* vol. 101, no. 23, p. 236806, 2008.
[99] Y. Ma, P. Lehtinen, A. S. Foster, and R. M. Nieminen, "Magnetic properties of vacancies in graphene and single-walled carbon nanotubes," *New Journal of Physics,* vol. 6, no. 1, p. 68, 2004.
[100] M. Hashemi, K. Sääskilahti, and M. J. Puska, "Local semiconducting transition in armchair carbon nanotubes: The effect of periodic bi-site perturbation on electronic and transport properties of carbon nanotubes," *Physical Review B,* vol. 83, no. 11, p. 115411, 2011.
[101] J. A. Rodriguez-Manzo and F. Banhart, "Creation of individual vacancies in carbon nanotubes by using an electron beam of 1 Å diameter," *Nano letters,* vol. 9, no. 6, pp. 2285-2289, 2009.
[102] Y. An *et al.*, "Negative differential resistance and rectification effects in step-like graphene nanoribbons," vol. 17, pp. 262-269, 2015.
[103] M. Sharifi, E. Akhoundi, and H. J. J. o. C. E. Esmaili, "Negative differential resistance in new structures based on graphene nanoribbons," vol. 15, no. 4, pp. 1361-1369, 2016.
[104] T. Wakai, S. Sakamoto, and M. J. J. o. P. C. M. Tomiya, "I–V characteristics of graphene nanoribbon/h-BN heterojunctions and resonant tunneling," vol. 30, no. 26, p. 265302, 2018.
[105] H. Teong, K.-T. Lam, and G. Liang, "A computational study on the device performance of graphene nanoribbon resonant tunneling diodes," *Japanese Journal of Applied Physics,* vol. 48, no. 4S, p. 04C156, 2009.
[106] M. Zoghi and A. Y. Goharrizi, "Strain-Induced Armchair Graphene Nanoribbon Resonant-Tunneling Diodes," *IEEE Transactions on Electron Devices,* 2017.
[107] G. J. Ferreira, M. N. Leuenberger, D. Loss, and J. C. J. P. R. B. Egues, "Low-bias negative differential resistance in graphene nanoribbon superlattices," vol. 84, no. 12, p. 125453, 2011.
[108] V. Nam Do and P. J. J. o. A. P. Dollfus, "Negative differential resistance in zigzag-edge graphene nanoribbon junctions," vol. 107, no. 6, p. 063705, 2010.
[109] Z. Zhang, K. Chang, and K. S. J. A. P. L. Chan, "Resonant tunneling through double-bended graphene nanoribbons," vol. 93, no. 6, p. 062106, 2008.
[110] S. I. A. J. h. w. i. net, "International technology roadmap for semiconductors," 2009.
[111] K. Cheng, D. Chidambarrao, R. Divakaruni, and O. G. Gluschenkov, "Structure of vertical strained silicon devices," ed: Google Patents, 2007.
[112] J.-J. Lee, S. T. Hsu, D. J. Tweet, and J.-s. Maa, "Strained silicon finFET device," ed: Google Patents, 2006.
[113] D. Lembke, S. Bertolazzi, and A. J. A. o. c. r. Kis, "Single-layer MoS2 electronics," vol. 48, no. 1, pp. 100-110, 2015.

[114] A. A. Fouladi, "Effect of uniaxial strain on the tunnel magnetoresistance of T-shaped graphene nanoribbon based spin-valve," *Superlattices and Microstructures,* vol. 95, pp. 108-114, 2016.
[115] Y. Xue, Y. Chen, K. Cai, Z.-Y. Liu, Y. Zhang, and N. Wei, "Local strain field engineering on interfacial thermal resistance of graphene nanoribbon," *Applied Physics Letters,* vol. 112, no. 2, p. 021604, 2018.
[116] M. Akbari, A. Baghai-Wadji, and R. J. a. p. a. Morad, "Uniaxial Strain Effects on Graphene-Nanoribbon Resonant Tunneling Transistors," 2018.
[117] C. Si, Z. Sun, and F. Liu, "Strain engineering of graphene: a review," *Nanoscale,* vol. 8, no. 6, pp. 3207-3217, 2016.
[118] J. Tan, X. Zhang, W. Liu, X. He, and M. J. N. Zhao, "Strain-induced tunable negative differential resistance in triangle graphene spirals," vol. 29, no. 20, p. 205202, 2018.
[119] M. Teague *et al.*, "Evidence for strain-induced local conductance modulations in single-layer graphene on SiO2," *Nano letters,* vol. 9, no. 7, pp. 2542-2546, 2009.
[120] J. Borysiuk *et al.*, "Transmission electron microscopy and scanning tunneling microscopy investigations of graphene on 4 H-SiC (0001)," vol. 105, no. 2, p. 023503, 2009.
[121] B. Huang *et al.*, "Quantum manifestations of graphene edge stress and edge instability: A first-principles study," vol. 102, no. 16, p. 166404, 2009.
[122] J. Kang, Y. He, J. Zhang, X. Yu, X. Guan, and Z. Yu, "Modeling and simulation of uniaxial strain effects in armchair graphene nanoribbon tunneling field effect transistors," *Applied Physics Letters,* vol. 96, no. 25, p. 252105, 2010.
[123] H. Fang, R.-Z. Wang, S.-Y. Chen, M. Yan, X.-M. Song, and B. Wang, "Strain-induced negative differential resistance in armchair-edge graphene nanoribbons," *Applied Physics Letters,* vol. 98, no. 8, p. 082108, 2011.
[124] S. Prabhakar and R. J. a. p. a. Melnik, "Band engineering and elastic properties of strained armchair graphene nanoribbons: semiconductor vs metallic characteristics," 2019.
[125] Y. Lu and J. J. N. R. Guo, "Band gap of strained graphene nanoribbons," vol. 3, no. 3, pp. 189-199, 2010.
[126] L. Sun, Q. Li, H. Ren, H. Su, Q. Shi, and J. Yang, "Strain effect on electronic structures of graphene nanoribbons: A first-principles study," *The Journal of chemical physics,* vol. 129, no. 7, p. 074704, 2008.
[127] S. B. Mamaghani, F. Eslaminasab, and A. Y. Goharrizi, "Armchair graphene nanoribbons: A synthesis precision study," in *2017 Iranian Conference on Electrical Engineering (ICEE)*, 2017, pp. 349-354: IEEE.
[128] Y.-W. Son, M. L. Cohen, and S. G. J. N. Louie, "Half-metallic graphene nanoribbons," vol. 444, no. 7117, p. 347, 2006.
[129] H. J. P. E. L.-d. S. Mohammadpour and Nanostructures, "Quantum dot resonant tunneling FET on graphene," vol. 81, pp. 91-95, 2016.
[130] G. Fiori and G. Iannaccone, "Simulation of graphene nanoribbon field-effect transistors," *IEEE Electron Device Letters,* vol. 28, no. 8, pp. 760-762, 2007.
[131] B. Fallahazad *et al.*, "Gate-tunable resonant tunneling in double bilayer graphene heterostructures," *Nano letters,* vol. 15, no. 1, pp. 428-433, 2014.
[132] Y. Wu *et al.*, "Three-terminal graphene negative differential resistance devices," *ACS nano,* vol. 6, no. 3, pp. 2610-2616, 2012.

[133] C. Soldano, A. Mahmood, and E. Dujardin, "Production, properties and potential of graphene," *Carbon,* vol. 48, no. 8, pp. 2127-2150, 2010.
[134] A. Y. Goharrizi, M. Pourfath, M. Fathipour, and H. Kosina, "Device performance of graphene nanoribbon field-effect transistors in the presence of line-edge roughness," *IEEE Transactions on electron devices,* vol. 59, no. 12, pp. 3527-3532, 2012.
[135] G. Liang, S. B. Khalid, and K.-T. Lam, "Influence of edge roughness on graphene nanoribbon resonant tunnelling diodes," *Journal of Physics D: Applied Physics,* vol. 43, no. 21, p. 215101, 2010.
[136] F. Xu, J. W. Durham III, B. J. Wiley, and Y. Zhu, "Strain-release assembly of nanowires on stretchable substrates," *ACS nano,* vol. 5, no. 2, pp. 1556-1563, 2011.
[137] J. Kang, Y. He, J. Zhang, X. Yu, X. Guan, and Z. J. A. P. L. Yu, "Modeling and simulation of uniaxial strain effects in armchair graphene nanoribbon tunneling field effect transistors," vol. 96, no. 25, p. 252105, 2010.